ANNUAL REPORT

Center for Experimental Nuclear Physics and Astrophysics
University of Washington
April, 2011

Sponsored in part by the United States Department of Energy
under Grant #DE-FG02-97ER41020.

Cover design by Nora Boyd. Top photos, left to right: Graduate student Ran Hong examining the ^{6}He collection system in experimental cave 1 (see Sec. 3.3.1). Photo by Greg Harper. Gravity graduate student Charlie Hagedorn, self portrait, with the submillimeter parallel-plate torsion balance (see Sec. 2.1.3). Photo by Charlie Hagedorn. Postdoc Andrew Wagner, research engineer Nora Boyd, graduate student Michael Hotz, postdoc Gray Rybka, and senior research engineer Doug Will removing the bottom of the ADMX insert (see Sec. 5.1). The ADMX magnet cryostat is in the background. Photo by Greg Harper. Bottom photo: Instrument maker Jim Elms discussing the new NCD end cap assemblies for the HALO experiment (see Sec. 1.6) with Hamish Robertson. The end caps are being manufactured in production mode with our new CNC lathe. Photo by Greg Harper.

INTRODUCTION

The Center for Experimental Nuclear Physics and Astrophysics, CENPA, was established in 1998 at the University of Washington as the institutional home for a broad program of research in nuclear physics, astrophysics and related fields. Research activities are conducted locally and at remote sites. CENPA has been a major participant in the Sudbury Neutrino Observatory (SNO) and is presently contributing substantially to the KATRIN tritium beta decay experiment, the MAJORANA ^{76}Ge double beta decay experiment, and the SNO+ ^{150}Nd double beta decay experiment in Canada. With the arrival of the Muon Physics group from Illinois we have new activities at the Paul Scherrer Institute in Switzerland, and development of a new program to measure the anomalous magnetic moment of the muon at Fermilab. The fundamental symmetries program also includes "in-house" research using the local tandem Van de Graaff accelerator, and neutron physics at other locations. We conduct user-mode research on relativistic heavy ions at the Relativistic Heavy Ion Collider at Brookhaven.

The year 2010–2011 has been filled with new activity at CENPA. Professors David Hertzog and Peter Kammel arrived from the University of Illinois, bringing with them Postdoctoral Fellow Peter Winter and students Michael Murray and Sarah Knaack. They will continue to receive support for some of their research for the duration of their 3-year NSF grant until April 2012, thanks to the cooperation of the University of Illinois and the NSF. Worldwide interest in their previous result for muon $g-2$, which shows approximately 3σ disagreement with the Standard Model calculation, continues unabated, and their new proposal to mount a still more precise measurement at Fermilab has been greeted with enthusiasm.

The KATRIN experiment, sited in Karlsruhe, continues to move forward with construction. The difficult task of building the windowless gaseous tritium source passed a major milestone with the delivery and testing of the "demonstrator", a cryogenic-performance prototype. Remarkably, temperature stability of 4 mK at 30 K was achieved, almost 10 times better than the specification. Here at CENPA, good progress on the detector system has brought us close to a successful conclusion to commissioning, and the complete system will be shipped in the spring of 2011.

Professor Leslie Rosenberg's group succeeded, with the skillful support of Doug Will, in bringing the 12-tonne superconducting magnet for the axion experiment ADMX from Livermore to Seattle. There was no damage or misadventure, as determined by a complete cooldown and ramping of the magnet field to 6 T. We await completion of the modification to our high-bay area east of the tandem which will allow sufficient headroom to install and remove the insert.

We are very interested in the potential of "Project 8," a possible approach to extending the sensitivity of direct neutrino mass measurements below even the 200-meV level accessible to KATRIN. A prototype microwave receiver and antenna are being installed in the bore of a superconducting magnet that was formerly used by Professor Bob Van Dyck. We take this opportunity to congratulate CENPA Fellow Mike Miller and Postdoctoral Fellow Gray Rybka, who teamed up to write a successful proposal to the Royalty Research Foundation for Project 8.

With Associate Director Greg Harper assuming his new duties, we carried out a search for a professional staff member to maintain our strength in technical support, especially in the face of so much new activity. We are very pleased to welcome Nora Boyd to our professional staff.

Two senior Postdoctoral Fellows, Seth Hoedl and Brent VanDevender, took up positions elsewhere, Seth moving to a startup company in North Carolina, and Brent taking a staff position at Pacific Northwest National Lab. We were successful in recruiting Diana Parno from Carnegie-Mellon University into a postdoc position, and she joined us in April, 2011. Frederik Wauters from Leuven, Belgium, will join us in June, 2011.

The DOE Office of Nuclear Physics, which provides operating support through programs in Low Energy Nuclear Physics and Heavy Ion Physics, has renewed our support under Grant DE-FG02-97ER41020 for FY11, which began December 1, 2010, and is the third of the current 3-year cycle. In the following paragraphs we record some more of the highlights of our past year in research.

- Analysis of the data from emiT-II has been completed. We have not found evidence for Time-Reversal symmetry breaking, but we have placed the best limit on the D coefficient significantly below any previous experiment. This important achievement had a strong contribution from UW. The apparatus upgrade from emiT-I was performed mostly at UW. Over the last few years, at UW, we remained responsible for the Monte Carlo calculations, which played an important role in understanding systematic uncertainties in the experiment. We are presently writing a paper for publication.

- We have determined the ^{22}Na(p, γ) thermonuclear reaction rate for novae and have found large discrepancies with a previous experiment. Our results imply that the chance of observing the highly-sought (but so-far elusive) evidence of production of ^{22}Na in novae is a bit harder than previously thought.

- We have performed and published the results of several experiments related to understanding details of nova nucleosynthesis.

- We have succeeded in our efforts on production of ^{6}He with the aim of searching for tensor contributions to the weak current. We demonstrated that we can consistently get $\sim 10^9$ atoms/s of ^{6}He delivered to a clean room. We are now on the process of moving the laser systems from Argonne National Lab to UW.

- The UCNA collaboration has published a determination of the beta asymmetry to approximately 1%. We have played a supporting role in experimental shifts, data analysis, and in writing the publications.

- The earthquake and tsunami that struck Japan March 11, 2011, caused severe damage to the reactor complex at Fukushima. We set up a monitoring system that took advantage of the very high airflow rates through intake filters at the Physics-Astronomy Building, as well as a test PPC detector for MAJORANA that was available. We were able to see the arrival of fission products, quantify their activity in the air, and draw conclusions about some of the circumstances of events at Fukushima.

- The UW URHI group has established accurate systematic trends for minimum-bias jet (minijet) production in Au-Au and Cu-Cu collisions by application of pileup correction techniques developed by our group (collision-event pileup is increasingly significant for higher-luminosity RHIC operation). After pileup corrections the previously-observed "sharp transition" in minijet properties now clearly occurs at a specific mean projectile-nucleon path length for all collision systems corresponding to at least two dijets per collision. We have converted jet angular correlations into jet fragment yields via pQCD dijet cross sections. The fragment yields account for essentially all hadron yield increases beyond participant (wounded-nucleon) scaling in Au-Au collisions, indicating that jet absorption in an opaque medium is negligible, although jets are strongly modified.

- We have established an accurate global parametrization of our azimuth quadrupole measure $v_2\{2D\}$ which is factorized on centrality b, transverse momentum p_t and collision energy $\sqrt{s_{NN}}$. Our $v_2\{2D\}$ data, obtained by fits to 2D angular correlations, are precisely distinguished from jet correlations ("nonflow"). Our v_2 parametrization challenges conventional interpretations of published v_2 data in terms of hydrodynamic flows and constituent-quark recombination, suggesting instead a possible QCD field-field interaction mechanism for A-A collisions above $\sqrt{s_{NN}} \approx 13$ GeV.

- We have used our jet and quadrupole systematics to relate RHIC collisions to recent results from the LHC at 7 TeV, specifically the "ridge" observed by the CMS collaboration. We have demonstrated that jet correlations in 7 TeV p-p collisions are exactly as predicted by a simple extrapolation from 200 GeV data (multiplicative factor 2.3), and that the CMS ridge is the result of a subtle interplay between jet and quadrupole correlation components as affected by applied multiplicity and p_t cuts.

Three CENPA graduate students, Rob Johnson, Mike Marino, and Anne Sallaska, obtained their Ph.D. degrees during the period of this report. Rob is a postdoc at the University of Colorado in Boulder, Mike is a postdoc at the Technical University, Munich, and Anne is a postdoc at the University of North Carolina, Chapel Hill.

As always, we encourage outside applications for the use of our facilities. As a convenient reference for potential users, the table on the following page lists the capabilities of our accelerators. For further information, please contact Greg Harper, Associate Director, CENPA, Box 354290, University of Washington, Seattle, WA 98195; (206) 543 4080, or gharper@u.washington.edu. Further information is also available on our web page: http://www.npl.washington.edu.

We close this introduction with a reminder that the articles in this report describe work in progress and are not to be regarded as publications or to be quoted without permission of the authors. In each article the names of the investigators are listed alphabetically, with the primary author underlined, to whom inquiries should be addressed.

Hamish Robertson, Director
Greg Harper, Associate Director and Editor

Victoria Clarkson, Assistant Editor
Gary Holman, Technical Editor

TANDEM VAN DE GRAAFF ACCELERATOR

A High Voltage Engineering Corporation Model FN purchased in 1966 with NSF funds, operation funded primarily by the U.S. Department of Energy. See W. G. Weitkamp and F. H. Schmidt, "The University of Washington Three Stage Van de Graaff Accelerator," *Nucl. Instrum. Methods* **122**, 65 (1974). Recently adapted to an (optional) terminal ion source and a non-inclined tube #3, which enables the accelerator to produce high intensity beams of hydrogen and helium isotopes at energies from 100 keV to 7.5 MeV.

Some Available Energy Analyzed Beams

Ion	Max. Current (particle μA)	Max. Energy (MeV)	Ion Source
^{1}H or ^{2}H	50	18	DEIS or 860
^{3}He or ^{4}He	2	27	Double Charge-Exchange Source
^{3}He or ^{4}He	30	7.5	Tandem Terminal Source
^{6}Li or ^{7}Li	1	36	860
^{11}B	5	54	860
^{12}C or ^{13}C	10	63	860
*^{14}N	1	63	DEIS or 860
^{16}O or ^{18}O	10	72	DEIS or 860
F	10	72	DEIS or 860
* Ca	0.5	99	860
Ni	0.2	99	860
I	0.001	108	860

*Negative ion is the hydride, dihydride, or trihydride.

Several additional ion species are available including the following: Mg, Al, Si, P, S, Cl, Fe, Cu, Ge, Se, Br and Ag. Less common isotopes are generated from enriched material. We recently have been producing the positive ion beams of the noble gases He, Ne, Ar, and Kr at ion source energies from 10 keV to 100 keV for implantation, in particular the rare isotopes ^{21}Ne and ^{36}Ar. We have also produced a separated beam of 15-MeV ^{8}B at 6 particles/second.

Contents

1 Neutrino Research

1.1 Neutrino research at CENPA

R. G. H. Robertson

Neutrino research is a major focus of CENPA's current research effort, and we are contributing significantly to 6 projects which are in different stages. The Sudbury Neutrino Observatory (SNO) project led to the resolution of the solar neutrino problem in favor of new neutrino properties (mass and oscillations). Data taking ended in 2006, but much interesting physics remained to be mined, and that process is now drawing to a conclusion. Recent publications include a very detailed re-analysis of the data from the first two phases with an improved rejection of low-energy backgrounds.

That neutrinos have mass is established from oscillations, but the mass itself is not known. Neutrino mass is not only an important fundamental constant, it influences the evolution of the cosmos. In 2000 we joined the KATRIN collaboration as founding members and took on the task of delivering the detector system for this complex experiment. The goal is a direct determination of neutrino mass from tritium beta decay with a sensitivity of 200 meV. Our construction of the detector system is nearly complete and it will be shipped to Germany in the spring of 2011.

The question of why the universe is mostly matter, with very little antimatter, may reflect a unique property of neutrinos. Alone among matter particles, neutrinos can be their own antiparticles, but it is not known if they are. If they are then they can provide a mechanism for the conversion of antimatter to matter. The only known approach to answering this question is to search for neutrinoless double beta decay. The MAJORANA DEMONSTRATOR is a search in ^{76}Ge using enriched and natural Ge detectors. At CENPA we are contributing mechanical design and fabrication, low-background cables and components, and electronics.

The SNO+ experiment is similarly motivated but will carry out the search for neutrinoless double beta decay in ^{150}Nd, making use of the former SNO detector in a new incarnation. The acrylic vessel will be filled with a Nd-doped liquid scintillator and a search made for a monoenergetic line at the known Q-value.

KATRIN is the most sensitive direct mass search experiment, but it may nevertheless turn out that the mass is less than 200 meV. Oscillations place a lower limit of 20 meV on the average mass of the 3 eigenstates. We are beginning experimental investigation of a new idea for a tritium beta decay search that might reach into this last window. "Project 8," as it is called, would make use of cyclotron radiation emitted by betas spiraling in a magnetic field.

The only supernova neutrino burst to be detected came from SN1987a. There is much to be learned about supernovae from neutrinos and an opportunity presented itself with the conclusion of the SNO experiment to make use of the neutral-current-detection (NCD) array that we built. A supernova detector, HALO, based on Pb as a target and using the NCD detectors is under construction in SNOLAB.

KATRIN

1.2 Overview of the KATRIN experiment

J. F. Amsbaugh, J. Barrett*, A. Beglarian†, T. Bergmann†, L. I. Bodine, T. H. Burritt, T. J. Corona‡, P. J. Doe, S. Enomoto, J. A. Formaggio*, F. M. Fraenkle‡, D. L. Furse*, G. C. Harper, M. Knauer†, A. Kopmann†, E. L. Martin, N. S. Oblath*, L. Petzold†, D. Phillips‡, A. W. P. Poon§, R. G. H. Robertson, M. Steidl†, D. Tcherniakhovski†, B. A. VanDevender*, T. D. Van Wechel, B. L. Wall, K. J. Wierman, J. F. Wilkerson‡, and S. Wüstling†

The KATRIN experiment aims to make an order of magnitude improvement in the direct measurement of the mass of the neutrino complementing the model-dependent measurements obtained via cosmology and searches for neutrinoless double beta decay. With a predicted sensitivity of 200 meV, KATRIN will investigate the neutrino hierarchy and address the value for the neutrino mass of 560 meV derived from a claimed observation of neutrinoless double beta decay[1]. KATRIN is currently under construction at the Karlsruhe Institute of Technology (KIT) in Germany. Data taking is expected to begin in early 2014 with final sensitivity reached 5 years later. KATRIN probes the neutrino mass by making a precision measurement of the electron energy spectrum associated with beta decay of tritium. Neutrino mass is evidenced in a distortion at the high energy tail of the spectrum, allowing a value for the mass to be derived solely from the kinematics of the reaction. The design of the KATRIN apparatus draws on some 40 years of tritium beta decay searches for the neutrino mass. The improved sensitivity of KATRIN arises primarily from increases in source luminosity and the physical size of the apparatus and probably represents the best one can practically expect to achieve with this technology. The layout of the KATRIN apparatus is shown in Fig. 1.2-1.

The tritium source is of the window-less, gaseous type, a 10-m long, 9-cm diameter tube containing tritium gas at an effective column density of 5×10^{17} molecules/cm^2 and a temperature of 30 K. Tritium escaping from the ends of the source is returned to the center by way of turbo molecular pumps, the differential pumping system. Electrons from tritium beta decay are constrained to escape from the ends of the source via a train of 3-T magnets. Those electrons escaping "downstream" pass towards the analyzing spectrometers via the cryogenic pumping system which consists of a chicane beam pipe whose walls are coated with argon frost to trap any escaping tritium molecules that would contaminate the spectrometer system. The tritium pressure at the entrance to the spectrometers is 11 orders of magnitude lower than the pressure at the outlet of the tritium source.

*Massachusetts Institute of Technology, Cambridge, MA.
†Karlsruhe Institute of Technology, Karlsruhe, Germany.
‡University of North Carolina, Chapel Hill, NC.
§Lawrence Berkeley National Laboratory, Berkeley, CA
*Pacific Northwest National Laboratory, Richland, WA.

[1] H. V. Klapdor-Kleingrothaus, I. V. Krivosheina, A. Dietz, and O. Chkvorets, Phys. Lett. B **586**, 198 (2004).

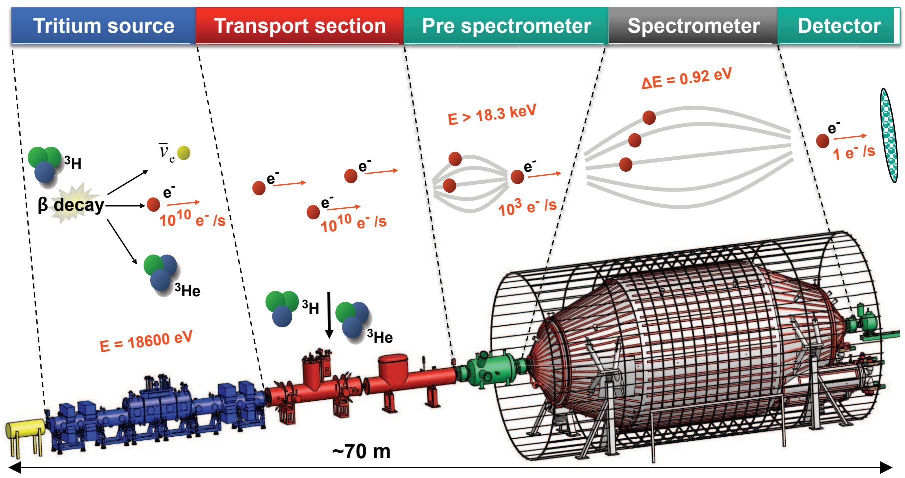

Figure 1.2-1. Layout of the KATRIN experiment showing the principal components. Also shown is the electron flux for each stage of the apparatus

KATRIN employs two spectrometers of the adiabatic retarding potential type which make use of a precise electrostatic potential to energy-select electrons for passage through the spectrometer. The purpose of the first spectrometer, the pre-spectrometer, is to reject all but the interesting highest energy electrons, within approximately 300 eV of the tritium endpoint. This reduces the flux of electrons from 10^{10} e^-/sec to 10^3 e^-/sec. The electrons then enter the main spectrometer. In order to reduce electron scattering, the pressure inside the spectrometer is maintained at 10^{-11} mbar. Both spectrometers have wire-planes that conform to the inner shell of the spectrometer vessel, both shaping the electric field potential and reducing sources of background electrons. By precisely controlling the retarding potential on these wire planes, an energy resolution of 0.93 eV is achieved. A monitoring spectrometer, observing a line from a Kr source and supplied with the same retarding potential as the main spectrometer, is used to record the stability of the retarding potential in the main spectrometer. Only those electrons with sufficient energy to overcome the variable retarding potential pass through the main spectrometer to the electron detector. Thus the spectrometer makes an integral measurement of the electron flux. The rate of tritium beta decay electrons exiting the main spectrometer and seen by the detector is approximately 1 Hz. In principle it is only necessary for the electron detector to count electrons. In practice, energy, spatial, and temporal information is very important in both understanding the operation of the apparatus and sources of systematic background. The detector, shown in Fig. 1.2-2, is a monolithic PIN diode array consisting of 148 pixels arranged in a "dart board" pattern which provides the spatial information.

Typical energy resolutions of individual pixels are 1.4 keV (FWHM). Signal to background rates directly effect the run time to reach maximum sensitivity. To suppress intrinsic backgrounds the detector is surrounded by lead and copper shielding. Backgrounds associated with cosmic rays are tagged using a cylindrical plastic scintillator veto surrounding the detector. Signals from the PIN diode array and the veto are read out using custom designed

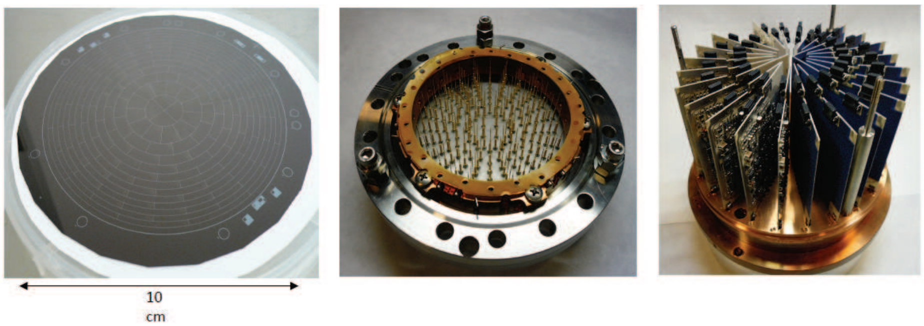

Figure 1.2-2. The KATRIN detector assembly. Left: the detector wafer showing "dart-board" layout of the pixels. Center: the detector mounting flange showing the pogo pin contacts to the pixels. Right: the preamplifier carousel mounted immediately behind the detector and connected by the pogo pins.

analog and digital electronics provided by KIT while data acquisition is controlled by software provided by the US collaborators. KIT is an ideal location for the KATRIN experiment since it has the necessary license and expertise to handle the large quantities of tritium required for a bright source. Currently the experiment is in an intense construction phase. The buildings housing the apparatus are complete. All three spectrometers are installed. The pre-spectrometer has been extensively used to understand sources of background such as Penning traps and to use this understanding to refine the design of the wire-planes of the main spectrometer. Installation of the wire-planes and other hardware associated with the main spectrometer is expected to be finished in August 2011 after which the US supplied detector system will be used in commissioning the main spectrometer. The detector system is described in detail below and is expected to meet the schedule and performance requirements of the main spectrometer commissioning. The differential pumping system was delivered to KIT in June 2010 and has successfully passed its acceptance test and is now undergoing tests to demonstrate that it can satisfy the physics criteria. The cryogenic pumping system is on track to be delivered to KIT in September 2011. The gaseous source is a technical challenge and therefore has been divided into two components. The "demonstrator" consists of the inner chamber of the source along with the cooling system used to maintain the temperature of the source to ± 30 mK. The demonstrator was delivered to KIT in October 2010 and has passed all its acceptance tests and is being shipped back to the manufacturer to be mated to the magnet system. The magnet system now sets the critical path for the project. The system consists of five, 3-T superconducting solenoids along the bore of the source and two pairs of magnet dipoles at each end that are used to steer a diagnostic electron beam down the source.

1.2.1 Status of the U. S. contribution to the KATRIN experiment

P. J. Doe

The University of Washington was among the founding institutes that submitted a Letter of Intent in September 2001 with the goal of reaching a sensitivity of 350 meV. The response to the LoI was to request an improvement in sensitivity. In February 2005 this request resulted in a design report with an improved sensitivity of 200 meV. At this time the Massachusetts Institute of Technology joined the US effort. In June 2007 funds were awarded by the DOE Office of Nuclear Physics to support construction of the KATRIN detector system and development of the data acquisition system. Additional US institutes involved in KATRIN include University of North Carolina, Chapel Hill (2008), the University of California Santa Barbara (2009) and the Lawrence Berkeley National Laboratory (2009). In addition to the detector task (led by UW) and the DAQ task (led by UNC), the US is also involved in the simulations task (led by MIT), the design of the rear calibration system (UCSB participation) and the US analysis program (led by LBNL). Only the status of the detector task is covered here.

In August 2007 a formal design review of the detector system determined that the design was compatible with the KATRIN system and would satisfy the physics goals, allowing the acquisition of long lead items to begin. The principal components of the design are shown in Fig. 1.2.1-1

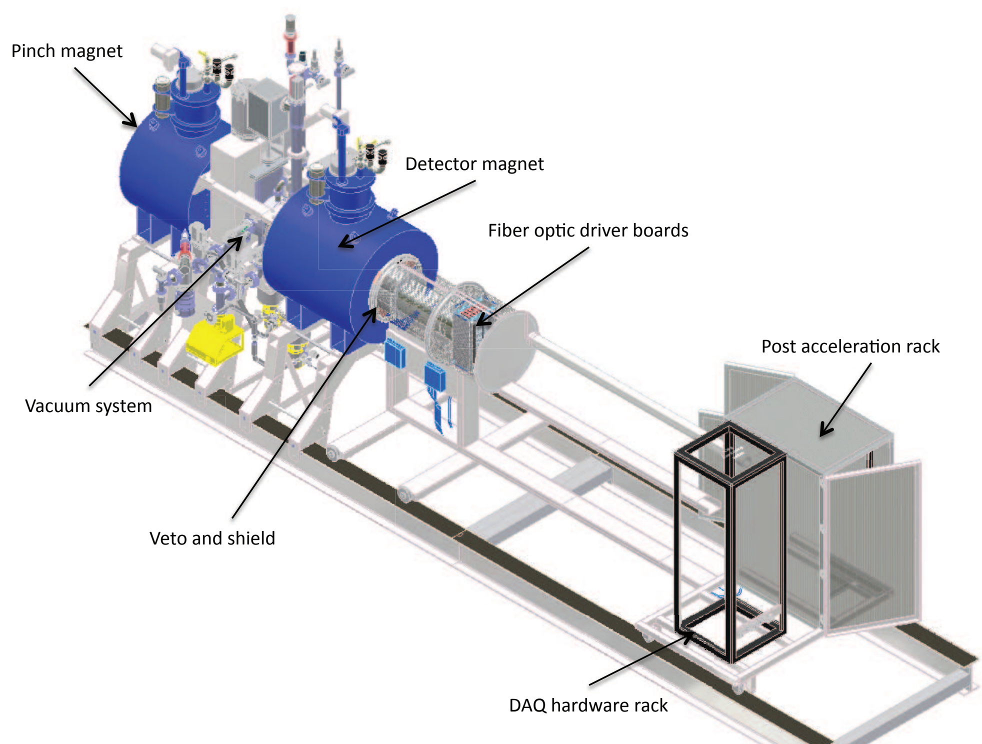

Figure 1.2.1-1. A schematic view of the KATRIN detector system showing the principal components.

The detector system contains two warm-bore solenoid magnets. The pinch magnet defines the highest magnetic field in the whole magnet train. Nominal fields of the pinch and detector magnets are 6 T and 3.4 T respectively. The magnets are operated in the persistent mode and are cooled using helium reliquefiers. The 10-cm diameter detector wafer is located on-axis at the center of the detector magnet bore. To be compatible with the extreme vacuum of the main spectrometer, a vacuum of better than 10^{-9} mbar is required in the detector chamber. To optimize performance while not degrading the vacuum, the preamplifiers are located in a separate vacuum chamber immediately behind the detector wafer operated at a pressure of better than 10^{-6} mbar. All vacua are maintained by vibration isolated cryopumps. To reduce thermal noise the detector and preamplifiers are cooled using a pulse tube cooler. Given the low end-point energy of the beta decay, intrinsic backgrounds are a concern. To reduce detector backgrounds, all materials in close proximity to the detector are chosen for low radioactivity, including the use of ceramic circuit boards for the preamplifiers. In addition the detector vacuum chamber is surrounded by 3 cm of lead, 1 cm of copper and a plastic scintillator veto. Furthermore, up to 30 kV post acceleration can be applied to the decay electrons to further raise the signal above the low energy backgrounds. Since the outputs of the preamplifiers may float at up to 30 kV, fiber optic drivers/receivers are used to pipe the signal to the data acquisition hardware which also receives signals from the veto system. The front-end electronics and DAQ hardware is supplied and maintained by KIT. The DAQ hardware is derived from the system developed for the Auger cosmic ray experiment and is under control of the ORCA software derived from the SNO experiment and maintained by UNC. All vital signs, temperatures, pressures, voltages, etc. are recorded by a slow controls system provided and maintained by KIT. A figure of merit has been defined based on fundamental detector performance parameters such as energy resolution and backgrounds that will be used to determine if the detector system is capable of meeting its physics goals. Table 1.2.1-1 shows minimum required values for the principal parameters along with the engineering design goals for that parameter. In the following section progress to meeting those goals during detector commissioning is described.

Parameter	**Minimum**	**Eng. Design**	**Units**
F	1.2	1.1	-
s	-	1	kev (σ)
b_d	-	0.4	mHz/keV
Area	63	80	cm^2
Spatial res.	20	20	pixels/detector dia.
Time res.	212	45	ns (σ)
Muon eff.	-	95	%
Post acc.	1	30	kV

Table 1.2.1-1. The minimum and engineering design performance specifications. The figure of merit, F, is an overall measure of the detector performance, s the detector resolution and b_d is the detector background.

1.2.2 Commissioning the KATRIN detector

P. J. Doe

The KATRIN detector system is currently in the commissioning phase during which the detector subsystems are exercised to determine whether they satisfy the performance criteria given in the detector design report and the minimum performance required to ensure that the physics goals can be achieved. The status of commissioning these subsystems is given below.

1.2.2.1 Commissioning the detector and electronics

B. L. Wall

Commissioning of the focal plane detector (FPD) and electronics is currently underway. The front-end electronics chain has been installed into the detector section vacuum system and connected to the DAQ via the fiber optic chain. The FPD and electronics have been operated at high voltage in conjunction with the post-acceleration electrode (PAE). The basic detector system characteristics, including the timing resolution, γ and electron energy response, and an initial estimate of the background have been determined.

The testing of the detector electronics at high voltage was carried out in two phases. In the initial phase the number of front-end electronics channels was reduced to 12. During this phase, the system was elevated to 20 kV. High voltage discharges in this phase damaged most of the preamplifiers in the vacuum. Transient suppression was added to the front-end electronics and other peripheral hardware to protect against discharges. The electronics have been operated at 10 kV for 24 hours without damage due to high voltage discharge.

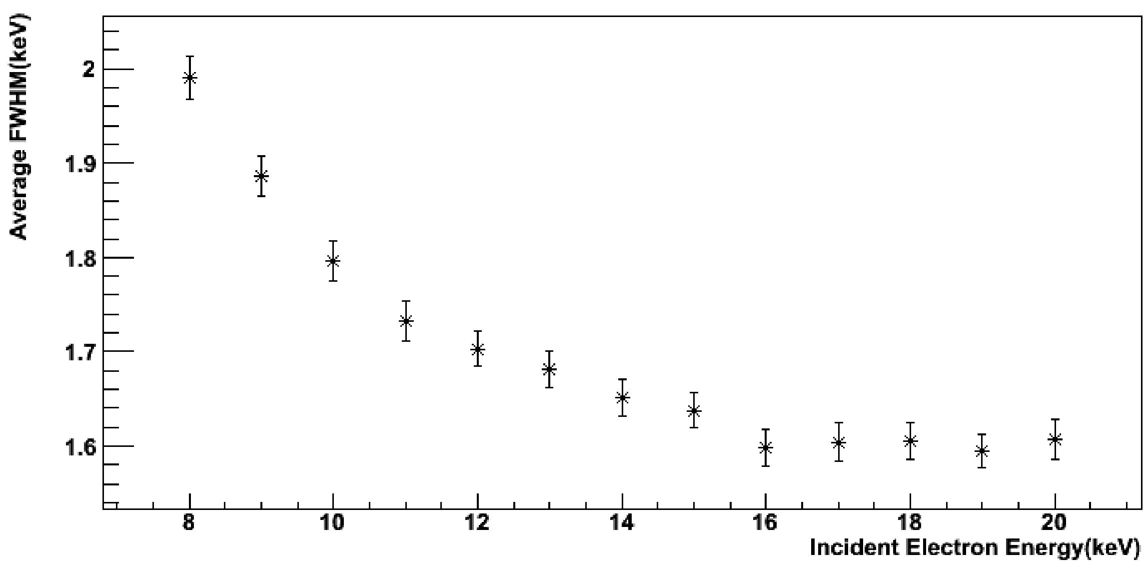

Figure 1.2.2.1-1. The focal plane detector energy response to electrons.

Initial tests of the FPD and electronics showed the γ resolution to be 1.67 ± 0.03 keV (FWHM). A major contributor to the resolution was microphonic impulse noise from the two vacuum cryopumps. Isolating the cryopumps with a set of bellows improved the γ resolution by 10% to 1.50 ± 0.03 keV. The FPD's electron energy response is shown in Fig. 1.2.2.1-1. The energy resolution for 18.6-keV electrons is 1.60 ± 0.02 keV.

A single pixel background rate of 17.1 ± 0.6 mHz was obtained for a region of interest of 16.6 to 20.6 keV. This is above the background goal of 1 mHz, but the data were taken with an incomplete shield and without the veto system. Many events were found to be correlated with high energy events from other channels. A timing cut on high energy events and the use of the veto system should significantly reduce the background rate.

The system timing resolution was determined to be less than 127 ns. It was measured by pulsing the photo-electron calibration source in sequence with an external sync pulse input to the data acquisition crate. Individual components of the system are capable of better performance and further tests are planned to look into contributions to the 127 ns. The current measured resolution, however, surpasses the detector specification of 212 ns.

1.2.2.2 Status of the magnets

L. I. Bodine

The superconducting magnets of the KATRIN detector section were commissioned at the University of Washington (UW) in February, 2010. They have been successfully ramped four times to the nominal field values of 3.6 T at the center of the detector magnet and 6 T at the center of the pinch magnet. They have also been ramped to lower field values for testing detector section components.

Slow controls monitoring of the magnets was modified to use the RS-232 protocol resulting in improved robustness of remote magnet monitoring. In addition, the helium recondenser system was upgraded to allow recording and remote monitoring of the pressure inside each cryostat.

In February, 2011, during a ramp of the magnet pair the pinch magnet quenched at 6 T. A vacuum leak into the cryostat has been identified as a possible cause. Cryomagnetics, Inc. will attempt to fix the leak in situ at the end of March, 2011. The detector magnet will remain at UW while the pinch magnet is repaired so that the complete magnet system can be tested in April, 2011.

1.2.2.3 Status of the vacuum system

J. F. Amsbaugh

The KATRIN focal plane detector (FPD) vacuum system is comprised of two systems; the extreme high vacuum (XHV) and the high vacuum (HVac). The XHV system supports the γ and electron calibration sources and the post acceleration electrode (PAE), on the end of which the FPD is mounted. The HVac system surrounds the PAE component of the XHV system where it extends into the magnet bore. The HVac provides thermal isolation. Cooling for the detector and electronics is provided by a pulse tube cooler. Both system vacua are maintained by cyropumps and are pumped down from atmospheric pressure with two turbo-molecular pump systems which can also provide bakeout pumping.

As reported before[1], the XHV system achieved 1.5×10^{-9} mbar with all components at room temperature and after a 120°C to 135°C bakeout. Testing the PAE assembly after vacuum brazing revealed that the PAE assembly had permanently deformed by about 1 cm. After several pump out and vent cycles the creep rate stabilized and we decided to continue our commissioning tests with this PAE. A redesigned version of the PAE is currently being manufactured. The measured displacement of the new PAE under vacuum loading is 0.011 ± 0.0005 inches, consistent with FEA estimates.

The vacuum systems have been vented, disassembled, reconfigured, and pumped out eight times in the last year as commissioning and testing have progressed. Typical XHV vacua prior to venting range from 2 to 3×10^{-9} mbar without the FPD assembly installed and 5×10^{-9} mbar with the FPD installed. All of these measurements had detector cooling present. The FPD cooling tests indicate that improvements in the cooling are needed. The current hard copper connection to the pulse tube cooler is being replaced with a higher efficiency thermo-siphon. The testing of the PAE voltage with a magnetic field present and a faraday cup in place of the FPD caused erosion and failure of the plated aluminum electrodes on the quartz tubes. These have been replaced by thin, stainless steel sheet and the electrical connection was improved. The as-delivered faulty vacuum gauge and controller have been repaired. Temporary bellows couplings were installed on both cryopumps and were found to be be very effective in reducing microphonics noise. Permanent edge welded bellows assemblies have been ordered that will not reduce the cryopump's effective pumping speed as much as the temporary ones.

1.2.2.4 Status of the calibration system

E. L. Martin

The electron source uses a titanium disc biased at high voltage and illuminated with a UV LED. The current from the electron source is measured by a precision current meter attached to the disc (PULCINELLA.) The γ source uses a radioactive isotope placed inside an aluminum tube. Both sources use pneumatic motor driven linear actuators to move the source in and out of the beam line. Both sources have been demonstrated suitable for detector calibration. Source movement as well as electron source voltage control have been successfully integrated with slow controls.

The γ source currently uses an Am-241 source. A Cd-109 source will also be used but has not yet been purchased due to the short life time. The γ source has been used to determine detector resolution by the width of the 56-keV Am-241 γ emission.

PULCINELLA has been installed in the detector and significant noise was discovered at high voltage due to mechanical vibration changing the capacitance of the electron source disc. Accuracy is expected to scale in proportion to electron source potential and be 1.7 pA/Hz at 18.6 kV, allowing absolute detection efficiency to be determined to 3% in one hour from

[1]CENPA Annual Report, University of Washington (2010) p. 5.

a detector rate of 10 MHz. The electron source has been used to determine detector timing resolution by pulsing the electron source.

A flood illumination device has been combined with the electron source illumination device for testing the linearity of the focal plane detector and electronics. Illumination is provided by a red LED stabilized by feedback from a pin-diode to produce light with intensity proportional to the input voltage. Testing is underway to determine if this will be sufficient.

1.2.2.5 Status of the veto

E. L. Martin

The veto uses six scintillator panels surrounding the lead and copper passive detector shield. Light from the scintillators are read out by wavelength shifting fibers and silicon photomultipliers (SiPMs.) The SiPM signals are read out by the detector DAQ system and coincidence between SiPM signals is used to detect the passing of a muon.

The SiPMs used for veto panel readout have been replaced with a different model allowing the readout fibers to be placed closer to the SiPM active surface. This resulted in improved detection efficiency due to less light loss. In addition a new trigger scheme requiring both a coincidence of individual readout fibers on a veto panel as well as a threshold on the sum of all fibers on the panel has been implemented to reduce noise. Combined with cooling the SiPMs using a Peltier cooling device to further reduce noise to allow lower thresholds without significant deadtime, the veto is expected to meet the design detection efficiency of 95%.

The passive shield and veto panels have been installed around the detector vacuum system. The veto signal summing boards and the new cooling box are still being constructed and tested. The veto DAQ firmware is still under development but the DAQ system can be operated using a focal plane detector readout mode to read out the veto signals. The system is expected to be installed in the detector and tested in February, 2011.

1.2.2.6 Status of the DAQ and slow controls

M. A. Howe*

The KATRIN version 4 first and second level trigger (FLT and SLT) electronics were built at Karlsruhe Institute of Technology (KIT) and delivered to the University of North Carolina (UNC) for testing. After ORCA support for the SLT and FLT cards was completed and verified, the electronics were shipped to UW to be used in the final commissioning of the KATRIN focal plane detector (FPD) and cosmic-ray veto system.

For the FPD, the KATRIN DAQ electronics uses a trapezoidal filter to detect and record energy information from the detector pixels. In order to verify the function of the FPGA

*University of North Carolina, Chapel Hill, NC.

coded filter, a software version of the filter was developed. The results of both filters were compared and it turned out that there was a malfunction of the FPGA filter, which created a random shift of the calculated energy values at each run start. After a revision of the FPGA code at KIT, a comparison with the software filter showed that the FPGA filter is now working correctly. The DAQ system has been collecting commissioning data and assisting in commissioning the FPD detector and electronics.

A new version of the FLT FPGA firmware was developed at KIT to support the KATRIN veto system as a run-time option. This allows one IPE crate to support both veto and the FPGA readout modes simultaneously. The ORCA FLT support software was expanded to support the new veto parameters. The veto configuration of the FPGA firmware has undergone verification at the University of Washington (UW), UNC and KIT. The task of verification included the analysis of output from pulser, scintillator and silicon photomultiplier (SiPM) electronics analogous to the configuration intended for use in the KATRIN experiment. During this testing, synchronization issues within the system's readout and problems with dropped events were observed. These problems require a subsequent redesign of the FPGA code at KIT, which is currently underway.

The ZEUS slow control system was installed at UW to monitor the KATRIN magnet temperatures, power supplies, cryogen levels, and other parameters. All of the slow control parameters are inserted into an ADEI database (also running at UW). ORCA can link to the ADEI database and use selected parameters in its slow control subsystem where users can set up custom monitoring and alarms. A number of new features were added to the ORCA slow control subsystem. It now auto-starts with ORCA, email reports can be sent upon process start and stop, heartbeat emails can be sent, and a confirmation alert is posted if a user tries to stop ORCA while a slow control process is running. In addition, a high-level display was added to optionally hide the complex low-level slow control set up display. Several ORCA systems are being used in production running to monitor the conditions during the commissioning.

A major upgrade of the slow control for the KATRIN Detector system has been carried out. The field point program has been migrated and adapted to a new, more powerful, field point controller, the National Instruments cFP-2220. An additional digital input module has been added to the slow control system hardware to monitor the vacuum valve outputs. This allows monitoring the interlock and/or fuse status of the vacuum system valves. A new GUI slow control interface program has been developed and installed on the new ZEUS PC. It is a web-based application that can be remotely interfaced from a web browser providing full control and monitoring of the detector slow control systems.

1.2.2.7 Near-time analysis tools

S. Enomoto

A set of software tools has been developed for the on-going KATRIN detector commissioning at the University of Washington (UW) and forthcoming detector and main spectrometer commissioning at Karlsruhe Institute of Technology (KIT). The tools were designed for the rapidly progressing commissioning phase, where quick analysis investigations by on-site people are crucial for timely trouble shooting and performance evaluation, while predictions of what will be necessary are generally difficult. Due to the heuristic nature of commissioning activities, it is quite common that people are inclined to write application-specific one-time-use quick-and-dirty programs. Although such programs are intended for single use, they are a logical record of the investigation activities and experiences, and if accumulated properly, they will be a valuable knowledge base at later stages.

The KATRIN near-time analysis tools were designed with these things in mind: they are designed to be adaptive to unexpected applications, to be quickly applicable to specific purposes by end-users, and to make all investigation outcomes reusable and traceable. Two different types of tools are provided: interactive and batch-oriented (Fig. 1.2.2.7-1).

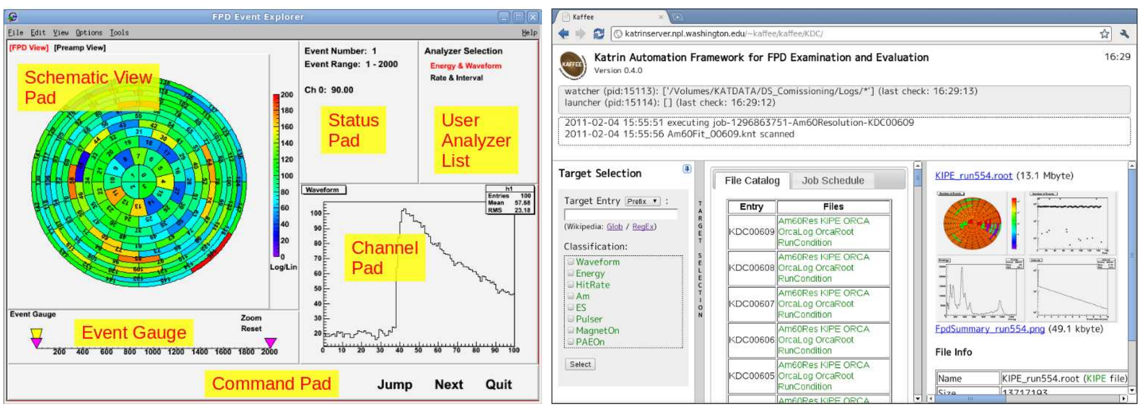

Figure 1.2.2.7-1. Left: Interactive tool, with user FPD pixel view plugin and user waveform plugin. Right: Automation tool, used for detector commissioning processing and analysis.

The interactive tool serves to co-ordinate analysis logic, data, and human operation. Analysis logic is implemented by runtime user plug ins. The tool is solely written with ROOT without any external libraries, thus a user ROOT program can be directly used as an analysis plug in. One typical application of the tool is as an event browser with runtime choice of user analyzers. There are also plans to use it for the main spectrometer and detector system.

The batch-oriented tool automates any type of routine processing and summarizes the processing status and results. It automatically solves dependencies for chained processing. It automatically recognizes data content, classifies the data, and then determines which processor to execute. It can run any user executable according to a user configuration written in XML and the output from the user executable is traced by the tool. The status and results can be accessed with RESTful Web APIs, interfacing web browsers, and user programs. For the on-going detector commissioning at UW, several data analyzers are setup for automatic execution among other automated processing such as format conversion (from ORCA files to ROOT objects) and slow-control data extraction (ADEI interface).

Majorana

1.3 Majorana Demonstrator Activities

J. F. Amsbaugh, T. H. Burritt, J. Diaz Leon, P. J. Doe, G. C. Harper, M. A. Howe*, R. A. Johnson†, M. G. Marino‡, M. L. Miller, D. A. Peterson, R. G. H. Robertson, A. G. Schubert, T. D. Van Wechel, J. F. Wilkerson*, D. I. Will, and B. A. Wolfe

The Majorana Collaboration is performing R&D to demonstrate the feasibility of building a 1-tonne modular array of 86% enriched ^{76}Ge capable of searching for neutrinoless double-beta ($0\nu\beta\beta$) decay in the inverted mass hierarchy region ($\sim$30 meV). A cornerstone of the plan is the development and construction of the Majorana Demonstrator, a R&D module comprised of 30 kg of 86% enriched ^{76}Ge and 30 kg of non-enriched Ge detectors. The use of a mixture of both enriched and natural or depleted Ge, has the advantages of lowering the costs in the R&D phase, accelerating the deployment schedule, and also giving the Majorana Demonstrator an opportunity to verify that any observed peak in the $0\nu\beta\beta$ region of interest is directly associated with the presence of ^{76}Ge. The broad goals for the Demonstrator are:

- Show that backgrounds, at or below 1 count/ton/year in the $0\nu\beta\beta$ - decay peak 4-keV region of interest, can be achieved, a necessary condition for scaling to a 1-tonne or larger mass detector.
- Demonstrate sensitivity by testing the validity of the Klapdor-Kleingrothaus reported ^{76}Ge $0\nu\beta\beta$ observation[1].
- Show successful long-term operation of crystals in their respective environments.
- Demonstrate a cost-effective and scalable approach.

The proposed method uses the well-established technique of searching for $0\nu\beta\beta$ in high-purity Ge (HPGe) diode radiation detectors that play both roles of source and detector. These detectors will be located in specially fabricated ultra low-background, electroformed Cu cryostats. The technique is augmented with recent improvements in signal processing, detector design, and advances in controlling intrinsic and external backgrounds. Major advances in detector R&D (both laboratory and industrial) have lead to the choice of p-type point-contact (PPC) detectors for the demonstrator module. These detectors offer low capacitance and excellent resolution, providing the ability to (1) tag and veto two-site background interactions via pulse shape analysis and (2) probe ultra low-energy events (E>$\sim$300 eV) to competitively search for dark matter candidates (WIMPs, axions, etc)[2].

Project execution of the Majorana Demonstrator is currently underway at full steam. Items on the overall project critical path are addressed below:

*University of North Carolina, Chapel Hill, NC.
†University of Colorado, Boulder, CO.
‡Excellence Cluster Universe, Munich, Germany.

[1] H. V. Klapdor-Kleingrothaus, I. V. Krivosheina, A. Dietz, and O. Chkvorets, Phys. Lett. B **586**, 198 (2004).
[2] C.E. Alseth *et al.*, http://arxiv.org/abs/1002.4703.

- Funding. The Majorana Demonstrator project passed the major DOE CD1 review in 2010 and is preparing for CD2 review in 2011.
- Host Lab. The 4850 ft laboratory at Sanford Underground Laboratory (SUL) is nearly ready for beneficial occupancy.
- Electroforming. Copper growth has begun in earnest at a temporary underground cleanroom at SUL as well as PNNL.
- Detector Procurement. The natural germanium detectors have been purchased and are stored underground at SUL, and we are preparing to procure enriched germanium in 2011.

The Majorana group at the University of Washington is playing a leading role on many levels including project management, software and computing, technical R&D, engineering, and fabrication:

- Project Management. Robertson continues to serve as a member of the Majorana governing board (SAC) and Miller is deputy task leader for the module task
- Software and computing. Holman maintains the core collaborative tools (wiki, calendar and wiki) on virtualized UW servers as well as exposing the Athena computing cluster for general Majorana simulations and data analysis. Miller is designing and implementing the data management and workflow management tools for the collaboration.
- Simulation and analysis. Schubert continues to develop tools to describe, simulate and validate our understanding of radioactive backgrounds in both the Majorana Demonstrator as well as prototype detectors (e.g. MALBEK)
- Host lab infrastructure. Diaz and Will have nearly completed major effort to extract, package and ship 40 tons of old lead that was previously used in an early radio carbon dating experiment at UW. This lead is highly valuable due to its low radioactivity and will form the inner shield of the Majorana Demonstrator.
- Detector R&D. We are involved on many fronts. Knecht and Miller are leading the design, fabrication and testing of ultra low-background parylene cables and connectors for both the detector signals and high voltage. Leon is performing additional characterization of PPC detectors as well as testing, evaluation and commissioning of digitizers. Robertson is leading design, fabrication and testing of a highly innovative preamplifier design for ultra-low noise. Miller is leading the effort to validate long-term operation and stability of a PPC detector (CoGeNT) with an emphasis on the low-energy spectrum for cosmogenic background identification and suppression as well as opportunistic Dark Matter searches.
- Engineering. Burritt remains an invaluable resource for design and fabrication of innumerable key components, including the tooling for parylene fabrication, detector mounts into strings, the thermosyphon and cryostat. Harper has led the design and fabrication of multiple cryostats for string testing and storage underground.

In the following articles we briefly highlight selected accomplishments in the past year.

1.3.1 A Monte-Carlo model of the background energy spectrum of the MALBEK detector

J. I. Collar*, P. S. Finnerty†, G. K. Giovanetti†, R. Henning†, M L. Miller,
A. G. Schubert, and J. F. Wilkerson†

A good understanding of the MAJORANA DEMONSTRATOR background energy spectrum will be required to project background rates for a tonne-scale germanium experiment and to interpret results of a neutrinoless double-beta decay search. A modified CANBERRA Broad-Energy germanium (BEGe) detector has been deployed in a low-background shielded environment at the Kimballton Underground Research Facility (KURF), in Ripplemead, VA. This detector, the MAJORANA Low-background BEGe at KURF (MALBEK), provides an opportunity to study the background energy spectrum of a well-understood low-background germanium detector. Studies of the MALBEK detector and simulations of detector response to background radiation can be used to inform a background energy spectrum model for the MAJORANA DEMONSTRATOR.

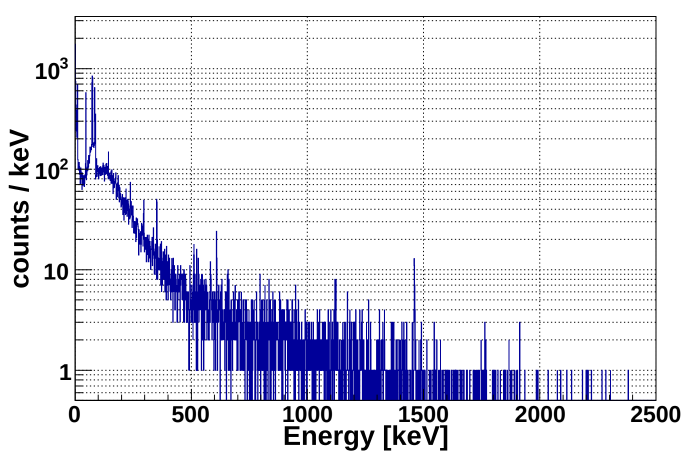

Figure 1.3.1-1. A background energy spectrum collected from the MALBEK detector in September through November of 2010; 56 days of live time.

A model of the MALBEK detector has been created in MaGe, a physics simulation software package jointly developed by the MAJORANA and Gerda collaborations. MaGe was used to simulate the response of the MALBEK detector to decays of naturally-occurring radioactive contaminants in the MALBEK cryostat and shield. Results of these simulations are combined with information on material radiopurity to create a model of the MALBEK background energy spectrum. This model can be compared to the spectrum collected at KURF

*Kavli Institute for Cosmological Physics and Enrico Fermi Institute, University of Chicago, Chicago, IL.
†University of North Carolina, Chapel Hill, NC, USA and Triangle Universities Nuclear Laboratory, Durham, NC.

to verify understanding of backgrounds and the performance of the simulation software. A background energy spectrum collected from KURF appears in Fig. 1.3.1-1.

1.3.2 Pre-amplifier with forward biased reset for Majorana

D. A. Peterson, R. G. H. Robertson, and T. D. Van Wechel

Development continues on a charge sensitive pre-amplifier which is continuously reset by the forward biased gate to source junction of the input JFET. The DC stabilization of a conventional charge sensitive amplifier is provided by a high-value feedback resistor in parallel with the feedback capacitor. This resistor provides a DC path for the net input bias and detector currents at the amplifier input, so that the feedback capacitor does not eventually charge to the output saturation voltage. It would be advantageous to eliminate the feedback resistor as it is a major noise source.

It is possible to operate a JFET with zero volts on the gate, or even a small forward bias. A JFET has an operating point where the current of the forward biased gate cancels the reverse leakage current. The detector leakage of a positive biased detector can also be cancelled. A feedback resistor is not required when the JFET operates with the gate open eliminating its noise contribution. Charge feedback can still be applied to the gate through a feedback capacitor. Some other means is needed to stabilize the DC operating point.

We are using a tetrode JFET that has superior noise performance and provides a means of DC stabilization without a DC connection to the gate. A tetrode JFET has two gates: – the control gate has small capacitance for improved performance, while the substrate gate can be used to set the drain-source current I_{DS}. There are two feedback loops, one operating at high frequencies, which provides charge feedback to the control gate. The other, low-pass, loop is connected to the substrate gate, stabilizing the DC operating point so that the average net charge at the input is zero.

The pre-amplifier transfer function is affected by the two low-frequency corners in the feedback paths. One is that of the low pass loop for the stabilization of the DC operating point. The other low frequency corner is that of the high-pass charge loop, which depends on the dynamic resistance at the JFET control gate and the input capacitance (detector, gate and feedback). The dynamic input resistance seen at the gate is inversely proportional to the gate current and is on the order of 25 GΩ at a gate current of 1 pA at room temperature. As a result, the low-frequency corner of the charge loop is proportional to detector leakage current. Above the corner of the low-pass loop the feedback phase lags by 90° and below the corner of the high-pass loop it leads by 90°. If the corner frequency of the low-pass loop is lower than that of the high pass loop, the total feedback at the intersection vanishes because of their relative phases. The amplifier output will be large and noisy near that frequency, as we found experimentally with the prototype pre-amplifier, which had excessive low frequency noise. We learned that the low frequency corner of the low pass loop needs to be set above that of the low frequency corner determined by the highest operational detector current.

The output noise level of our prototypes has been higher than predicted by circuit simulation. It is now believed that the bipolar transistors on the HFA3096 transistor array that we are using, have excessive noise at low frequencies. Recent measurements show that when a diode connected transistor that biases the base of the cascode transistor was replaced with a conventional diode, that the series noise voltage decreased by more than 20%. We are now constructing a new prototype with discrete transistors to see if there is an improvement in the output noise.

The cascode amplifier stage was also improved. Circuit simulation showed that the impedance looking into the emitter of the cascode transistor was much higher than it should be. The output of the cascode drives a bootstrapped voltage follower stage with a very high effective input impedance which is partially reflected back to the cascode input. This was solved by stacking two cascode transistors in series. Originally less than half the JFET ac drain current was coupled into the emitter of the cascode transistor. Now more than 95% of the ac drain signal is coupled into the cascode.

1.3.3 Digitizer evaluation with PPCII

J. Diaz Leon, A. Knecht, and M. L. Miller

A critical element of the MAJORANA data acquisition system is the analog-to-digital converter, which allows for the fast triggering and digitization of pulses from germanium detectors. Several digitizer cards have been tested for compatibility with the needs of the MAJORANA collaboration[1], and currently the Struck SIS3302[2] digitizer is being evaluated. Signals from PPCII[3], a P-type point-contact germanium detector, have been used for this purpose and this setup has also proven to be invaluable for testing analysis software.

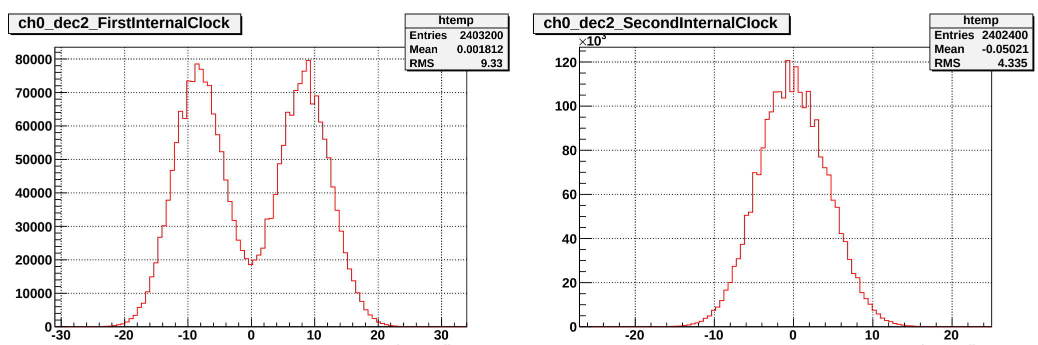

Figure 1.3.3-1. Distribution of ADC value about the waveform baseline using the first internal clock (left) and the second internal clock (right). A wider distribution corresponds to a noisier waveform.

Each digitized waveform of the PPCII preamp consists of up to 65536 (16-bit width) samples at 100 MS/s. The energy and timing parameters obtained from these waveforms

[1]CENPA Annual Report, University of Washington (2010) p. 18.
[2]Struck Innovative Systeme, www.struck.de.
[3]On loan from John Orrell, Pacific Northwest National Laboratory, Richland, WA.

can be used to determine the location and nature of the interaction which caused them. Furthermore, analysis of the digitized waveform's shape is used to distinguish multi-site vs. single-site interactions, which is relevant for suppression of backgrounds (e.g. γs from thorium series). Efforts were made to characterize the electronic noise of the system which revealed some undesirable behavior from one of the digitizer card's internal clocks. Jitter generated by the DLL/PLL of the card's FPGAs every other clock edge manifests itself as extra noise in the waveforms. Use of the other internal clock in the card corrects this (see Fig. 1.3.3-1), an example of valuable progress made with this system.

A recent firmware upgrade of the SIS3302 aimed at extending the card's ability to collect longer pre-trigger data, which would improve triggering at low amplitudes, will be tested at CENPA with this setup. This entails measurements of the digitizer dead-time, low energy threshold and triggering efficiency, and optimization of online triggering parameters. In addition, by scanning a source along the detector it is possible to measure its response to position dependent interactions, i.e. how waveform rise-time distribution depends on the location of the interaction.

1.3.4 Design, fabrication and testing of HV and signal cables and connectors for the MAJORANA experiment

N. M. Boyd, T. H. Burritt, A. Knecht, M. L. Miller, D. A. Peterson, R. G. H. Robertson, and B. A. Wolfe

We have produced several prototype parylene cables using the apparatus and methods described in last year's report[1]. For the first time, we produced a full cable in our class-1000 clean room (see Fig. 1.3.4-1) in order to meet the low radioactivity requirements. Initial results were ~ 3 times higher than expected. We are currently investigating the source of a possible contamination and refining our vacuum system.

In addition to the signal parylene cables we started to produce a high voltage compatible cable. We chose a 25-mil copper wire with 3 mils of parylene coating in order to withstand nearly 10 kV without breakdown. Due to its larger diameter we were able to hang the cable directly into the coating machine instead of working with a mandrel and thus were able to apply the 3 mil parylene coating in one pass. After the parylene coating we used our sputter source to deposit 100 nm of copper onto the outside of the parylene thereby producing a shielded coaxial cable. As the cable withstands the required voltage without breakdown, we are currently investigating its microdischarging properties.

In addition to the actual cables we started designing connectors which will be mounted onto the cold plate directly above the germanium detectors. These will allow for easier installation of the detectors without having to route the appropriate cables all the way out of the shielding to the electronics. However, this means that we need to meet stringent background requirements which severely constrain the choice of materials thus excluding any commercial solutions.

[1] CENPA Annual Report, University of Washington (2010) p. 24.

For the signal cable, we chose boards made of fused silica which are coated with gold traces. The copper wires of the signal cable are wedge bonded onto those gold traces and the two boards are pressed together such that the gold traces make contact. We then assemble the boards for a total of 5 cable connections in a copper garage (see Fig. 1.3.4-1) for testing.

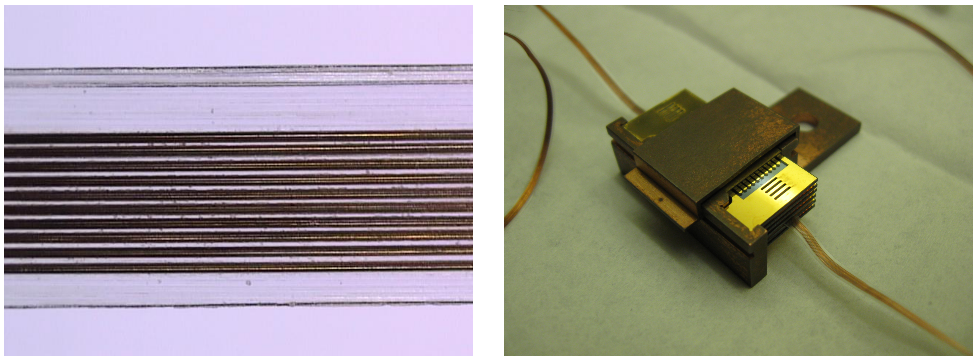

Figure 1.3.4-1. Left: Microscopic picture of our produced 10-wire parylene cable. The wires have a diameter of 3 mils and are separated by 6 mils. Right: Connector "garage" to connect five signal cables. The size of the garage is approximately $30 \times 20 \times 10$ mm^3.

The high voltage cable connector is based on a PTFE block into which the cables are inserted. For the actual connection of the two bare high voltage leads we are currently finalizing two designs based on either clamping or crimping scenarios.

1.3.5 Searches for dark matter with a Majorana prototype

J. I. Collar*, A. Knecht, M. G. Marino†, M. L. Miller, J. L. Orrell‡, and J. F. Wilkerson§

Since the end of 2009 we have been operating a low background P-type point contact (PPC) germanium detector at the Soudan Underground Laboratory in Soudan, MN. This detector exhibits low noise allowing for a very low threshold (below 0.5 keV). Due to this low threshold, the detector is very sensitive to low-mass WIMPs despite its small mass (0.5 kg) and is sensitive to a new region of parameter space. The setup at Soudan has been described in last year's report[1]. The data from the first 50 days have been published[2] while the data from the first 150 days served as the basis of M. Marino's thesis[3].

Over the course of the last year the detector was continuously running underground without any modification. That amount of data will allow us to search for an annually modulated dark matter signal, a sensitive test of the WIMP hypothesis. In order not to bias

*University of Chicago, Chicago, IL.
†Excellence Cluster Universe, Munich, Germany.
‡Pacific Northwest National Laboratory, Richland, WA.
§University of North Carolina, Chapel Hill, NC.

[1] CENPA Annual Report, University of Washington (2010) p. 19.
[2] Aalseth *et al.*, arXiv:1002.4703v2.
[3] M. G. Marino, Ph. D. thesis University of Washington (2010).

our data quality cuts and selections towards an annual modulation, we devised a doubly-blind method by randomly redistributing the day of the event and suppressing the actual time of exposure.

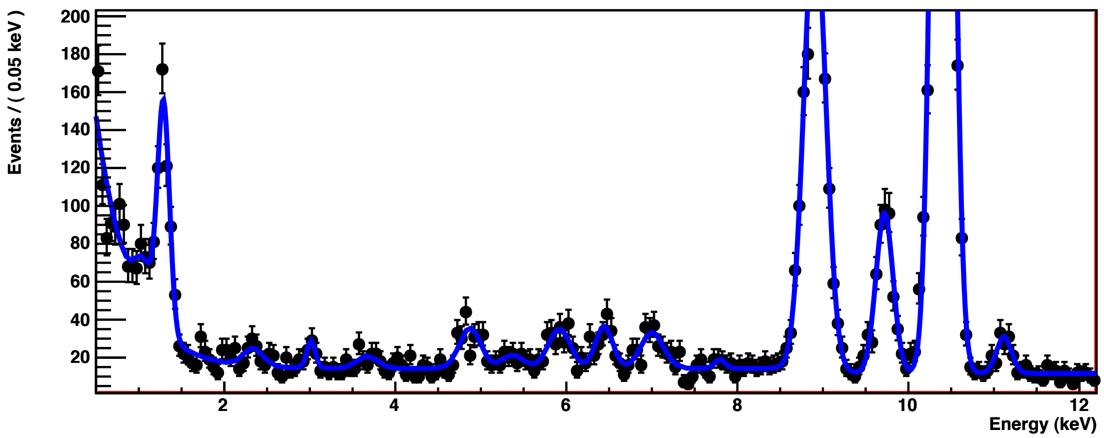

Figure 1.3.5-1. "High energy" spectrum for the first full year of data collection.

The goal for the analysis is to finalize the cuts and selection criteria on the blinded data before moving on to the actual modulation analysis and hypothesis testing. The biggest challenge of the analysis will be to correctly take into account the several background peaks present in the spectrum (see Fig. 1.3.5-1), their decaying amplitudes, and their contributions to the flat background.

1.3.6 Data management and workflow management for the MAJORANA DEMONSTRATOR

B. A. Wolfe, M. G. Marino*, M. L. Miller

The MAJORANA DEMONSTRATOR experiment is targeted squarely at scaling the deployment of enriched ^{76}Ge detectors from the well established scale of 1-10 kg to 100 kg and, ultimately, up to 1 tonne. A major challenge in this enterprise is the automation of the data management and processing workflow management (DMWM). In the following we briefly highlight the design of a prototype DMWM system for the MAJORANA DEMONSTRATOR, lessons learned from continued operation with the prototype detector systems at Soudan, and the anticipated design for a system that scales to support 1 tonne of detectors.

The MAJORANA DEMONSTRATOR will consist of 105 BEGe detectors, each having a low- and high-energy channel to span the energy range from ~300 eV to 10 MeV. A parallel DAQ system powered by ORCA has been field tested at Soudan. The DAQ system generates data files in the ORCA binary format. These ("Tier-1") files are buffered underground, transferred via the WAN to CENPA for archival on durable storage, and converted to ROOT format ("Tier-2") for further processing. The ROOT files are next passed through iterative series of

*Excellence Cluster Universe, Munich, Germany.

processing applications to create the MGDO encapsulation ("Tier-3") of event information (energy, timing, wave form data, etc). Finally, a series of flyweight analysis trees ("Tier-4") suitable for final analysis and publication are skimmed from the MGDO objects and published to a common cloud repository (Dropbox) for consumption by the entire collaboration. Every step in this process, including automated handling of calibration, run selection, etc., is fully automated and provenance tracked in the CouchDB database system that drives a custom python based workflow management package. A prototype system was developed in Spring 2009 and deployed in Summer 2009 for DMWM of the Soudan prototype. It has been running reliably and efficiently for nearly a year and has managed data from three separate detectors installed at various times in Soudan.

Additionally, we have developed tools for managing simulation workflow and cataloging and indexing all forms of simulation output at the PDSF computing facility. This system has been tested extensively for intermediate simulation studies and will be used for the upcoming Majorana Demonstrator simulation campaign in preparation for DOE CD2 consideration. Finally, we have also developed software and tools to make the Majorana Demonstrator software environment and data files secure and available for authenticated collaborators on the Amazon Web Services cloud. This has proven invaluable for overflow computing during the past year's research and development phase.

SNO+

1.4 Overview of the SNO+ experiment and CENPA's contribution

S. Enomoto, J. Kaspar, J. N. Kofron, D. J. Scislowski, N. R. Tolich, and
H. S. Wan Chan Tseung

SNO+ is a large-volume underground liquid scintillator neutrino experiment presently under development at the SNOLAB facility, in Sudbury, Ontario, Canada. It is a multi-purpose detector whose reach extends to the following areas of neutrino physics: neutrinoless double beta decay (with Nd-loaded scintillator), geo-neutrinos, reactor and low-energy solar neutrinos. In addition, a large liquid scintillator detector serves as an excellent supernova neutrino monitor.

SNO+ will use a lot of the infrastructure left behind by the completed Sudbury Neutrino Observatory (SNO) experiment, including the acrylic vessel (AV), photomultiplier tubes and most of the electronics. The main engineering work concerns the AV, which will have to be anchored to the floor after scintillator filling. A hold-down system has been designed, and the ropes are now being manufactured. Data-taking is scheduled to start in late 2012.

In SNO+ the data rate is expected to be two orders of magnitude higher than in SNO, and therefore updates to the SNO electronics and data acquisition (DAQ) system are needed. CENPA is responsible for updating the DAQ into a faster, ORCA-based system compatible with the electronics upgrades that are being planned by the University of Pennsylvania. These include new XL3 cards for controlling the 19 data crates. Software for operating the

XL3's through ORCA has been written and tested at the typical rates expected from SNO+. The full DAQ system will be available for commissioning this year. The status of the DAQ work is described in more detail (see Sec. 1.4.1).

CENPA is also responsible for the SNO+ slow control system, which records and monitors a large number of detector-related variables at a rate of ∼1 Hz. Good progress has been made during the past year towards testing and interfacing with the I/O servers that will be used in the slow control system. Data readout and monitoring at the expected rate have been tested for a single I/O server. Work done on the slow control hardware (see Sec. 1.4.2) and software (see Sec. 1.4.3) are described in more detail.

The proposed scintillator is linear alkylbenzene (LAB) with ∼3 g/L of 2,5-diphenyloxazole (PPO). To achieve the goals of the experiment, it is imperative to understand the properties of this scintillator. At CENPA, we have an active experimental program geared towards scintillator characterization. Two experiments have been carried out: (1) a test of the electron energy scale linearity of LAB-PPO, which was found to be non-linear below ∼0.5 MeV, and (2) a first measurement of the refractive index of LAB-PPO from 210 to 1000 nm. The test of the electron energy scale linearity of LAB-PPO is described (see Sec. 1.4.4), as well as reports on the dispersion measurement (see Sec. 1.4.5). A third experiment to study Rayleigh scattering in LAB-PPO is currently being developed.

1.4.1 Status of the SNO+ data acquisition software

M. A. Howe*, J. Kaspar, N. R. Tolich, and J. F. Wilkerson*

The new DAQ software to handle the data rate expected in SNO+ is based on ORCA: a general purpose, highly modular, object-oriented, acquisition and control system that is easy to use, develop, and maintain. The DAQ pulls data from the VME trigger crate. Nineteen data crates operating in an independent asynchronous way push data into the DAQ system.

In 2010, new XL3 controllers for the data crates were developed by the University of Pennsylvania group. They were demonstrated to deliver up to 15 Mb/s of data per single crate—at least 10 times more than the previous generation XL2 controllers could deliver from all the SNO crates together. On the ORCA side, the XL3s are served by circular buffers running in parallel in independent threads. A data manager pulls data from the buffers and serializes them into the data stream to be pushed to an event builder. Fig. 1.4.1-1 shows parts of the user interface to control XL3.

A DB specification to replace an unportable old Sun DB was released and is being implemented to provide a unified interface to run time parameters for DAQ, MC, slow control, and monitoring tools. The new solution is based on replicated CouchDB servers and all the data are served in JSON format.

Two test-stands for DAQ commissioning were in use during this year. A test stand located in Sudbury has been used for most of DAQ development. The second test-stand at Penn was

*University of North Carolina, Chapel Hill, NC.

added to debug the new XL3 data crate controller. These test-stands allow us to run both the former SNO DAQ and the present ORCA system in parallel to cross-check the outputs. The agreement between the systems is excellent and the speed improved to 13Mb/sec.

Figure 1.4.1-1. A GUI of the new XL3 data crate controller is shown.

1.4.2 Status of the SNO+ slow control hardware readout

J. N. Kofron

The SNO+ experiment relies on the accurate collection of data from the hardware by the data acquisition system (DAQ). The DAQ must, therefore, be at all times aware of the current state of the hardware, and in particular must have assurances that the hardware is operating within specified tolerances. In order to accomplish this we have developed a slow control system.

Conceptually, there are two parts to the slow controls, the low level hardware readout and the high level interface. The low level hardware readout is written in a combination of Erlang and C, and has been completed. The Erlang code passes binary encoded messages to the C code, which interprets them, performs operations on the hardware, and returns data to the Erlang code using another binary message format. These data are then decoded and returned to the requesting process.

The system as engineered has been found to perform at a level that is more than adequate for our purposes, and is able to collect data at a rate more than 1000 times that which is necessary. It has also been demonstrated to handle the case of concurrent requests gracefully, without loss of information. Up to 100 concurrent clients have been tested with no degradation of data or availability.

The SNO+ slow control system is therefore complete from the standpoint of hardware readout and is scheduled to be deployed on site at Sudbury, Ontario this year. A test deployment is currently in service at CENPA.

1.4.3 Status of the SNO+ slow control software

D. J. Scislowski

In order to make data acquisition from the SNO+ slow control hardware system portable and accessible to different clients, an HTTP brokerage layer was designed and implemented. It takes requests from any user-end HTTP client, relays them to the native Erlang code running on the IO servers, then parses, formats, and returns any output to the user client. Standard HTTP return codes indicate the success or failure of the request, and attached JSON message bodies contain either the data requested, or details of any errors.

Card voltages and configurations can be read with HTTP GET requests, while POST requests allow the user client to change card modes and channel gains by supplying the desired parameters in a JSON data structure.

Making use of the widely used Erlang based `webmachine`[1] web framework ensures reliable, fault tolerant communication to the hardware layers, and a high performance under many operating conditions.

1.4.4 The electron energy scale linearity of SNO+ scintillator

N. R. Tolich and H. S. Wan Chan Tseung

It is commonly assumed that the response of a liquid scintillator (LS) to e^- is linear except at very low energies, where ionization quenching becomes significant. However, there have been some reports from the KamLAND collaboration that the observed non-linearity of the e^- energy scale in their LS cannot be solely described by Birks' law[2]. It was suggested that there is a contribution from Cherenkov UV photons which are absorbed and re-emitted at longer wavelengths. Here, we report on results from an experiment to investigate the e^- energy scale linearity of SNO+ LS between 0.075 and 3 MeV.

To investigate the e^- energy scale of the scintillator LAB-PPO (linear alkylbenzene with $\sim$3 g/L of 2,5-diphenyloxazole), mono-energetic electrons were produced by the Compton scattering of a collimated γ-ray beam inside an LAB-PPO target coupled to a PMT. The scattering angle of the γ measured with a NaI detector is directly related to the e^- energy in the LAB-PPO target by the Compton formula. A Compton scattering event results in a coincidence signal from the NaI and LS target PMTs. γ rays originated from sealed ^{137}Cs and ^{60}Co sources as well as the ^{12}C(p,p$'$)^{12}C reaction. The UW tandem Van de Graaff accelerator supplied a $\sim$2-μA beam of 5.7-MeV protons onto a 5-mm thick $^{\mathrm{nat}}$C target, producing a high intensity 4.43-MeV γ source.

[1] https://bitbucket.org/justin/webmachine.

[2] O. Perevozchikov, *Search for electron anti-neutrinos from the Sun with KamLAND detector*, Ph. D. thesis, The University of Tennessee, Knoxville (2009).

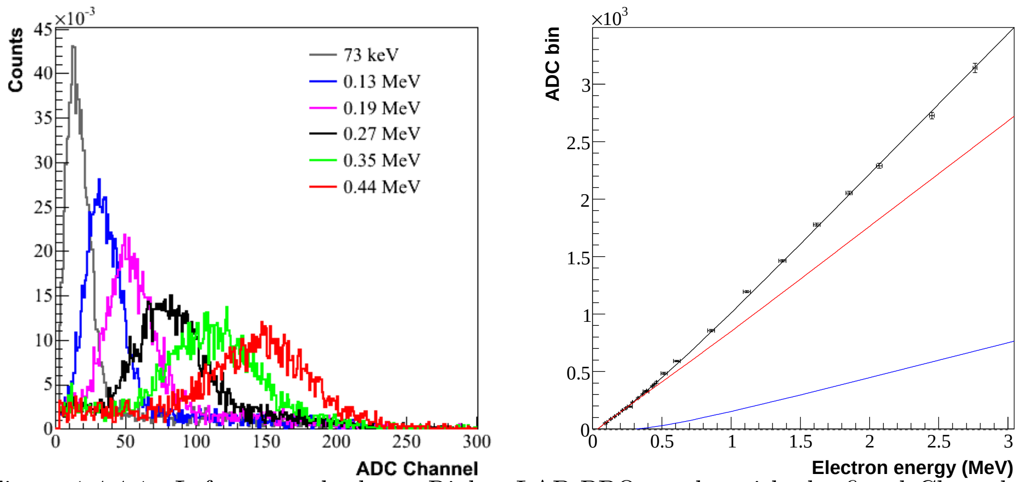

Figure 1.4.4-1. Left: example data. Right: LAB-PPO results with the fitted Cherenkov and scintillation components in blue and red.

Fig. 1.4.4-1 (left) shows the spectra of integrated PMT pulses from the LS that are in coincidence with the NaI detector at 6 scattering angles. In Fig. 1.4.4-1 (right) the peak positions, *i.e.* relative light output, as a function of e^- energy for LAB-PPO are shown in black markers. It is seen that the LS response becomes non-linear in the energy region around the Cherenkov threshold. This non-linearity cannot be explained solely by Birks' model of ionization quenching. The black line is a fit to the data assuming a two-component light model, Cherenkov (blue curve) and scintillation (red line). The relative magnitudes of these two contributions as extracted in this work will be included empirically in the SNO+ Monte Carlo package. Further work is in progress to verify the linearity of the PMT and electronics used in this experiment.

1.4.5 Measurement of the refractive index of SNO+ scintillator

N. R. Tolich and H. S. Wan Chan Tseung

In SNO+, an accurate knowledge of the scintillator refractive index as a function of wavelength is essential for reconstructing events, optical modeling, and performing reliable calculations of the Cherenkov light yield of charged particles. The refractive index of linear alkylbenzene (LAB) has so far been measured at only a few wavelengths in the visible region. Here we report on the first measurement of the refractive index within ± 0.005 for both LAB-PPO and Nd-doped LAB-PPO at 500 points in the wavelength range 200–1000 nm using ellipsometry[1]. Fig. 1.4.5-1 shows our results for LAB with 3 g PPO/L. The yellow curve is the average refractive index from the five angles while the 1-σ band is shown in red. Also shown between 400 and 650 nm are previous measurements by our collaborators at Queen's University and Brookhaven National Laboratory, Petresa, and the RENO collaboration[2]. The Nd-doped LAB-PPO results agree very closely with those from the undoped sample.

[1] R. A. Synowicki *et al.*, J. Vac. Sci. Technol. B **22** (2004) 3450.
[2] I. S. Yeo *et al.*, Phys. Scr. **82** (2010) 065706.

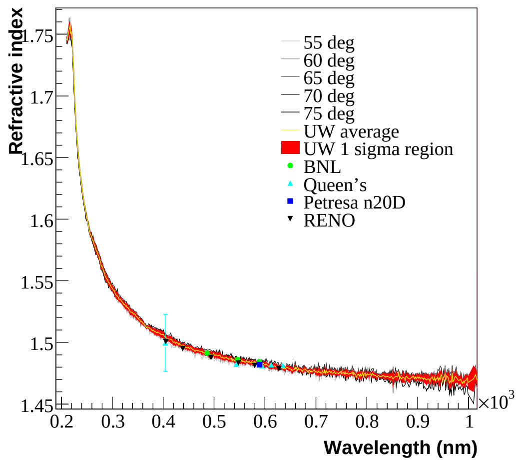

Figure 1.4.5-1. Refractive index of LAB-PPO as a function of wavelength.

The experimental set-up uses a Woollam M2000 ellipsometer[1]. A thin film of liquid scintillator was deposited on a frosted glass slide. A beam of polarized light from a Xe lamp is specularly reflected off the liquid surface undergoing a change of polarization that is characterized by two ellipsometric parameters. These are evaluated by the apparatus and can be directly related to the real and imaginary components of the refractive index. Light that is transmitted into the liquid is diffusely reflected off the frosted glass and does not impact the measurements significantly. Readings were taken at five different angles at room temperature. We first verified the validity of this method with a distilled water sample.

Project 8

1.5 Status of the Project 8 neutrino mass measurement prototype

L. I. Bodine, R. F. Bradley[*], P. J. Doe, J. A. Formaggio[†], D. L. Furse[†], R. A. Johnson[‡], J. Kaspar, M. L. Leber[§], M. L. Miller, B. Monreal[§], M. F. Morales, R. G. H. Robertson, L. J. Rosenberg, G. Rybka, W. A. Terrano, T. Thuemmler[¶], and B. A. VanDevender[‖]

Neutrino mixing experiments indicate the average neutrino mass must be greater than 0.02 eV. The KATRIN experiment has a target neutrino mass sensitivity of 0.2 eV. If the neutrino mass is not within the reach of the KATRIN experiment, it will almost certainly be within

[*]National Radio Astronomy Observatory, Charlottesville, VA.
[†]Massachusetts Institute of Technology, Cambridge, MA.
[‡]University of Colorado, Boulder, CO.
[§]University of California, Santa Barbara, Santa Barbara, CA.
[¶]Karlsruhe Institute of Technology, Karlsruhe, Germany.
[‖]Pacific Northwest National Laboratory, Richland, WA.

[1]Access to this equipment was provided by the University of Washington NanoTech User Facility.

the reach of an experiment an order of magnitude more sensitive. The Project 8 group is exploring ideas for a next-generation experiment sensitive to neutrino masses in the 0.02 to 0.2-eV mass range. Even in the event of a null measurement, such an experiment will be able to distinguish between normal and inverted hierarchies of neutrino mass.

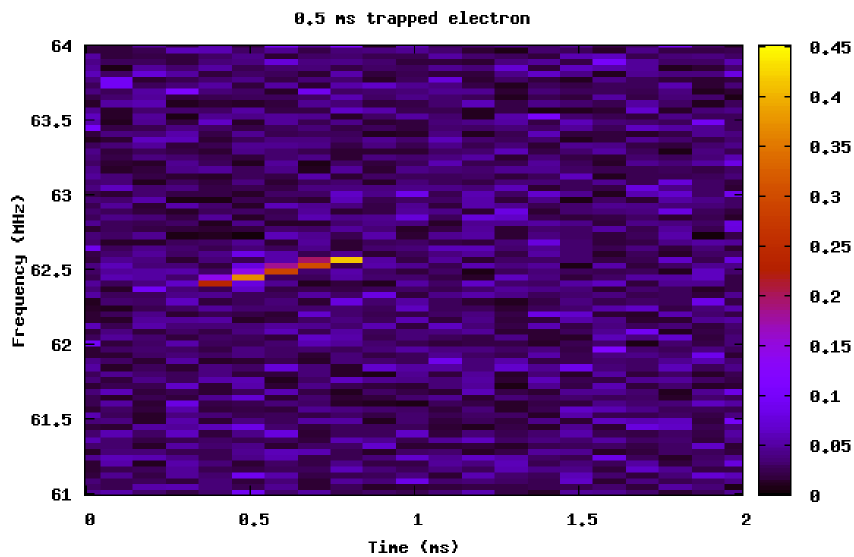

Figure 1.5-1. Simulation of the signal from an electron trapped in the prototype. Color indicates relative power in receiver. Energy loss from cyclotron radiation is noticeable as an increase in frequency over time.

Measuring the frequency of the cyclotron radiation emitted by electrons with tritium endpoint energies in a magnetic field should be able to increase electron energy resolution, and therefore neutrino mass resolution, by an order of magnitude over current experiments[1]. We are currently constructing a prototype to detect electron cyclotron radiation and characterize the experimental issues that need to be addressed to scale the method to a neutrino mass experiment.

The Project 8 prototype consists of a small magnetic bottle placed into a recently recommissioned 1-T superconducting magnet with a near-field transmission-line antenna to detect the cyclotron radiation of electrons trapped in the bottle. Electrons will be supplied by $^{83\mathrm{m}}$Kr, which has been successfully produced using the CENPA tandem accelerator. Because thermal noise will be the primary background to detecting the cyclotron radiation, the entire system will be cooled to roughly 30 K to maximize the signal to noise necessitating a cryogenic microwave amplifier on loan from NRAO. Simulations indicate the signal from a single electron should be clear, with an energy resolution limited primarily by the uncertainties in the magnetic field as shown in Fig. 1.5-1.

[1]B. Monreal and J. Formaggio, Phys. Rev. D **80**, 051301, 2009.

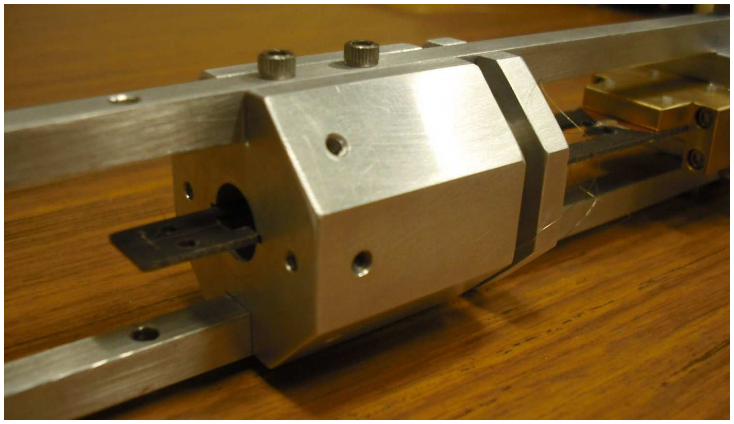

Figure 1.5-2. Partially assembled prototype detector showing the bottle coil (silver), the antenna support (black), and the cryogenic amplifier (gold).

Prototype construction (Fig. 1.5-2) is being overseen by visiting graduate student Dan Furse, and is providing excellent hands-on education in cryogenics and RF receivers to a group of three undergraduates (Fig. 1.5-3). Cryogenic tests of the detector are expected to begin early Spring 2011, with electron measurements made by the end of the year.

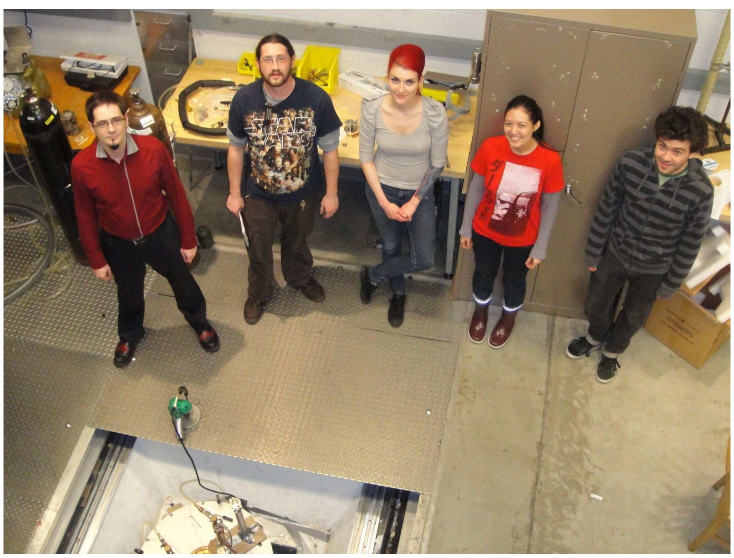

Figure 1.5-3. Project 8 insert construction team posing by the magnet top. Left to right: Gray Rybka, Aaron Stoll (undergraduate), Brynn MacCoy (undergraduate), Lisa McBride (undergraduate), Dan Furse.

HALO

1.6 The HALO supernova detector

C. A. Duba[*], F. Duncan[†‡], J. Farine[‡], A. Habig[§], A. Hime[¶], M. A. Howe[††], C. Kraus[‡], R. G. H. Robertson, K. Scholberg[‖], M. Schumaker[‡], J. Secrest[**], T. Shantz[‡], C. J. Virtue[‡], J. F. Wilkerson[††], S. Yen[‡‡], and K. Zuber[§§]

HALO (Helium and Lead Observatory) is under construction at SNOLAB. It will be a detector of supernova neutrinos with sensitivity covering most of the galaxy, but nevertheless compact, low in cost, and low in maintenance. These features are obtained through the use of Pb as a neutrino target. Neutrino interactions on Pb, both charged-current and neutral-current, populate neutron unstable states in product nuclei, and the neutrons emitted can be moderated and detected in ^{3}He-filled proportional counters. The counters are the ones used in the final stage of the SNO experiment to detect neutrons produced by the neutral-current interaction of solar neutrinos on deuterium. The Pb itself is also reused, originally a part of the cosmic-ray neutron detection array sited at Deep River beginning with the International Geophysical Year in 1957-58. About 76 tonnes of Pb have been preserved from that detector.

The past year has seen excellent progress in the construction of HALO, beginning with the initiation of an award to the Canadian participants from NSERC (Natural Sciences and Engineering Research Council). A robust steel framework was built and the lead forms (of a special shape designed for the IGY array) installed. A water moderator and reflector surrounding the detector consists of cubical liquid container boxes that have been filled with ultrapure water.

Since UW built the original NCD array (in collaboration with Los Alamos National Laboratory), our role has been to help with recommissioning the detectors for the new application. We have designed and built new endcaps for connecting cables individually to the 2.5-m and 3.0-m counters that will be used in HALO. The endcaps have been machined from 303 stainless steel with the help of our new CNC lathe (see cover photograph). The endcaps accept SHV cables and contain gold-plated ball-and-socket spring-loaded connections inside (see Fig. 1.6-1). A new cutting apparatus was also built and shipped to site where it is being used to cut apart the counter "strings" that are still welded together in places. All the counters have now been moved from the storage location near the deck of the SNO cavity to a new location near HALO in the 'ladder lab' part of SNOLAB. We continue to work on modifying the electronics to reconfigure the readout to charge mode instead of current mode.

[*]Digipen Institute of Technology, Redmond, WA.
[†]SNOLAB, Sudbury, ON, Canada.
[‡]Laurentian University, Sudbury, ON, Canada.
[§]University of Minnesota Duluth, Duluth, MN.
[¶]Los Alamos National Laboratory, Los Alamos, NM.
[††]University of North Carolina, Chapel Hill, NC.
[‖]Duke University, Durham, NC.
[**]Armstrong Atlantic State University, Savannah, GA.
[‡‡]TRIUMF, Vancouver, BC, Canada.
[§§]TU Dresden, Dresden, Germany.

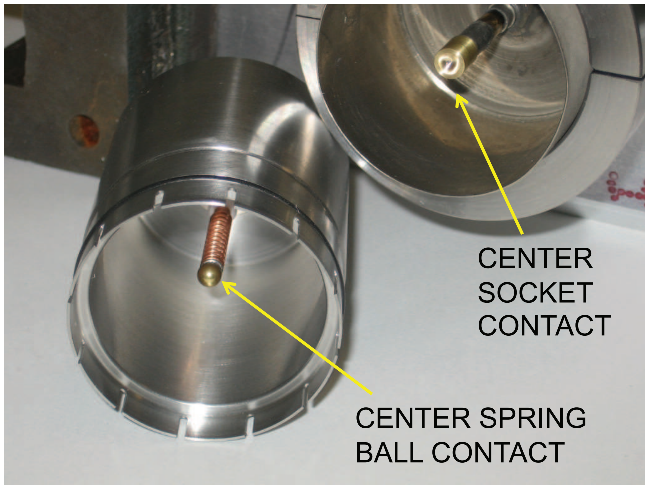

Figure 1.6-1. The contacts inside the new endcaps made for the neutron detectors recycled from the third phase of SNO.

SNO

1.7 Overview of the SNO experiment and CENPA's contribution

R. G. H. Robertson, R. C. Rosten, N. R. Tolich, B. VanDevender, H. S. Wan Chan Tseung, plus the SNO Collaboration.

The primary scientific goal of the Sudbury Neutrino Observatory (SNO) experiment was to measure the flux of the different neutrino flavors coming from the Sun in order to understand the solar neutrino anomaly. There were three distinct phases of the experiment, each of which measured the total fluxes for all three light neutrino flavors in a different way. For the first and second phases, respectively, neutrons produced by neutrino neutral current interactions in the D_2O were observed by the gammas emitted from the subsequent neutron capture on ^{2}H and ^{35}Cl. For the third phase, proportional counters filled with ^{3}He were deployed within the D_2O, to detect the neutrons. Since data taking ended in November, 2006, all efforts have focussed on analysis of the recorded data.

During the past year we have been working on a final analysis of the SNO data combining in a single analysis results from all three phases. This will be the most accurate result possible with the SNO data, and will likely be the most accurate solar neutrino measurement for the foreseeable future. This analysis is currently under review by a committee within the SNO collaboration before it will be distributed to the entire collaboration and published. During this analysis a number of inconsistencies in the previous analyses were investigated and resolved.

The combined analysis described above is for neutrinos from the decay of ^{8}B within the Sun. We have also completed an internal review and are working on the publication of a search for neutrinos from the reaction $^3\mathrm{He} + {}^1\mathrm{H} \rightarrow {}^4\mathrm{He} + e^+ + \nu_e$ within the Sun. The standard model prediction for the flux of these neutrinos at SNO is $8.0 \times 10^3\,\mathrm{cm}^{-2}\mathrm{s}^{-1}$. By doing an analysis including the expected neutrino energy spectrum and all the available data, this analysis reached a sensitivity at 90% confidence level of $13.0 \times 10^3\,\mathrm{cm}^{-2}\mathrm{s}^{-1}$, which is more than a factor of two improvement on the previous best sensitivity, also obtained from SNO. In the past year the SNO collaboration has published a null search for neutrinos from supernova with no optical signal[1].

Along with these collaboration-wide analysis efforts that have been led by Tolich; Rosten, Robertson, and VanDevender, together with a small group of other collaborators submitted for publication in Nucl. Instrum. Methods their work[2] to identify two "hotspots" of backgrounds on the proportional counters. Robertson, Tolich, and Wan Chan Tseung, together with a small group of other collaborators submitted for publication in New J. Phys. their work[3] developing the proportional counter simulations.

The above publications complete what has been a main area of research at CENPA for more than a decade. The work has led to some very exciting results confirming that the solar neutrino anomaly was caused by neutrino oscillations.

[1] B. Aharmim, *et al.* Astrophys. J. **728**, 83 (2011)
[2] CENPA Annual Report, University of Washington (2008) p. 7.
[3] CENPA Annual Report, University of Washington (2008) p. 5.

2 Fundamental symmetries and non-accelerator based weak interactions

Torsion balance experiments

2.1 Overview of the CENPA torsion balance experiments

E. G. Adelberger

A surprisingly large number of ideas for solving open problems in fundamental physics, many of which are directed at unifying gravity with the rest of physics, predict new ultra-weak forces mediated by conjectured low-mass particles. String-theory ideas are particularly prolific in this regard, as the conjectured extra dimensions and the large number of low-mass particles all produce new forces. The discovery of such forces would have a revolutionary impact, and sufficiently sensitive upper bounds on the forces severely constrain the theories. Motivated by these considerations, the CENPA Eöt-Wash group develops advanced torsion-balance techniques for sensitive mechanical measurements and applies them to address problems of current interest. We have produced the most sensitive tests of the equivalence principle[1], tested the Newtonian inverse-square law to the shortest distances[2], and have tested certain Lorentz-violating properties of electrons five orders of magnitude below the Planck scale and non-commutative geometry at the 10^{13}-GeV level[3]. We currently operate 7 different torsion-balance instruments. Each one is devoted to a particular topic and is often the thesis project of an individual graduate student. At this moment one of the instruments is used for tests of the equivalence principle, two are used to probe short-range gravity, two to search for new electron-spin-dependent forces, and two are dedicated to investigate the subtle factors that limit the sensitivities of delicate mechanical experiments. The contributions below outline our progress in this area during the past year.

This work is primarily supported by NSF grant PHY-0969199 and the salaries, etc. of faculty, students and postdocs are covered by the NSF. Costs of some equipment used in both NSF and DOE sponsored research are shared between the two funding sources.

2.1.1 Testing an equivalence principle pendulum with hydrogen-rich test bodies

E. G. Adelberger, J. H. Gundlach, B. R. Heckel, S. Schlamminger*, W. A. Terrano

Ordinary luminous matter is believed to be less than one quarter of the total mass of the universe, however these estimates rely on the assumption that the only long-range interaction between dark and luminous matter is gravity. This important assumption can be tested in

*National Institute of Standards and Technology, Gaithersburg, MD.

[1] S. Schlamminger *et al.*, Phys. Rev. Lett. **100**, 041101 (2008).
[2] D. J. Kapner *et al.*, Phys. Rev. Lett. **78**, 092006 (2008).
[3] B. R. Heckel *et al.*, Phys. Rev. D **78**, 092006 (2008).

the lab by looking for an equivalence-principle violating interaction between the dark matter in our galaxy and a composition dipole in our pendulum, as any non-gravitational interaction is expected to violate the equivalence principle. The sensitivity of an equivalence principle test is proportional to the degree to which the test bodies differ. To date, all equivalence-principle tests have employed test bodies that have varying degrees of neutron excess. One can gain roughly a factor of 10 in sensitivity by using test bodies of polyethylene (which has a 1 in 7 proton excess) and beryllium (which has a 1 in 9 neutron excess)[1].

We are gearing up for a new version of the classic torsion balance tests of the equivalence principle with this test-body pair. The major difficulty at this point is working with a plastic material. All of our previous test bodies consisted of metals. We have built the prototype that was proposed earlier[2]. This prototype will allow us to take data evaluating the thermal and mechanical stability of the ultra high molecular weight polyethylene.

In order to take this data, we needed to upgrade and repair parts of the original Eöt-Wash rotating pendulum after 19 years of continuous operation. In particular the laser used to read out the twist of the pendulum was replaced with a new higher power laser that greatly increased the intensity of the angle readout signal. We also replaced the gear reducer driving the large turntable and the bearing in the co-rotating feed thru stage.

2.1.2 Progress toward improved equivalence principle limits for gravitational self-energy

E. G. Adelberger, J. H. Gundlach, B. R. Heckel, S. Schlamminger*, and T. A. Wagner

We are currently completing the analysis of our equivalence principle test using test bodies that model the difference in composition between the Earth and Moon. This experiment complements lunar laser ranging efforts by placing limits on the composition dependent portion of any equivalence principle violation. By combining these experimental results, a limit on equivalence principle violation due to the difference in the gravitational self-energy content of the Earth and Moon can be determined. Previously, a value of $\eta_{CD} = (+0.1 \pm 2.7 \pm 1.7) \times 10^{-13}$ was reported by Baeßler *et al.*[3] Due to improvements made to our apparatus over the course of this experiment, much improved noise levels were achieved in the past year. Our preliminary results with $1-\sigma$ statistical uncertainty are $\eta_{CD} = (7 \pm 5) \times 10^{-14}$. In conjunction with improvements in lunar laser ranging[4], we expect to set a limit on η for gravitational self-energy of $\sim 10^{-4}$.

Systematic and statistical uncertainties contribute approximately equally to our lab frame results. To address two of our major systematic effects, we installed lower noise tilt sensors

*National Institute of Standards and Technology, Gaithersburg, MD.

[1] E. G. Adelberger, J. H. Gundlach, B. R. Heckel, S. Hoedl, and S. Schlamminger, Prog. Part. Nucl. Phys. **62**, 102 (2009).

[2] CENPA Annual Report, University of Washington (2009) p. 31.

[3] S. Baeßler, B. R. Heckel, E. G. Adelberger, J. H. Gundlach, U. Schmidt, and H. E. Swanson, Phys. Rev. Lett. **83**, 3585 (1999).

[4] J. G. Williams, S. G. Turyshev, and T. W. Murphy, Jr., Int. J. Mod. Phys. D, **13**, 567 (2004).

(Fig. 2.1.2-1) on the apparatus this year. We began testing installation and measurement practices for these tilt sensors with a goal of obtaining a measurement of the gravity gradient field using the tilt sensors. The gravitational gradient systematic is one of our largest due to seasonal changes of the water table. Currently, we change out the pendulum for one with large gravitational moments to measure the environmental gravity gradients. If ongoing tilt sensor measurements resolve the seasonal change of the gravity gradient, we can interpolate the more sensitive pendulum measurements of the field.

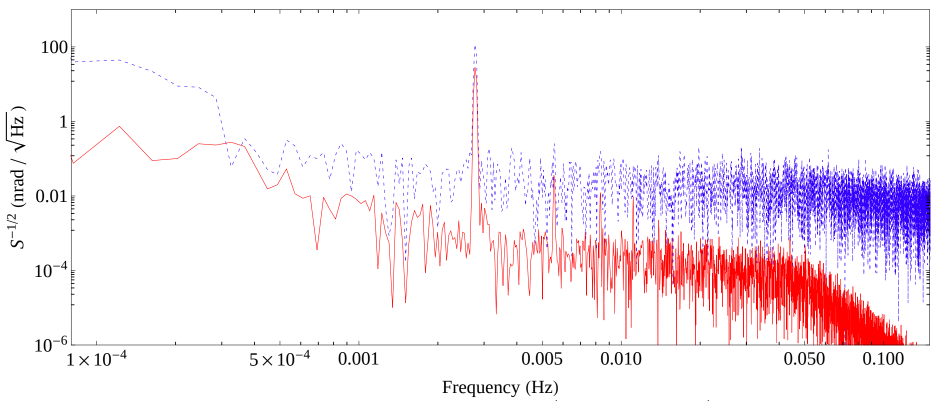

Figure 2.1.2-1. The noise amplitude of the existing (blue, dashed) and new, lower noise (red, solid) tilt sensors. The turntable rotation frequency is 7×10^{-4} Hz and the large peak is the 4th harmonic of the rotation frequency due to a four-fold symmetry of the apparatus support structure.

2.1.3 Submillimeter parallel plate test of gravity update

J. H. Gundlach, C. A. Hagedorn, S. Schlamminger*, and M. D. Turner

Work continues on a parallel-plate torsion balance test of the gravitational inverse square law at submillimeter scales[1]. In this test, a pendulum torsion balance is used to measure the gradient of the gravitational field of an "infinite" sheet attractor at distances shorter than 100 μm. The experiment is a null-test search for violations of the inverse square law. The torsion pendulum and attractor are physically isolated by a thin metal foil held at a defined electric potential.

A summer/autumn measurement campaign gave inconsistent results. Our measurements resolved a large signal (in conflict with previous experiments) that varied with time and with changes to the apparatus. We interpret the signal as being most probably caused by an unknown systematic instrumental effect.

To further control possible systematic effects, we made a number of upgrades. Electrically: isolated battery-powered application of the pendulum-foil and attractor-foil voltages, battery-powered isolation amplifiers for the pendulum feedback electrodes. Pneumatic attractor drive:

*National Institute of Standards and Technology, Gaithersburg, MD.

[1]CENPA Annual Report, University of Washington (2010) p. 35.

electronic reed valve replaced with a quieter and faster fuel injector, TTL-controlled solenoid valve installed to fully shield the attractor from external pressure disturbances, and a precision absolute pressure gauge in the bellows line to allow precise determination of the attractor position without electrical connection to the apparatus.

The interferometric foil monitor laser was temperature stabilized with a commercial controller. It is now stable enough to produce reliable measurements, but is slightly noisier than expected. An upgrade to a 660-nm fiber-coupled laser increased the intensity significantly, improving both SNR and ease-of-use. See Fig. 2.1.3-1.

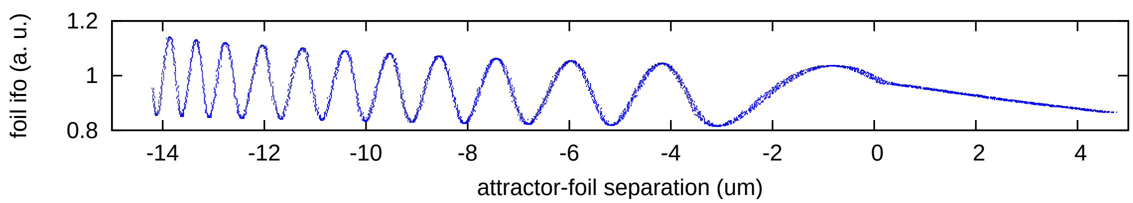

Figure 2.1.3-1. Foil interferometer output as attractor presses on foil. Variable spatial frequency is due to attractor-foil misalignment. Signal variation at positive attractor-foil separation is due to interferometer drift.

Improvements in data analysis include the trial implementation of bootstrapped Monte Carlo techniques for both uncertainty estimation and signal extraction.

Present work includes the installation of in-vacuum motors that will allow on-line realignment of the foil to the attractor and repositioning of the interferometer tip. Realignment may allow a 20-micron reduction in pendulum-attractor separation. A new measurement campaign will begin in Spring 2011.

2.1.4 Progress on the wedge-pendulum probe of short-range gravity

E. G. Adelberger, T. S. Cook, B. R. Heckel, and H. E. Swanson

A second complete set of data has been taken with the wedge pendulum (see Fig. 2.1.4-1). Despite efforts to improve the performance of the system over the first set of data (primarily through flattening of the pendulum[1]), this set has proved to be of roughly equal quality, and did not provide the clean noise performance we hoped to obtain at close separations.

As the data set was collected, it quickly became apparent that something was again wrong with the ratio of the 18-fold to 120-fold signals. The problem appeared to be in the 18-fold signal as the fit to just the 120-fold data gave very good results. Much time was spent exploring possible models to account for the discrepancy, but to no avail. The apparatus was opened to search for the causes of these problems.

We believe the primary culprit for the poor noise was a piece of dust (or pieces of dust) discovered on the attractor surface and observed to be touching the electrostatic screen.

[1] CENPA Annual Report, University of Washington (2010) p. 36.

Additionally, detailed scans of the outer edge of the pendulum and attractor have revealed 18-fold structure in phase with the wedges that should explain the additional amplitude in our 18-fold signal. This analysis is currently in progress.

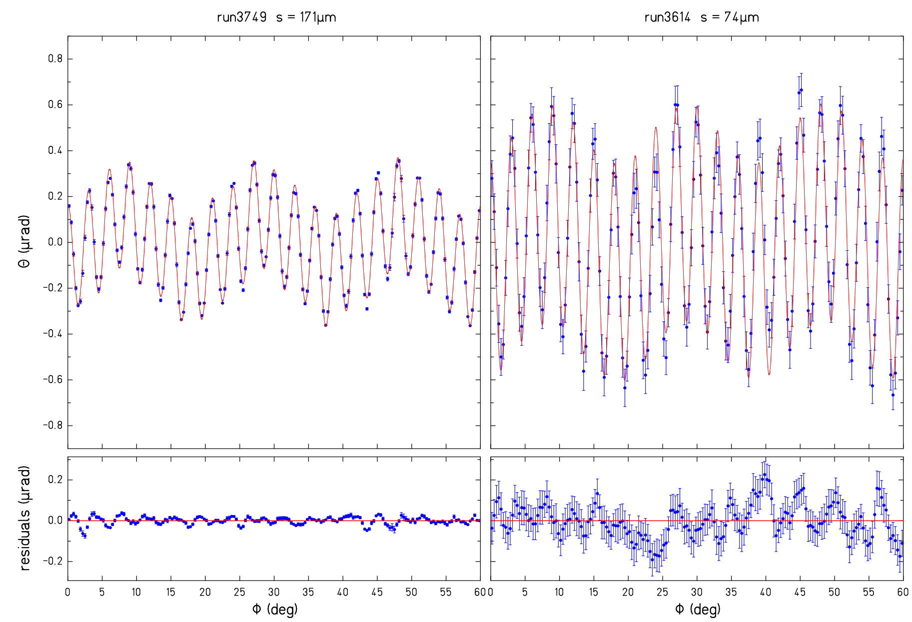

Figure 2.1.4-1. Twist data binned over 60° of attractor rotation showing prominent 120-fold and 18-fold signals. The data at closer separation (right) have atypically low noise for that distance; most similar runs have considerably more noise. We hope to achieve consistently less noise in the upcoming data set.

Preparations are underway to attempt to collect a final set of data. The goal is to achieve reasonably clean data at attractor to pendulum separations of ≤ 60 μm.

2.1.5 Experimental limits on a proposed signature of space-time granularity from a spin polarized torsion pendulum

E. G. Adelberger, B. R. Heckel, S. Schlamminger*, W. A. Terrano

Attempts at detecting a fundamental granularity of space-time have often looked for violations of Lorentz symmetry as a signal. Bonder and Sudarsky[1] propose a phenomenological signature of a Lorentz invariant granularity that would manifest itself in the lab as a coupling between (1) the curvature of space due to the Earth and local masses, (2) the angular momentum of the Earth, and (3) the spin of the particle. We are looking for this signal using the spin-polarized pendulum[2] and a large quadrupole source that can be rotated between data taking runs. Rotating the Q22 source by 90° changes the relative orientation of the

*National Institute of Standards and Technology, Gaithersburg, MD.

[1]Y. Bonder and D. Sudarsky, Class. Quantum Grav. **25**, 105017 (2008).
[2]CENPA Annual Report, University of Washington (2003) p. 11.

local curvature and the Earth's angular momentum and shifts the lowest energy orientation of the accumulated electron spin in the pendulum. Comparing runs taken with different Q22 configurations allows us to isolate effects due to the proposed signal of Bonder and Sudarsky.

In certain mass distributions used with the Q22 source we saw a non-gravitational systematic effect on the pendulum. By changing the mass distributions of the sources relative to the turntable without changing the Q22 moments we found that the signal was presumably due to thermal gradients between the turntable and our Q22 source. In fact, we were able to correlate the observed twist signal with a thermal gradient across the can lid. Redesigning our Q22 source to eliminate assymetric cooling paths reduced the thermal gradient by a factor of 20. This pushes the associated systematic effect down well below our statistical uncertainty. Our results have been submitted to the Journal of Classical and Quantum Gravity.

2.1.6 Status update on a new torsion balance test of spin coupled forces

E. G. Adelberger, B. R. Heckel, and W. A. Terrano

The torsion balance experiment to measure spin dependent forces[1] is nearly ready for commissioning. All that remains is assembling it in the vacuum with the torsion fiber attachments.

Since our pendulum will have large numbers of aligned spins in order to be sensitive to spin coupled forces, an essential component to the experiment is demonstrating that its magnetic couplings can be controlled.

To this end, after assembling the ring we tune the magnetizations of each individual segment. This reduces the measured peak to peak magnetic field 0.070 inch above the rings from 600 G to 30 G. Measurements of magnetic shielding factors on preliminary shields[2] led us to a design for a set of magnetic shields which will magnetically isolate the pendulum from the attractor. These have been manufactured and annealed. We have had to redesign our system for measuring the leakage magnetic fields in order to pick up the tiny 10-ω leakage fields. This involved adding an encoder to the rotating stage so that we can average the readings from many rotations of the pendulum, and using a magneto-resistant probe instead of a hall probe for improved sensitivity. This setup should allow us to see magnetic field inhomogeneities of less than 1 μgauss.

2.1.7 Progress towards an equivalence principle test using a cryogenic torsion balance

E. G. Adelberger, F. Fleischer, B. R. Heckel and H. E. Swanson

As described in previous annual reports[3,4], we have built a torsion balance designed to be operated near LHe temperature. The setup will be used to investigate the limiting factors in

[1] CENPA Annual Report, University of Washington (2007) p. 38.
[2] CENPA Annual Report, University of Washington (2010) p. 38.
[3] CENPA Annual Report, University of Washington (2009) p. 28.
[4] CENPA Annual Report, University of Washington (2010) p. 40.

torsion-balance performance, and then to test the equivalence principle, using the Sun and the center of the galaxy as attractors.

First tests showed excess noise significantly above the expected thermal noise level even at room temperature. This excess noise has been investigated and we have successfully identified and mitigated its sources. So far we have not yet seen an improvement in the quality factor Q of the torsion balance on cooling. There are strong hints that this may be due to eddy current damping of the pendulum motion. To overcome this limitation, a magnetic shield has been designed and is being made.

Furthermore we have built a new moment-free test pendulum. Its design allows for a more sensitive and easily aligned optical readout of the twist angle. It should considerably improve the pendulum's ability to withstand thermal cycling as well.

2.1.8 Development of an ultrasensitive interferometric quasi-autocollimator

J. H. Gundlach, C. A. Hagedorn, S. Schlamminger*, and M. D. Turner

We have developed an angular deflection measurement device called the interferometric quasi-autocollimator (iQuAC). This has potential use in any of our group's torsion balance experiments. It uses the quantum weak value amplification effect[1] and is based on the setup described by Dixon *et al.*[2]

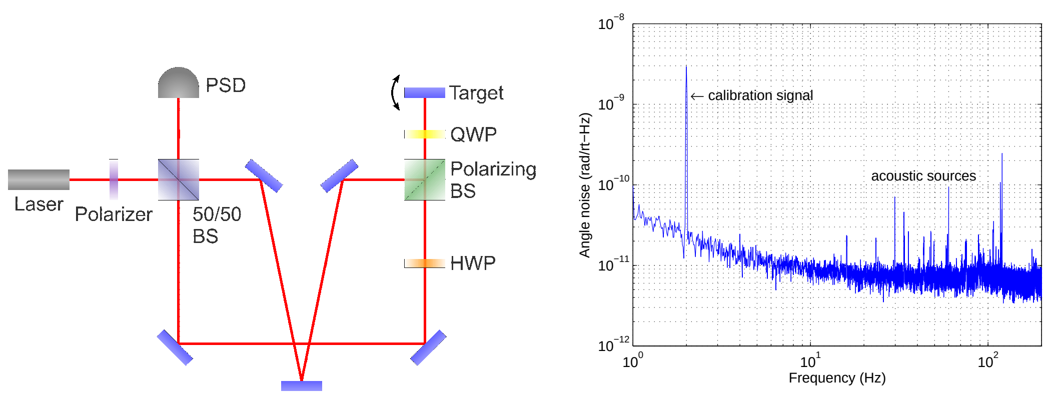

(a) (b)

Figure 2.1.8-1. (a) A schematic diagram of the iQuAC device. (b) The noise floor of an implementation of the iQuAC design. A 620-prad calibration signal at 2 Hz is used to calibrate the device.

Our torsion balances are monitored by autocollimators that our group has designed and constructed. The best of these autocollimators has a sensitivity of $\sim$ 1 nm. Although the amplification scheme used by Dixon *et al.* can measure much smaller angles, it is sensitive

*National Institute of Standards and Technology, Gaithersburg, MD.

[1]Y. Aharonov, D.Z. Albert, and L. Vaidman, Phys. Rev. Lett. **60**, 1351 (1988).
[2]P. B. Dixon, D. J. Starling, A. N. Jordan, and J. C. Howell, Phys. Rev. Lett. **102**, 173601 (2009).

to translations of the target. We developed a design, shown in Fig. 2.1.8-1(a), which uses the same amplification scheme but is insensitive to target translations. An implementation of the device using standard optics equipment has a noise floor below 10 prad/$\sqrt{\mathrm{Hz}}$ in the range 10-200 Hz, as shown in Fig. 2.1.8-1(b).

Non-accelerator based weak interactions and fundamental symmetries

2.2 Overview of non-accelerator based weak interactions studies

A. García

The mercury-EDM group has made progress on several improvements to their system which will allow for a more sensitive search for time reversal symmetry violation.

The neutron spin-rotation collaboration (parity violating neutron spin-rotation in ^{4}He) has worked to analyze sources of systematic uncertainties and published their results[1].

This last year was one of intense work on analysis for the emiT collaboration, searching for time-reversal symmetry breaking in the decay of neutrons. The collaboration is now satisfied with the analysis, has opened the box, and publication of the results are imminent.

The UCNA collaboration continued to take data towards a precise determination of the beta asymmetry and published the 2008-2009 data[2].

2.2.1 Status of the UCNA experiment

A. García, A. Knecht, and C. Wrede for the UCNA collaboration

The goal of the UCNA collaboration is a precise measurement of the beta asymmetry in neutron decay. The experiment utilizes ultra-cold neutrons produced at the Los Alamos Neutron Science Center (LANSCE). Ultra-cold neutrons are polarized by passage through a 7-T superconducting magnet and fed into a decay trap within a 1-T superconducting solenoidal magnet. Two electron detectors at the ends of the solenoidal magnet measure the beta decay asymmetry directly. From the measured decay asymmetry one can extract the ratio of axial to vector coupling constants g_A/g_V. With the neutron lifetime as an additional input, it is then possible to calculate V_{ud}, the up-down element of the weak quark mixing matrix. All these values are basic elements of the standard model. In addition, comparing these results to measurements of nuclear beta decay serves as a stringent test of our current understanding.

The group at the University of Washington worked on producing a ^{114m}In source[3] (see Sec. 3.3.5) which can be used for electron energy calibration, and also contributed to experimental shifts.

[1] Phys. Rev. C **83**, 022501(R) 2011.
[2] J. Liu *et al.* (UCNA collaboration), Phys. Rev. Lett. **105**, 181803 (2010).
[3] C. Wrede *et al.*, Nucl. Instrum. Methods B **269**, 1113 (2011).

Last year we published the combined data from 2008 and 2009 leading to a precision on the asymmetry measurement of 1.3%[1]. In addition, data taking continued with several improvements in place that should allow us to reach a precision of $\sim 0.6\%$. The measurement period starting in the summer of 2011 will eventually bring us another factor of 2 improvement in sensitivity.

2.2.2 Permanent electric dipole moment of atomic mercury

J. Chen, E. N. Fortson, B. Graner, B. R. Heckel

Atomic electric dipole moment (EDM) experiments offer perhaps the most sensitive probe of CP violation in theories of physics beyond the standard model, and our measurements of the ^{199}Hg EDM over the years have achieved the most precise EDM limit on any system. The leading theoretical extension to the standard model, supersymmetry (SUSY), is expected to generate a ^{199}Hg EDM comparable to our experimental limit. By increasing the precision of our result, we can provide important information about the model parameter space of SUSY and other theories. We recently published a new upper limit[2] for the EDM of ^{199}Hg: $|d(^{199}\mathrm{Hg})| < 3.1 \times 10^{-29} e\,\mathrm{cm}$ (95% confidence level), a seven-fold improvement in the upper limit over previous work. The experiment uses a frequency-quadrupled laser diode on the 254-nm mercury absorption line to orient the ^{199}Hg nuclear spins and to measure their Larmor frequency.

In the past year we have been preparing for a new round of EDM measurements. To improve upon our current results requires better precision in measuring the ^{199}Hg Larmor frequency, better magnetic field stability, and reduced systematic errors. Last year's report[3] described the development of a detection scheme that measures both polarization states of the light transmitted through the cells and a leakage current monitoring scheme that isolates the currents flowing down the cell walls, the most serious source for systematic error. In the past year we have implemented these improvements to the apparatus and have made other significant improvements. Our major accomplishments are listed below.

Optical components to measure both polarization states of the laser beams through each of the four vapor cells have been assembled and tested. The data acquisition system has been modified to read eight optical signals and to allow data taking "in the dark"; the Larmor frequency is extracted from the spin phases measured at the start and end of the precession interval with the light turned off in between. This eliminates a systematic error associated with the light and reduces noise associated with light shifts. A new cell vessel has been constructed that incorporates additional leakage current channels to measure the currents flowing down the vapor cells independently from the currents discharged to the air. The ground plane was changed from gold coated glass to tin oxide coated glass to reduce magnetic field noise from fluctuating currents in the gold. A new magnetic field coil form, wound on an insulating cylinder, was built and installed. This coil form replaces a similar

[1] J. Liu *et al.* (UCNA Collaboration), Phys. Rev. Lett. **105**, 181803 (2010).
[2] W. C. Griffith, *et al.*, Phys. Rev. Lett. **102**, 101601 (2009).
[3] CENPA Annual Report, University of Washington (2010) p. 48.

one wound on an aluminum cylinder; the fluctuating currents in the aluminum cylinder were a major source of magnetic field noise. The new coil form includes eight gradient coils and produces a five times more uniform field than the coil it replaced.

As the ^{199}Hg signal in the old cells has vanished the remaining task is to construct new ^{199}Hg vapor cells ; the ^{199}Hg atoms "disappear." We have recently discovered that out-gassed vapor from the glue used to bond the cells reacts with ^{199}Hg forming stable compounds. We are in the process of making new cells that do not require glue and hope for cells that will not fade with time.

2.2.3 Parity non-conserving neutron spin rotation experiment

C. Bass*, K. Gan†, B. R. Heckel, D. Luo‡, D. Markoff§, A. M. Micherdzinska†, H. P. Mumm*, J. Nico*, A. Opper†, W. M. Snow‡, and H. E. Swanson

The experiment measures the parity-violating neutron spin rotation angle that neutrons experience as they pass through liquid ^{4}He. In the previous CENPA annual report[1] we reported an upper bound on this rotation angle. The collaboration has so far produced three publications, two in Nuclear Instruments and Methods[2,3], and one in Physical Review C[4]. Partially motivated by a comment from one of the reviewers, we used the wavelength sensitivity of our neutron detector to determine the ambient longitudinal B-field averaged over the measurement. We then computed the factor by which the apparatus suppresses this magnetic systematic and it is in good agreement with calculations.

A second phase of the measurement is planned using a more intense neutron beam in an improved beam line under construction at NIST

2.2.4 Progress in analysis of emiT data

A. García for the emiT collaboration

The emiT collaboration worked on an experiment to search for the breaking of the time-reversal symmerty in neutron beta decay.[5] The beta decay rate depends on correlations between the momenta of the electron, $\vec{p_e}$, and neutrino, $\vec{p_\nu}$, and the average neutron angular

*NIST Center for Neutron Research, Gaithersburg, MD.
†Department of Physics, The George Washington University, Washington, DC.
‡Department of Physics, Indiana University Cyclotron Facility, Bloomington, IN.
§North Carolina State University, TUNL, Raleigh, NC.

[1] CENPA Annual Report, University of Washington (2010) p. 50.
[2] Nucl. Instrum. Methods A **612**, 69 (2009).
[3] Nucl. Instrum. Methods A **631**, 80 (2011).
[4] Phys. Rev. C **83**, 022501(R) (2011).
[5] See Mumm et al, Rev. Sci. Instr. **75** , 5343 (2004) for a description of the apparatus.

momentum $\langle\vec{J}\rangle$:

$$d\Gamma \propto \left[1 + a\frac{\vec{p_e}}{E_e}\cdot\frac{\vec{p_\nu}}{E_\nu} + \frac{\langle\vec{J}\rangle}{J}\cdot\left(A\frac{\vec{p_e}}{E_e} + B\frac{\vec{p_\nu}}{E_\nu} + D\frac{\vec{p_e}}{E_e}\times\frac{\vec{p_\nu}}{E_\nu}\right)\right]$$

The triple correlation is even under parity (P), but odd under motion reversal - the combination of time-reversal (T) and exchange of initial and final-states. A measurement of D is sensitive to T-odd/ P-even interactions among light quarks, which could arise from new physics that would not contribute to the neutron EDM, for example leptoquarks. For vector-axial-vector interactions only, D is also a measure of the complex phase of g_A/g_V.

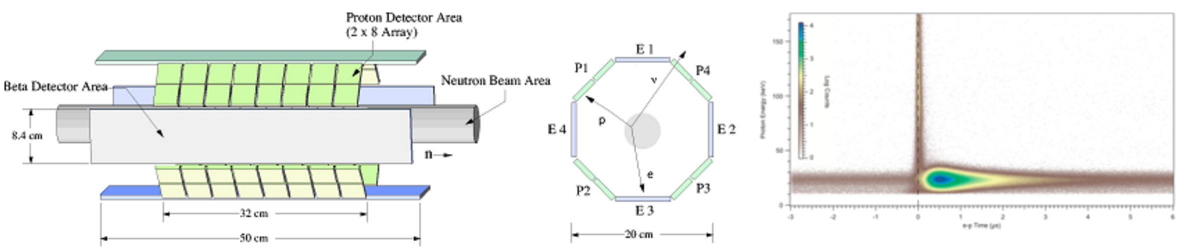

Figure 2.2.4-1. Left: Sketch of the emiT apparatus. Scintillating paddles were used as electron detectors and Si surface barrier were used as proton detectors. The Si detectors were set at ~ -30 kV so protons can be detected. Right: Si surface barrier amplitude versus proton-electron time difference. Events near $\delta t \approx 0$ are prompt coincidences due primarily to beam-related backgrounds. The very low background rate is apparent.

Two emiT runs have now been completed at NIST. The first run, in 1997, used PIN-diode proton detectors with the result[1] $D = [-0.6 \pm 1.2(stat) \pm 0.5(sys)] \times 10^{-3}$. The 1997 NIST run and study of systematic effects led to an upgrade of the apparatus, most importantly improved electronics, proton-acceleration geometry and implementation of surface-barrier detectors for protons. The improved emiT-II apparatus took data at NIST over 14 months in 2002-2003 collecting over 300 million proton-electron coincidence events. Cuts in proton-energy/time-of-flight plane isolate neutron decays as shown in the figure. A blind analysis and extensive study of all significant systematic effects has recently been completed. The last couple of years have demanded significant attention from García who has been responsible for Monte Carlo calculations. The latter have played an important role in analyzing data and understanding systematic uncertainties. The emiT-II analysis has revealed several ways in which the apparatus can be improved to reduce systematic effects. This will be crucial to assessing the feasibility of a higher statistics run with significantly higher sensitivity. A publication is in the works.

[1]L.J. Lising et al. Phys. Rev. C 62, 055501 (2000).

3 Accelerator based physics

Nuclear astrophysics

3.1 Overview of the CENPA nuclear astrophysics program

A. García and C. Wrede

During last year several of us (Adelberger, García, Robertson, Snover) contributed to a paper summarizing conclusions of the Solar Fusion II workshop. The paper is now in press in Rev. Mod. Phys. and includes several sections that benefited significantly from work performed using our local accelerator[1].

^{22}Na is one of the main radionuclides that can be observed with γ-ray telescopes and used to confirm calculations of novae. Taking advantage of our expertise and capabilities for radiative capture experiments we undertook the determination of ^{22}Na(p,γ). The work concluded last year with the publication of the work and the successful defense by Anne Sallaska of her thesis[2]. Our results indicate that previous experiments had underestimated the ^{22}Na(p,γ) reaction rate by factors of 2-3!

Led by C. Wrede several other experiments related to hydrogen burning and nova explosions were pursued. Some have been successfully approved for running at other facilities[3], successfully carried out, analyzed and published[4], or submitted for publication[5].

3.1.1 Direct measurements ^{22}Na(p,γ)^{23}Mg resonances

T. A. D. Brown[*], L. Buchmann[†], J. A. Caggiano[†,‡], A. García, D. A. Hutcheon[†], J. José[‡], D. F. Ottewell[†], C. Ruiz[†], A. L. Sallaska[§], K. A. Snover, D. W. Storm, C. Vockenhuber[†,¶], and C. Wrede

The ^{22}Na(p,γ)^{23}Mg reaction is the primary destruction mechanism for the cosmic γ-ray emitter ^{22}Na in classical novae. For the past several years, we have been working on a project to measure resonances in this reaction using ion-implanted targets from TRIUMF-ISAC and an intense proton beam from CENPA's tandem Van de Graaff accelerator. In last year's

[*]Mary Bird Cancer Center, Baton Rouge, LA.
[†]TRIUMF, Vancouver, BC, Canada.
[‡]Lawrence Livermore National Laboratory, Livermore, CA.
[‡]Departament Física i Enginyeria Nuclear and Institut d'Estudis Espacials de Catalunya, Barcelona, Spain.
[§]University of North Carolina, Chapel Hill, NC.
[¶]Swiss Federal Institute of Technology (ETH), Zurich, Switzerland.

[1]Solar Fusion II, to be published in Rev. Mod. Phys., arXiv:1004.2318.
[2]A. Sallaska *et al.*, Phys. Rev. Lett. **105**, 152501 (2010); Phys. Rev. C, **83**, 034611 (2011).
[3]C. Wrede *et al.*, NSCL PAC35, Proposal 10034.
[4]C. Wrede *et al.*, Phys. Rev. C **82**, 035805 (2010).
[5]B. M. Freeman *et al.*, Phys. Rev. C **83**, 048801 (2011).

annual report, we reported the completion of our analysis of absolute resonance strengths for this reaction. In the past year we have refined our analysis of resonance energies and γ-ray branches, initiated a fruitful collaboration with nova modeler Jordi José, and prepared two manuscripts for publication. The first manuscript reports resonance strengths – that are higher than those from previous measurements by factors of 2.4 to 3.2 – and resonance energies. This manuscript has been published as a Letter[1]. The second manuscript contains a much more detailed discussion of the experiment, reports the branches, and discusses the substantial influence of our measurements on the production of ^{22}Na in hydrodynamic nova models. This manuscript has been published[2]. Anne Sallaska successfully defended her Ph.D. thesis on this work in December of 2010.

3.1.2 Thermonuclear ^{25}Al(p,γ)^{26}Si reaction rate from ^{26}P beta decay

J. Brown[*], R. Casten[†], A. Chen[‡], K. Chipps[§], J. Clark[¶], N. Cooper[†], C. Deibel[‖,¶], A. García, D. Irvine[‡], J. José[**,††], A. Knecht, A. Laird[*], S. Liddick[‡‡], F. Montes[‡‡,‖], A. Parikh[**], H. Schatz[‡‡,‖], K. Setoodehnia[‡], V. Werner[†], and C. Wrede

Observations using space-based γ-ray telescopes have determined that the Galaxy contains roughly 3 solar masses of the radionuclide ^{26}Al and classical novae could contribute significantly to its production. The thermonuclear rate of the ^{25}Al(p,γ)^{26}Si reaction is the largest nuclear-physics uncertainty associated with the production of ^{26}Al in novae. The strength of the key $J^{\pi} = 3^{+}$, ^{25}Al(p,γ)^{26}Si resonance has not been measured directly because intense ^{25}Al beams are not available. Since Γ_p for the corresponding level in ^{26}Si has been measured recently, it is now possible to determine the resonance strength indirectly by measuring Γ_γ/Γ.

The key ^{26}Si level is fed significantly (18 %) in the β decay of ^{26}P and decays primarily via proton emission. We are leading an experiment to measure the β-delayed γ decay of ^{26}P and determine Γ_γ/Γ for this level at the National Superconducting Cyclotron Laboratory (NSCL). We will produce ^{26}P using the in-flight fragmentation of a 150-MeV/u ^{36}Ar beam incident upon a thin Be target. Samples of ^{26}P will be implanted in a segmented Ge detector surrounded by Ge clover detectors to detect γ rays (Fig. 3.1.2-1). Our formal proposal[3] has been approved by the NSCL's PAC35.

[*]University of York, York, UK.
[†]Yale University, New Haven, CT.
[‡]McMaster University, Hamilton, ON.
[§]Colorado School of Mines, Golden, CO.
[¶]Argonne National Laboratory, Argonne, IL.
[‖]Joint Institute for Nuclear Astrophysics.
[**]Departament Física i Enginyeria Nuclear, Barcelona, Spain.
[††]Institut d'Estudis Espacials de Catalunya, Barcelona, Spain.
[‡‡]Michigan State University, East Lansing, MI.

[1]A. Sallaska *et al.*, Phys. Rev. Lett. **105**, 152501 (2010).
[2]A. Sallaska *et al.*, Phys. Rev. C **82**, 034611 (2011).
[3]C. Wrede *et al.*, NSCL PAC35, Proposal 10034.

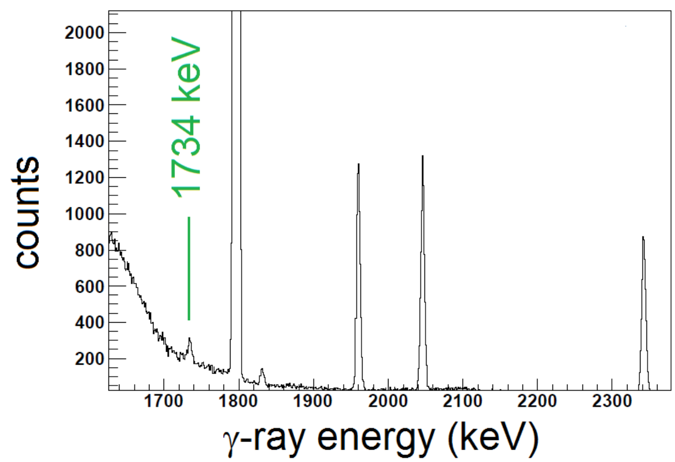

Figure 3.1.2-1. Simulation of ^{26}P β-delayed γ-decay spectrum assuming a very conservative 0.1% absolute ^{26}P β-decay branch for the 1734-keV γ ray of interest.

3.1.3 Measurements of ^{33}S(p,γ)^{34}Cl at nova temperatures: results

B. G. Delbridge, B. M. Freeman, A. García, A. Knecht, A. Parikh*, A. L. Sallaska†, and C. Wrede

Presolar grains are micron-sized grains of material, with isotopic ratios that differ from those in the solar system at large. Classical novae are thermonuclear runaways on white dwarf stars that are potential sources of presolar grains. The ^{32}S/^{33}S isotopic ratio has been suggested as having the potential to provide a clear signature for grains of nova origin. However, the value from models is currently subject to large uncertainties due to insufficient experimental information on the ^{33}S(p,γ)^{34}Cl reaction, the main destruction mechanism for ^{33}S in nova[1]. The ^{33}S(p,γ)^{34}Cl reaction may also be relevant to γ-ray astronomy as ^{34}Cl has an isomeric state (^{34m}Cl E_x = 147 keV $t_{1/2}$ = 32 min), the decay from which has been suggested as a possible nova observable[2].

Since our previous report on this experiment[3], we have finished data analysis and submitted our results for publication[4]. We looked for ^{33}S(p,γ)^{34}Cl resonances at energies suggested by previous experiments[5,6] with the main intent of determining the γ-ray branches. We did not discover any statistically significant branches at recently discovered[5] potential ^{33}S(p,γ)^{34}Cl resonances E_r = 214, 244, 260, 281, 301, 342, and 399 keV. However, we provided the first measurements that include reliable uncertainties of branches for the known

*Physik Department, Technische Universität München, Garching, Germany.
†University of North Carolina, Chapel Hill, NC.

[1] S. Amari *et al.*, Astrophys. J. **551**, 1065 (2001); J. José *et al.*, Astrophys. J. **612**, 414 (2004).
[2] M. D. Leising and D. D. Clayton, Astrophys. J. **323**, 159 (1987); A. Coc, M. Porquet, and F. Nowacki, Phys. Rev. C **61**, 015801(2000).
[3] CENPA Annual Report, University of Washington (2010) p. 60.
[4] B. M. Freeman *et al.*, Phys. Rev. C **83**, 048801 (2011).
[5] A. Parikh *et al.*, Phys. Rev. C **80**, 015802 (2009); A. Parikh private communication.
[6] F. B. Waanders *et al.*, Nucl. Phys. **A411**, 81 (1983).

resonances at $E_r = 432, 492, 529$ keV that are most important for novae. We also provided 18 previously unreported upper limits for branches from these resonances.

3.1.4 Miscellaneous studies of nova nucleosynthesis

C. Wrede and outside collaborators[*,†,‡]

In the past year we have contributed to studies of a variety of reactions that are important for understanding nucleosynthesis in classical novae.

For example, our work on the first direct measurement of the ^{23}Mg(p,γ)^{24}Al reaction using the DRAGON facility at TRIUMF-ISAC was published[1]. This reaction can influence production of the cosmic γ-ray emitters ^{22}Na and ^{26}Al.

In addition, we have investigated the structure of ^{31}S states above the proton-emission threshold in order to constrain the thermonuclear rate of the ^{30}P(p,γ)^{31}S reaction that strongly influences nucleosynthesis in the $A > 29$ region and the identification of presolar nova grains via Si isotopic ratios. These studies of the ^{31}P(^{3}He,t)^{31}S and ^{32}S(d,t)^{31}S reactions have been conducted using the Q3D magnetic spectrograph at Maier Leibnitz Laboratorium. The (^{3}He,t) work has provided crucial spin constraints on known ^{31}S levels and has been submitted for publication[2]. The (d,t) work is expected to yield additional spin constraints after the second experimental run in February 2011.

The ^{29}P(p,γ)^{30}S reaction also influences the expected Si isotopic ratios that are used for the identification of presolar nova grains. In 2007-08 we made measurements of the ^{32}S(p,t)^{30}S reaction using Yale University's tandem Van de Graaff accelerator and Enge magnetic spectrograph to explore the structure of proton-unbound levels in ^{30}S. This experiment has located the two most important resonances in this reaction at nova temperatures. The results were prepared for publication in 2010 and published as a Rapid Communication[3]. The article was also selected for a *Physics* Synopsis.

[*]Work on ^{23}Mg(p,γ)^{24}Al: TRIUMF experiment S810, C. Vockenhuber and U. Greife spokespersons; the collaboration is formed by approximately 30 scientists from Argonne National Lab., Univ. of British Columbia, McMaster Univ., Colorado School of Mines, Tech. Univ. München, Univ. of Northern British Columbia, Simon Fraser Univ., TRIUMF, Univ. of Washington, and Univ. Wien.

[†]Work on ^{31}P(^{3}He,t)^{31}S and ^{32}S(d,t)^{31}S: A. Parikh and A. A. Chen spokespersons, respectively; the collaborations are formed by approximately 20 scientists from Argonne National Lab., Ludwig-Maximilians-Univ. München, Maier-Leibnitz-Lab., McMaster Univ., Tech. Univ. München, Univ. Politecnica de Catalunya, and Univ. of Washington.

[‡]Work on ^{32}S(p,t)^{30}S: K. Setoodehnia, A. A. Chen, J. Chen, S. D. Geraedts, and D. Kahl (McMaster Univ.); J. A. Clark, C. M. Deibel, and P. D. Parker (Yale Univ.); D. Seiler (Tech. Univ. München).

[1]L. Erikson *et al.*, Phys. Rev. C **81**, 045808 (2010).
[2]A. Parikh *et al.*, submitted to Phys. Rev. C.
[3]K. Setoodehnia *et al.*, Phys. Rev. C **82**, 022801(R) (2010).

Nuclear structure

3.2 Overview of the CENPA nuclear structure program

A. García and C. Wrede

During last year we took data to determine the electron capture branch from ^{116}In to contribute to understanding the nuclear structure related to double beta decays[1]. The data analysis is ongoing.

We worked on developments of thin ion-implanted targets which were used for determination of spectroscopic properties of ^{20}Na, ^{24}Al, ^{28}P, ^{32}Cl, and ^{36}K[2]. The motivation was partly from nuclear astrophysics[3] and partly from weak-interactions related studies[4]. In particular the determination of the mass of ^{32}Cl contributed to determining with precision the $T = 2$ multiplet in $A = 32$. Presently we are collaborating with theorists in our department to understand these.

3.2.1 Electron capture on ^{116}In and 2β decay

A. Algora*, J. Äystö†, V. V. Elomaa†, T. Eronen†, A. García, J. Hakala†,
V. S. Kolhinen†, I. D. Moore†, H. Penttilä†, M. Reponen†, J. Rissanen†,
A. Saastamoinen†, S. K. Sjue‡, H. E. Swanson, and C. Wrede

Searches for neutrinoless double-beta ($0\nu\beta\beta$) decay can be used to place limits on the effective neutrino mass under the assumption that the neutrino is its own antiparticle. Such limits are dependent on theoretical calculations of the matrix elements that differ by factors as high as ≈ 2 for each candidate depending on the method employed. However, the calculations may be benchmarked by experimental measurements of certain nuclear properties that are not currently known with sufficient precision. For example, in cases where the parent has $J^\pi = 0^+$ and the intermediate nuclide has $J^\pi = 1^+$ the electron capture-decay branch of the intermediate nuclide provides a valuable constraint. In 2009, we carried out an experiment using CENPA detectors and electronics at the IGISOL facility of the University of Jyväskylä to measure the electron capture-decay branch of ^{116}In to ^{116}Cd, a $0\nu\beta\beta$ decay candidate. In the past year, we have started to analyze the data. We also prepared and submitted an invited manuscript[1] for publication in a special issue of Hyperfine Interactions devoted to the IGISOL facility.

*Instituto de Física Corpuscular, University of Valencia, Valencia, Spain.
†Department of Physics, University of Jyväskylä, Jyväskylä, Finland.
‡TRIUMF, Vancouver, BC, Canada.

[1] A. García *et al.*, submitted to Hyperfine Interactions.
[2] C. Wrede *et al.*, Nucl. Instrum. Methods B **268**, 3482 (2010).
[3] C. Wrede *et al.*, Phys. Rev. C **82**, 035805 (2010).
[4] C. Wrede *et al.*, Phys. Rev. C **81**, 055503 (2010).

3.2.2 Properties of ^{20}Na, ^{24}Al, ^{28}P, ^{32}Cl, and ^{36}K

S. Bishop*, A. A. Chen†,‡, J. A. Clark§, C. M. Deibel§,¶, K. Eppinger*, T. Faestermann*, B. M. Freeman, A. García, R. Hertenberger‖, R. Krücken*, O. Lepyoshkina*, A. Parikh*, G. Rugel*, K. Setoodehnia†, H.-F. Wirth‖, and C. Wrede

In late 2009, we completed precision measurements of the ^{20}Ne(^{3}He,t)^{20}Na, ^{24}Mg(^{3}He,t)^{24}Al, ^{28}Si(^{3}He,t)^{28}P, ^{32}S(^{3}He,t)^{32}Cl, and ^{36}Ar(^{3}He,t)^{36}K reactions using ion-implanted targets developed at CENPA and the Q3D magnetic spectrograph at Maier Leibnitz Laboratorium[1].

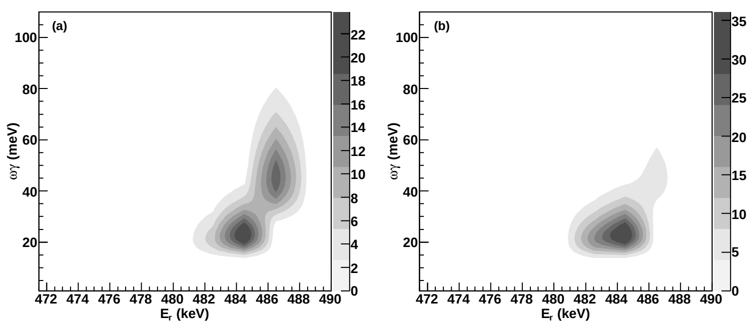

Figure 3.2.2-1. Two-dimensional probability density functions (PDFs) for the strength $\omega\gamma$ and c.m. energy E_r of the lowest energy resonance in the ^{23}Mg(p,γ)^{24}Al reaction. Panel (a) is the result from the direct measurement of Erikson, *et al.*, Phys. Rev. C **81**, 045808 (2010). Panel (b) is a new PDF derived by combining the PDF from panel (a) with the present constraint on resonance energy, $E_r = 482.1(20)$ keV.

In 2010, we investigated the scientific implications of our measurements of the masses and excitation energies of ^{20}Na, ^{24}Al, ^{28}P, ^{32}Cl, and ^{36}K and prepared two publications on this work that have both been published in Physical Review C. The first publication[2] describes our improvements on the Q_{EC} values for the superallowed $0^+ \to 0^+$ β decays of $T = 2$ nuclides. The second publication[3] describes our improvements on resonance energies for radiative proton-capture reactions that occur on unstable nuclides during explosive hydrogen burning in astrophysical environments such as classical novae and type I x-ray bursts (Fig. 3.2.2-1).

*Physik Department, Technische Universität München, Garching, Germany.
†Department of Physics and Astronomy, McMaster University, Hamilton, ON, Canada.
‡DFG Cluster of Excellence Universe, Technische Universität München, Garching, Germany.
§Physics Division, Argonne National Laboratory, Argonne, IL.
¶Joint Institute for Nuclear Astrophysics, Michigan State University, East Lansing, MI.
‖Fakultät für Physik, Ludwigs-Maximilians-Universität München, Garching, Germany.

[1] C. Wrede *et al.*, Nucl. Instrum. Methods B **268**, 3482 (2010).
[2] C. Wrede *et al.*, Phys. Rev. C **81**, 055503 (2010).
[3] C. Wrede *et al.*, Phys. Rev. C **82**, 035805 (2010).

3.2.3 Development of thin ion-implanted targets for precision studies

K. Deryckx, B. M. Freeman, A. García, G. C. Harper, A. S. C. Palmer, D. A. Short, D. I. Will, and C. Wrede

The precision of nuclear-reaction measurements that employ high-resolution magnetic spectrographs for momentum analysis of charged particle-reaction products to determine Q values and excitation energies is often limited by systematic effects associated with target properties that are difficult to characterize. Specifically, the energies of charged-particle reaction products depend sensitively on the target's areal density, uniformity, composition, and composition depth profile. Often the unique chemical properties of a particular element will influence one or more of these factors, complicating comparisons between spectra acquired with targets composed of different chemical elements or compounds (i.e. calibrations).

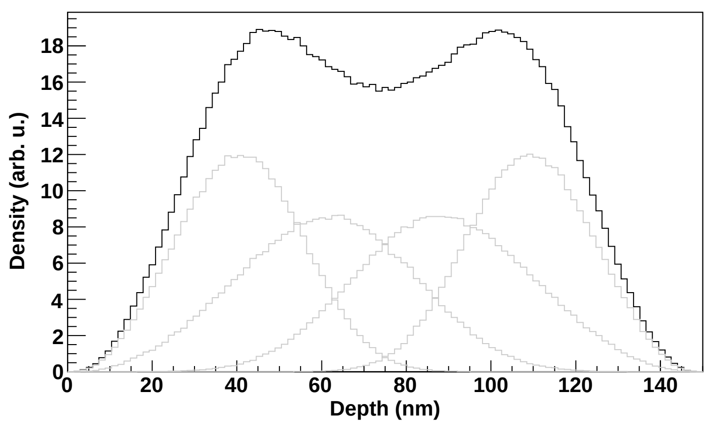

Figure 3.2.3-1. Symmetric depth distribution of ^{24}Mg implanted in a 150-nm thick carbon foil substrate, simulated using the Monte-Carlo code TRIM, with the known energies of 25 keV and 37.5 keV for the incident MgH$^-$, and a C density of 2.00 μg/cm^2. The gray histogram shows the contributions of the four implantation layers individually, assuming they do not interfere with each other, and the black histogram shows their sum.

Historically, thin ion-implanted targets have only been used when special circumstances (e.g. chemistry, radioactivity) have prohibited the use of solid targets prepared by more conventional techniques (e.g. rolling foil, chemical deposition, vacuum evaporation). In order to minimize uncertainties in our precision (^{3}He,t) measurements of masses and excitation energies of ^{20}Na, ^{24}Al, ^{28}P, ^{32}Cl, and ^{36}K with the Q3D magnetic spectrograph at Maier Leibnitz Laboratorium, we prepared similar ion-implanted targets of ^{20}Ne, ^{24}Mg, ^{28}Si, ^{32}S, and ^{36}Ar using thin carbon-foil substrates and the low-energy beam line at CENPA (see Fig. 3.2.3-1). To our knowledge, this is the first time an entire set of ion-implanted targets have been prepared solely to minimize uncertainties associated with target properties. In 2010, our work on this project consisted of preparing a manuscript that has now been published[1].

[1] C. Wrede *et al.*, Nucl. Instrum. Methods B **268**, 3482 (2010).

3.2.4 Calculations of isospin symmetry breaking in nuclei

G. Bertsch*, A. García, T. Lesinski*, and C. Wrede

Recent efforts at CENPA have contributed to precise experimental mass-excess values for the members of the lowest $A = 32$, $T = 2$ quintet. The highly successful quadratic Isobaric Multiplet Mass Equation yields a very poor fit to the data at this level of precision. In order to explain this deviation, we have initiated second-order calculations of isospin symmetry breaking in nuclei. We hope that our calculations will also help to improve isospin symmetry-breaking corrections to the ft values for the superallowed $0^+ \rightarrow 0^+$ β decays that are used to determine the value of the Cabibbo-Kobayashi-Maskawa matrix element V_{ud}.

Accelerator based weak interactions

3.3 Overview of the CENPA accelerator based weak interactions program

A. Knecht

The weak interaction program at CENPA greatly profits from having excellent access to our in-house tandem Van de Graaff accelerator. We follow two approaches: performing dedicated measurements here at CENPA and providing unique support for experiments at external facilities. Over the last year, there were three activities taking place at the accelerator within the field of the weak interaction program.

We are using the tandem accelerator to produce ^{6}He via the reaction ^{7}Li(d,^{3}He)^{6}He. ^{6}He undergoes β decay to ^{6}Li with a half life of 0.8 s and a Q-value of 3.5 MeV. Due to its $0^+ \rightarrow 1^+$ transition, it is a pure Gamow-Teller decay. The fact that it is a relatively simple nucleus facilitates the calculation of nuclear corrections and the theoretical understanding of its decay. In addition, ^{6}He is produced as a neutral noble gas which allows for a simple transport of the atoms away from the production target to a contaminant free and low background environment.

The main goal of our ^{6}He efforts is to measure the $\beta - \nu$ angular correlation and β spectrum. As it is a pure Gamow-Teller decay, only the axial component of the weak interaction should influence the correlation leading to a predicted value of $a_{\beta\nu} = -1/3$ (plus small corrections). By looking for a deviation from that value, or distortions of the β spectrum it is possible to search for tensor contributions in the weak interaction and exotic particles mediating such kind of couplings. The current best measurement of $a_{\beta\nu}$ was performed in 1963 and amounts to -0.3343 ± 0.0030[1]. We plan to improve this 0.9% measurement down to 0.1% by confining the ^{6}He atoms in a magneto-optical trap and detecting the β and recoiling nucleus in coincidence. In addition, we are working on determining the half life of ^{6}He with

*Institute for Nuclear Theory and Department of Physics, University of Washington, Seattle, WA.

[1] C. H. Johnson, F. Pleasonton, and T. A. Carlson, Phys. Rev. **132**, 1149 (1963).

high precision. Although it is quoted as 806.7 ± 1.5 ms, there is a discrepancy of 8.6 ± 1.8 ms between the most precise measured values.

For the UCNA experiment (see Section 2.2.1), we created a special conversion-electron source by implanting ^{113}In into an aluminum substrate using the low energy part of the accelerator and subsequently irradiating it with neutrons at the PULSTAR research reactor to produce ^{114m}In. UCNA measures the β-decay asymmetry by observing the number of emitted electrons with respect to the neutron spin direction. As this number is influenced not only by the underlying β-decay asymmetry but also by the energy of the electrons it is essential to have a well calibrated electron detection system.

A recent experiment measuring the $\beta - \gamma$ angular correlation in the β decay of ^{22}Na with the Gammasphere detector at LBNL[1] suggested a significant discrepancy with the Standard Model prediction. The discrepancy could be explained by a breakdown of the conserved vector current hypothesis and induced tensor (second-class) currents. In order to check some of the assumptions that went into the analysis, we are measuring the M1 width of the 2_1^+ state in ^{22}Na in order to assess the assumed recoil-order correction due to the weak magnetism form factor.

3.3.1 Production of ^{6}He at CENPA

B. G. Delbridge, A. García, G. C. Harper, R. Hong, A. Knecht, Z. T. Lu*, P. Müller*, R. G. H. Robertson, H. E. Swanson, D. I. Will, W. Williams*, C. Wrede, and D. W. Zumwalt

During the last year we had successful beam times during which we tested several improvements to our ^{6}He production scheme. The first concerned loading the lithium into our target cell. In the glove box, under an argon atmosphere, we now load the lithium into a 2.75-inch transfer tube that can be closed off by a valve. In the meantime, we pump down and heat up our target cell. Finally, we vent the target with argon, mount the transfer tube and let the lithium drop into the cell. This way, we were able to greatly reduce contaminations from the target cell that led to chemical reactions with the lithium. The second addition is a rotation and translation feed-through that gets installed once the transfer tube is removed. This allows us to break up any possible surface contamination on the lithium by stirring and to adjust the level of the lithium.

The last addition is a 6-inch diameter transfer tube between the target cell in the production area (cave 2) and a second experimental area (cave 1). A large 300-l/s turbomolecular pump improves the transmission from one cave to the other. The calculated transit time of about 2 s agrees with the measured loss of about a factor 2 - 3 in the number of ^{6}He atoms given the half-life of 0.8 s. Those two areas are separated by a $\sim$ 2-m thick concrete wall. That way we should be able to set up the ^{6}He trapping apparatus in an almost background

*Physics Division, Argonne National Laboratory, Argonne, IL.

[1] C. J. Bowers *et al.*, Phys. Rev. C **59**, 1113 (1999).

free environment. In Fig. 3.3.1-1, we show the measured rates of ^{6}He atoms at the place where the ^{6}He trapping apparatus will be installed. Our initial goal was to reach extracted rates in excess of 10^8 atoms/s reliably. After we achieved that, we were able to justify moving the trapping apparatus from Argonne National Laboratory to CENPA.

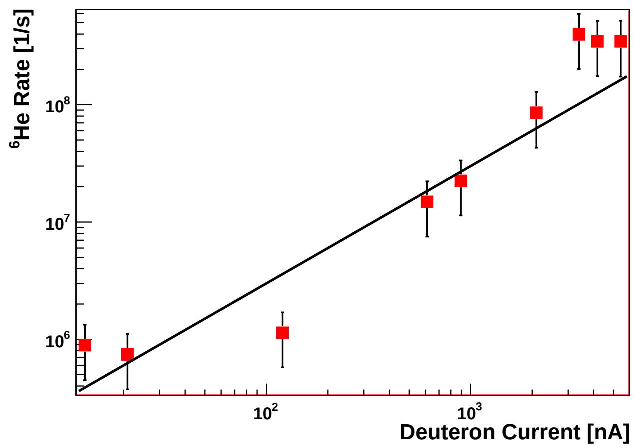

Figure 3.3.1-1. Measured ^{6}He rates in the low background area at the point where the ^{6}He trapping apparatus will be installed

Our plans for this year include installing the trapping apparatus and improving our ^{6}He production even further up to 10^9 atoms/s.

3.3.2 Neutron shield for ^{6}He β decay experiment

B. G Delbridge, A. García, G. C. Harper, R. Hong, A. Knecht, R. G. H. Robertson, H. E. Swanson, S. Utsuno, D. I. Will, C. Wrede, and D. W. Zumwalt

When a deuterium beam hits the liquid lithium target in cave 2 to produce ^{6}He, a large number of unwanted neutrons are also produced that can traverse the opening in the wall to cave 1. Using concrete blocks, solid paraffin wax, and polyethylene, we succeeded in decreasing the radiation level from 1 rem/hour to 10∼40 mrem/hour in cave 1 with a beam current of several μA, but this radiation level was still too high to ensure a safe, long-term working environment and low background level. Our final goal was to decrease the flux of neutrons to reduce the radiation level to below 1 mrem/hr in cave 1. We filled the opening with more concrete blocks, solid wax, and borax powder. We also built a 1”-thick 5%-borated polyethylene shield and set it on metal beams along the wall in cave 1. In addition, we placed several wooden boxes containing paraffin wax and boron around the lithium target in cave 2. Measuring the neutron flux using a Bonner sphere indicated that putting the shielding boxes near the lithium target was a very efficient way to reduce the neutron flux. After installing the aforementioned shielding the radiation level in the working area in cave 1 decreased to approximately 3.0 mrem/hour with a beam current of 3.8 μA. We currently believe that a significant fraction of the neutrons we detected reached cave 1 through an opening in the wall below the floor. In order to prevent these neutrons from passing into cave 1 through the opening, we put several of the shielding boxes both on the floor under the target in cave 2 and in the opening in the basement wall. Soon we will test the effectiveness of our present shielding configuration with the beam on target.

3.3.3 Helium recirculation developments for ^{6}He laser trap

A. García, R. Hong, A. Knecht, Z.-T. Lu*, P. Mueller*, H. E. Swanson, D. I. Will, W. Williams*, C. Wrede, and D. W. Zumwalt

Last year, we reported proposed adjustments to the Magneto-Optical Trap (MOT) to improve overall trapping efficiency. One such improvement was the inclusion of a helium recirculation system. In order to be trapped by the MOT, the helium must first be prepared in a metastable state. Only a small fraction is excited to the appropriate level after passing through an RF discharge tube, and the rest is ordinarily evacuated from the source chamber. However, the trap efficiency can be increased if we can send the remaining helium back through the discharge tube multiple times before the atoms decay.

Our collaborators at Argonne Laboratory have developed such a system to measure and improve recirculation times. After much work, improvements on recirculation times of approximately 2-3 were obtained. Further tuning and improvements may occur at CENPA once the system is put together.

Beyond recirculation, improvements to the trap efficiency include optimizing the transverse cooling lasers which effectively collimate the atomic beam. Another improvement is to bake the source chamber to minimize hydrogen backgrounds. Hydrogen, which is embedded in the walls of the chamber from its manufacturing process, limits the metastable population. Optimization of the transverse beams will take place in Seattle because alignments will be disturbed during the transport. The source will be baked before being shipped to Seattle, which is expected to take place near the end of March.

3.3.4 Precision determination of the ^{6}He half-life

B. G. Delbridge, A. García, G. C. Harper, A. Knecht, R. G. H. Robertson, H. E. Swanson, D. I. Will, C. Wrede, and D. W. Zumwalt

Although much has been discussed on the origin of the quenching of the axial coupling constant, it is not well understood how much of the effect is simply a renormalization of operators due to calculations performed in a finite shell-model space[1], versus a *real* physical effect of the renormalization of the coupling constant. Determinations of the half-lives of the lightest nuclei in combination with 'ab initio' Green Functions Monte Carlo calculations could allow one to disentangle the two effects. Our approach is to use the known ^{3}H and ^{6}He life-times in conjunction with the calculations of Bob Wiringa *et al.* and compare it to the

*Physics Division, Argonne National Laboratory, Argonne, IL.

[1]W.C. Haxton and C.-L. Song, Phys. Rev. Lett. **84** , 5484 (1995).

value extracted for the decay of the free neutron. Although the ^{6}He life-time is quoted as 806.7 $\pm$ 1.5 ms, there is a discrepancy of 8.6 $\pm$ 1.8 ms between the most precise measured values. We have worked towards reducing the error in this measurement by an order of magnitude. This fall we performed our first test run using a new data acquisition setup consisting of a VME crate, Caen ADC and scaler which was fed a 1-kHz clock. We collected data for beam currents ranging from 14 nA to 500 nA, and a beam energy of 17 MeV (see Fig. 3.3.4-1). Additionally we varied our deadtime from 10 μs to 500 μs. These variations resulted in initial ^{6}He decay rates of 0.3 kHz to 58 kHz. From this data we were able to extract half life values and test various analysis methods and error correction routines. These tests allowed us to understand the systematic and experimental errors present in our measurement. In the spring of 2011 we will make a complete measurement of the ^{6}He half life.

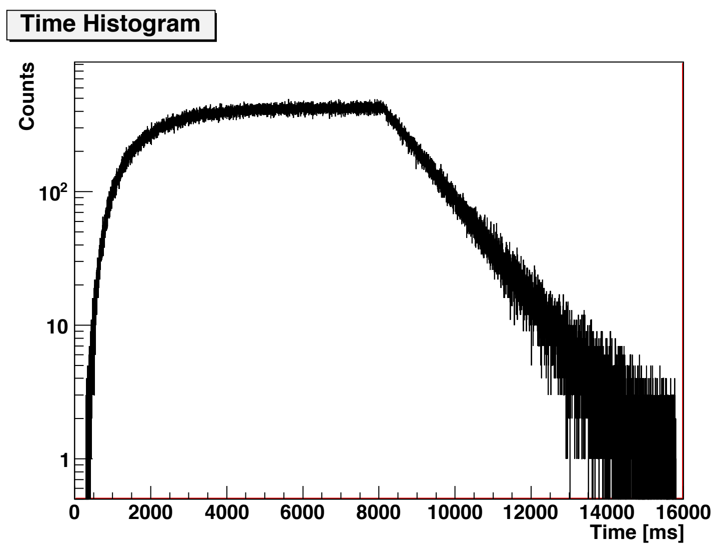

Figure 3.3.4-1. Example of raw ^{6}He decay data obtained from initial test run this fall. This run consists of 110 16-sec beam cycles and was taken with a beam current of 14 nA, and energy of 17 MeV. The deadtime was fixed at 64.4 μs.

3.3.5 Development of a ^{114m}In source of conversion electrons

B. W. Filippone*, A. García, G. C. Harper, S. Lassell†, J. Liu*, M. P. Mendenhall*, A. S. C. Palmer, R. W. Pattie, Jr.†, D. I. Will, C. Wrede, and A. R. Young†

The Ultra Cold Neutron β Asymmetry (UCNA) experiment measures the β asymmetry in polarized neutron decay to extract the axial-vector coupling constant, g_A. The experiment requires energy calibration points up to the β end point of 782 keV. Presently, there are only about five conversion-electron sources in this energy region that are available commercially, limiting the selection of electron energies. The 190.3-keV isomer ^{114m}In ($t_{1/2}$ = 49.5 d) decays to the ^{114}In ground state by internal conversion producing electrons in the energy

*California Institute of Technology, Pasadena, CA.
†North Carolina State University, Raleigh, NC.

range 162 − 190 keV. This potentially useful conversion-electron emitter is not currently available commercially in the form of a calibration source.

We have developed sources of ^{114m}In conversion electrons with customizable specifications by preparing thin samples of ^{113}In using ion implantation and irradiating them with neutrons in a reactor. Isotopically pure samples of ^{113}In were prepared using the low energy-beam line at CENPA by implanting ^{113}In^{16}O^{-} ions into aluminized mylar and pure Al-foil substrates. The implanted foils were irradiated with neutrons in the PULSTAR research reactor at North Carolina State University to produce ^{114m}In via the ^{113}In(n,γ) reaction. Neutron activation analysis was carried out there with a high-purity Ge detector (Fig. 3.3.5-1). Conversion electrons and β particles from the sources were measured using the UCNA spectrometer at the Los Alamos Neutron Science Center of Los Alamos National Laboratory.

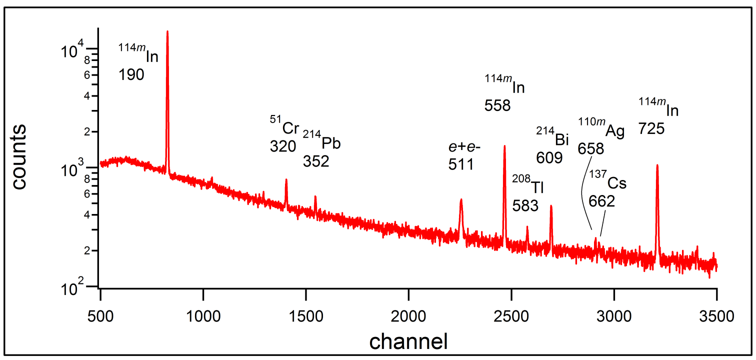

Figure 3.3.5-1. γ-ray spectrum acquired 24 days after a neutron irradiation of the ^{113}In-implanted Al sample. Room background lines include ^{110m}Ag, ^{137}Cs, ^{208}Tl, ^{214}Bi, and ^{214}Pb

In 2010, we carried out the analysis of our source-radiation measurements. CENPA led the preparation of a manuscript on these sources that has been published[1]. We have contacted the University of Washington's Center for Commercialization who encouraged us to submit a Record of Innovation and file a provisional patent. If a licensee for this technology can be found then we will consider obtaining a patent.

3.3.6 M1 width of the 2_1^+ state in ^{22}Na and searches for tensor contributions to beta decays.

E. G. Adelberger, A. Diaz Varela*, M. K. Djongolov†, R. Dunlop*, A. García, G. C. Harper, D. Jamieson*, J. N. Orce†, D. A. Short, S. P. R. Steininger, S. Triambak†, D. M. Williams, and C. Wrede

A determination of the β-γ angular correlation from ^{22}Na beta decay with the GAMMASPHERE array[2] has been used to extract induced tensor current contributions to the weak

*Department of Physics, University of Guelph, Guelph, ON, Canada.
†TRIUMF, Vancouver, BC, Canada.

[1] C. Wrede *et al.*, Nucl. Instrum. Methods B **269**, 1113 (2011).
[2] C. J. Bowers *et al.*, Phys. Rev. C **59**, 1113 (1999).

interaction. The result, together with other available experimental data, yielded an unexpectedly large breaking of the Conservation of the Vector Current (CVC) hypothesis, a fundamental assumption in the Standard Model. A weak link in the data used for this analysis is another recoil-order term, the weak magnetism form factor, which is extracted from an independent unpublished determination of the analog isovector magnetic dipole ($2^+ \rightarrow 3^+$) γ-ray transition strength in ^{22}Na. The state of interest in ^{22}Na at $E_x = 1952$ keV was produced using a ^{25}Mg(p,$\alpha\gamma$) reaction and the results were limited by low statistics[1]. We have run an experiment seeking to improve on the unpublished results by using a ^{21}Ne(p,γ) resonance at $E_p = 1112$ keV. This resonance leads to a γ cascade in ^{22}Na at $E_x = 7800 \rightarrow 1952 \rightarrow 0$ keV. Testing and optimization of our apparatus[2] was completed in summer 2010 and data was collected in September. Angular correlation data were taken to extract the M1-E2 mixing ratio. This in conjunction with the branch determination will allow for a reliable extraction of the M1 width. We are presently running Monte Carlo simulations that will help interpolate our efficiency determinations to extract the needed information.

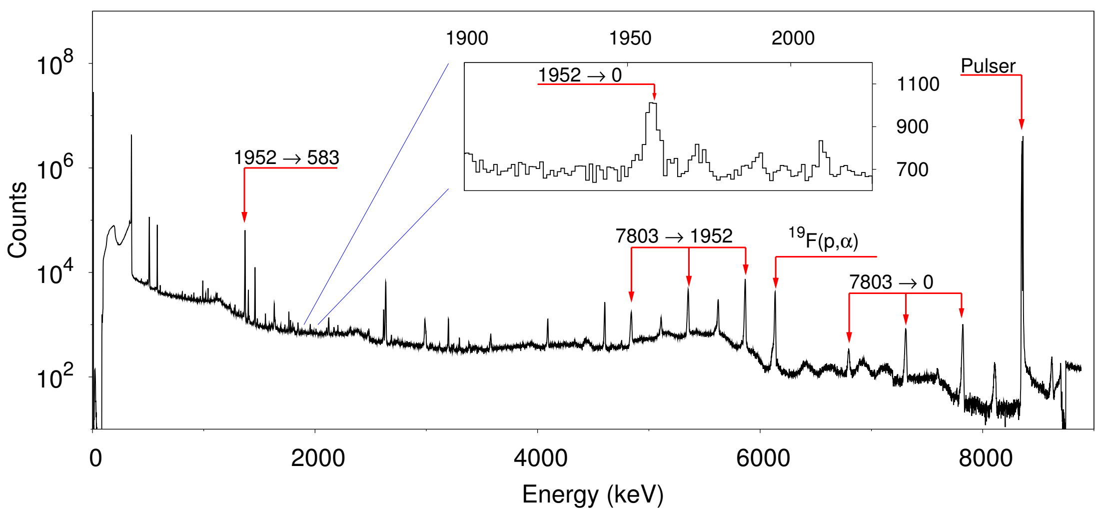

Figure 3.3.6-1. γ-ray spectrum showing observed gammas corresponding to energies in the ^{22}Na cascade. Our largest γ-ray background is from a ^{19}F(p,α) resonance.

[1] R. B. Firestone *et al.*, Lawrence Berkeley National Laboratory No. LBL-12219 (unpublished).

[2] CENPA Annual Report, University of Washington (2010) p. 52.

4 Precision muon physics

4.1 Overview of the muon physics program

J. Crnkovic, D. W. Hertzog, P. Kammel, B. Kiburg*, S. A. Knaack, M. H. Murray, A. Trautner, and P. Winter

The Precision Muon Physics program at the University of Washington (UW) represents a major new entry in the CENPA annual report. The group was formerly located at the University of Illinois at Urbana-Champaign, having moved to UW in the summer of 2010. We remain funded by our NSF medium energy physics grant, but are in transition to direct support of the program under the main CENPA DOE grant in the next funding cycle. The physics program is focused on five experiments involving muons and one analysis project, which is related to standard model theory for the muon $g-2$. These projects are in different stages from nearly complete to very long term development. Three of the experiments utilize the high-intensity muon beams available at the Paul Scherrer Institute (PSI) in Switzerland, and two will be located at Fermilab, representing key elements in the emerging Intensity Frontier initiative at the laboratory. We briefly summarize the projects here and provide details in subsections that follow:

- The MuLan experiment at PSI measured the positive muon lifetime to determine the Fermi constant, G_F. The experiment achieved its design precision goal of 1.0 ppm on the muon lifetime, representing an improvement in precision over any previous generation experiment by a factor of more than 25. The lead analysis was carried out by our graduate student David Webber, who received his Ph.D. in 2010. The final results were published[1] in January, 2011 and a long paper is in preparation. The experiment used a blind analysis technique—which is true for all of our muon projects—finding agreement at the sub-ppm level between two large data sets obtained in different years and under different running conditions. The new Fermi constant, obtained from the average of these data, implies that the weak force is ever so slightly stronger than previously thought (0.00075 percent greater), a result that has been covered well by the press.
- The MuCap experiment at PSI measures the negative muon lifetime in high-purity protium gas. The difference between τ_{μ^-} and τ_{μ^+} (from MuLan) determines the μp capture rate Λ_s. The capture rate can be used to obtain the weak-nucleon pseudoscalar coupling g_P, which is the poorest known of the weak-nucleon couplings, despite being precisely predicted by fundamental low-energy QCD-based theory. The data taking is complete and our first results were published in 2007, marking the first clear and unambiguous measurement of g_P. The result is in good agreement with theory. The final data sample, obtained in 2006 and 2007, is 10 times larger. These data have presented considerable challenges but in February, 2011 a relative unblinding of the two data sets found them to be in excellent agreement. We expect to do the final unblinding

*University of Illinois at Urbana-Champaign, Urbana, IL.

[1] D. M. Webber *et al.*, Phys. Rev. Lett. **106**, 041803 (2011).

in summer 2011. This project is led by Ph.D. candidate Brendan Kiburg in our group and by senior postdoc Peter Winter.

- MuSun is our new effort, built on the MuLan and MuCap techniques developed at PSI. Like MuCap, it is a measurement of the negative muon lifetime in a gaseous tracking chamber. Here we use ultra-pure deuterium and hold the temperature at 30 K to reduce unwanted molecular processes, including muon catalyzed fusion. The capture process on the deuteron is one of the simplest two-nucleon weak interactions and the physics involved has aspects in common with both *pp* fusion in the sun and neutrino breakup of deuterium, as used in the SNO experiment. For all three processes, effective field theory is quite precise, up to an unknown low-energy constant. By establishing a precise measurement for the μd capture rate, we will fix this LEC, which is common for the other two processes; thus, MuSun will help to "calibrate the sun." In the fall of 2011 we completed the commissioning run using a newly developed cryogenic time projection chamber and the full experimental equipment as designed for the physics runs. The data from this run are very encouraging and we have been actively analyzing them, led by UW graduate student Michael Murray. We are preparing a first long "physics run" for summer of 2011.

- One of the strongest hints at new physics is the persistent difference between the measurement and standard model prediction for the muon anomalous magnetic moment. Both are known to ~ 0.5 ppm precision. The current discrepancy $a_\mu(Expt - Thy) = (281 \pm 80) \times 10^{-11}$ is suggestive, but not yet definitive, about new physics at the TeV scale. Because the BNL experiment was statistics limited, we have been proposing a next-generation muon $g-2$ experiment with a factor of 4 or more improved overall precision. In January, 2011 our Fermilab proposal was approved, being endorsed with strong DOE support. Accordingly, we are redirecting our priorities towards the design and implementation of this proposal, which will be a central effort of our group. This includes detector and beamline developments and overall project management. A related project is our analysis of Belle initial-state-radiation data to determine multi-hadron cross sections, which are needed to reduce the uncertainty on the hadronic vacuum polarization contribution to the muon anomaly. Graduate student Jason Crnkovic is nearly complete with the analysis of two channels, which is described separately.

- In the longer term, we anticipate involvement in the approved muon-to-electron conversion experiment—Mu2e—which has the aim of a four-orders-of-magnitude improvement in sensitivity to this forbidden reaction compared to previous efforts. Our group has been official collaborators since its inception and in 2010 we led an experiment at PSI to measure low-energy proton and neutron emission following muon capture in candidate Al and Ti targets. As time permits, we intend to refine these measurements in parasitic operation to our MuSun effort and beamtime. With the approval of $g-2$, we will restrict our Mu2e contributions to "targeted" efforts that have technical overlap with our PSI or $g-2$ developments. Nevertheless, this is a very long-term experiment and we anticipate playing a strong role in the future.

MuCap

4.2 Overview of MuCap experiment physics and technique

D. W. Hertzog, P. Kammel, B. Kiburg*, S. A. Knaack, M. H. Murray, and P. Winter

The elementary electroweak process $\mu^- p \to n\,\nu_\mu$ of ordinary muon capture (OMC) is an excellent probe of the helicity structure of the weak interaction. The OMC process involves $g_V(q_0^2)$, $g_M(q_0^2)$, $g_A(q_0^2)$, and $g_P(q_0^2)$; i.e., the nucleon's vector, magnetic, axial, and pseudoscalar form factors, respectively. The relevant momentum transfer is given by $q_0^2 = -0.88 m_\mu^2$. Since $g_V(q_0^2)$, $g_M(q_0^2)$, and $g_A(q_0^2)$ are well known from other processes, the measurement of the singlet capture rate Λ_S of the OMC process allows for a determination of g_P. This quantity mainly arises from the coupling of the axial current to an intermediate pion. While the derivation of the dominant pion-pole term has been well established, it can now be precisely calculated within heavy baryon chiral perturbation theory and its underlying concept of chiral symmetry breaking. Thus, an experimental confirmation of the predicted ChPT result[1] $g_P = 8.26 \pm 0.23$ is an important test of QCD symmetries.

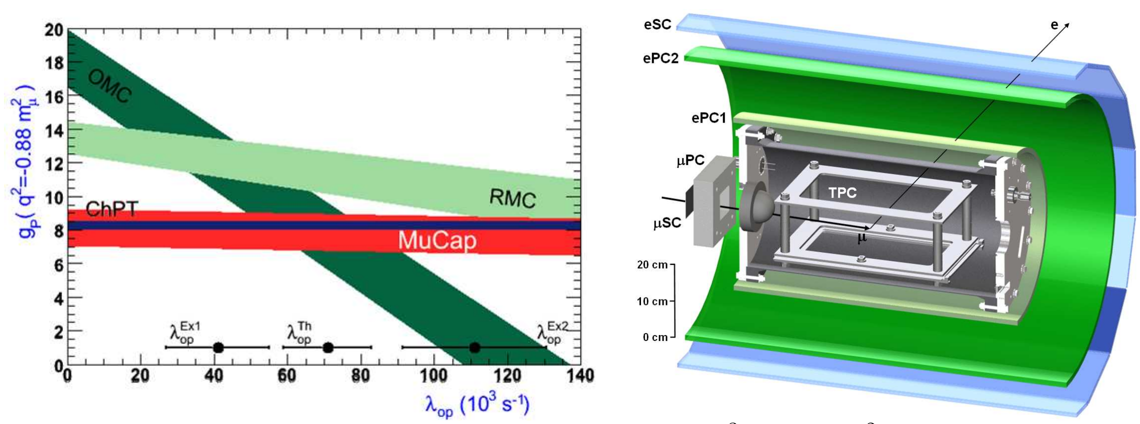

Figure 4.2-1. Left: Previous most precise result from OMC[3] and RMC[2] compared to the ChPT prediction[1] for g_P. Both experiments significantly depend on the poorly known molecular rate λ_{op}. The MuCap result[5] is almost independent on λ_{op} due to the chosen experimental conditions. Right: Simplified experimental setup of the MuCap detector.

The experimental determination of g_P spans a long history including both OMC efforts and one experiment[2] using radiative muon capture (RMC). As can be seen on the left side of Fig. 4.2-1, the interpretation of the data is unclear because the OMC[3] and RMC results depend significantly on the molecular ortho-para transition rate λ_{op}. While details about the formation of $pp\mu$ molecules can be found in reviews[4], it is important to note that the experimental conditions of MuCap using a low-density gas target at 1% liquid hydrogen density

*University of Illinois at Urbana-Champaign, Urbana, IL.

[1] V. Bernard, N. Kaiser, U.-G. Meissner, Phys. Rev. D **50**, 6899 (1994); N. Kaiser, Phys. Rev. C **67**, 027002 (2003).

[2] D. H. Wright *et al.*, Phys. Rev. C **57**, 373 (1998).

[3] G. Bardin *et al.*, Nucl. Phys. A **352**, 365 (1981).

[4] P. Kammel, K. Kubodera, Annu. Rev. Nucl. Part. Sci. **60**, 327 (2010); T. Gorringe, H. W. Fearing, Rev. Mod. Phys. **76**, 31 (2004).

are essential to suppress the relevance of the poorly known rate λ_{op}. The first published[5] MuCap result shown in the same figure reveals our almost negligible dependence on λ_{op} and gives a precise and unambiguous result for g_P in agreement with the ChPT prediction. The analysis of the full statistics of the MuCap experiment will determine the singlet rate Λ_S of the OMC process to 1% precision.

The MuCap detector schematically shown on the right of Fig. 4.2-1 is installed at the end of the πE3 beamline at the Paul Scherrer Institut, Switzerland. Muons produced at the proton target are entering the central time-projection chamber (TPC) where they stop in the hydrogen gas. The muon's arrival is initially registered in the muon entrance scintillator μSC and a two-plane wire chamber μPC. Upon registering a muon arrival, an electrostatic kicker deflects the incoming beam to prevent additional muons from entering the target during a 25-μsec measurement period in the TPC. Pileup of a second muon due to the finite beam extinction is detected in the entrance counters with high efficiency and only leads to a small systematic effect on the lifetime. High purity of the 10-bar ultra-pure hydrogen gas in the TPC was provided by constant circulation through an external cleaning unit[6] reducing chemical contaminants to concentrations of less than 10 ppb. Isotopic purity of better than 6 ppb was achieved by an initial purification using a cryogenic distillation column that separates isotopes based on the difference in vapor pressure for hydrogen and deuterium. Such high elemental and isotopic purity levels are crucial to reduce any effects from capture on non-hydrogen atoms which can distort the result for the singlet rate Λ_S. At our concentration levels, these effects are small and well under control. In addition, the experimental setup enables us to monitor and measure the effects stemming from muon capture on chemical impurities.

The full reconstruction of the muon track by means of the TPC data allows for the selection of muons stopping far away from any wall material. The decay electrons' trajectories are reconstructed in the cylindrical wire chambers surrounding the TPC. A segmented scintillator hodoscope on the outside provides the fast timing information of the decay electrons. The high statistics of $\sim 1.5 \times 10^{10}$ decays allows for a precise measurement of the negative muon's lifetime in hydrogen. The singlet capture rate Λ_S can then be inferred from the difference of the negative muon's lifetime in hydrogen measured in MuCap and the positive muon's lifetime measured in MuLan[7]. After the data for our published result was taken, the MuCap system underwent some important upgrades like the isotopic purification by means of the deuterium separation column, an improved electronics readout system and the integration of the electrostatic kicker. Since then, we have finished collecting the final statistics which will give an improvement in precision by another factor of about 2.5. The analysis of the full statistics as described in the following section (see Sec. 4.2.1) should be finalized by summer 2011 and will give g_P to the final precision of $\sim$7%. A dedicated measurement to reduce one of our main systematic errors in the published result stemming from the uncertainty in the molecular formation rate $\lambda_{pp\mu}$ is described thereafter (see Sec. 4.2.2).

[5] V. Andreev *et al.*, Phys. Rev. Lett. **99**, 032002 (2007).
[6] V. Ganzha *et al.*, Nucl. Instrum. Methods A **578**, 485 (2007).
[7] D. M. Webber *et al.*, Phys. Rev. Lett. **106**, 041803 (2011).

4.2.1 Singlet capture rate analysis

D. W. Hertzog, P. Kammel, B. Kiburg*, S. A. Knaack, M. H. Murray, and P. Winter

The main analysis of the MuCap experiment extracts the lifetime of negative muons stopped in the hydrogen gas in order to infer the singlet capture rate Λ_S for the OMC process. The decay time for each event is given by the time difference of the electron scintillator hodoscope and the muon entrance scintillator and histogrammed to extract the muon's lifetime. The TPC signals allow for a reconstruction of the stopping muon's track. The outgoing decay electron track is reconstructed from the signals of the electron wire chambers. While these muon and electron tracks are not necessarily needed for the timing measurement, they offer crucial handles on suppressing background events that could distort the measured lifetime. One of the most important classes of such events are muons that do not stop in the pure hydrogen gas but in some frame material introducing an additional fast capture time component. Hence, careful studies of the stability of the extracted lifetime for variation of these cut parameters was performed to exclude any significant time-distortions.

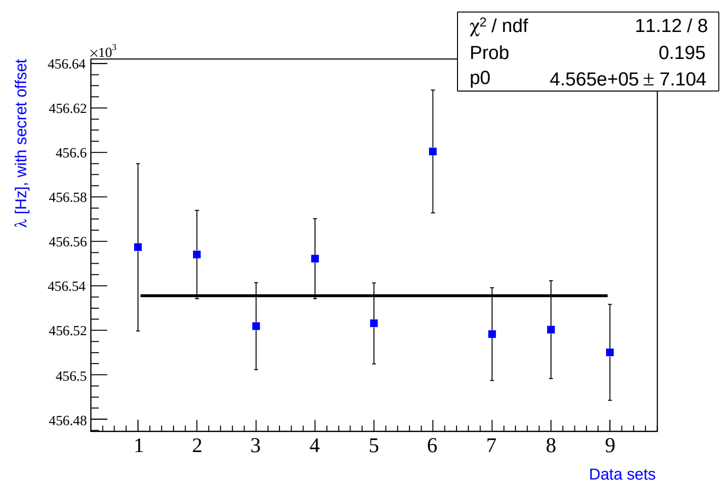

Figure 4.2.1-1. Lifetime versus subsets of our full statistics.

The final statistics resulted in $\sim 1.5 \times 10^{10}$ negative muon decays amounting to a total of 54 TB of stored data. In a first step, the raw information is translated into physical objects like muon and electron tracks. Due to its CPU intensiveness, this stage was only performed twice. The subsequent analysis involved the fine tuning of the selection criteria of muon-electron coincidences. Scanning this highly dimensional parameter space required several iterations of this subsequent analysis. The most crucial part was a careful fine-tuning of the requirements imposed on the muon track. While more stringent cuts would usually improve the suppression of time-distortions caused by physics effects (e.g. such as capture on frame material), they can also couple to subtle detector effects. Hence, a very careful optimization of the quest for stringent cuts due to physics and the necessity of relaxing these to avoid detector related systematics has been the major work over the last year. At this moment,

*University of Illinois at Urbana-Champaign, Urbana, IL.

our second full analysis pass over the entire data has successfully finished. Fig. 4.2.1-1 shows the current status for the lifetime of negative muons in hydrogen versus subsets of the full data. It shows an overall good stability of the lifetime versus groups of different detector performance and TPC gain. To avoid any bias, our clock frequency was blinded with an offset secret to the analyzers. Given the overall very good consistency of our capture rate analysis, we anticipate to unblind this secret offset in summer 2011 and obtain our final result for g_P with $\sim 7\%$ precision.

4.2.2 Molecular transfer analysis

D. W. Hertzog, P. Kammel, B. Kiburg*, S. A. Knaack, M. H. Murray, and P. Winter

As described before (see Sec. 4.2), the MuCap experiment measures the μ^- lifetime in a gaseous hydrogen TPC to obtain the μp singlet capture rate Λ_S. Due to the chosen experimental conditions, corrections to the extracted capture rate originating from the formation of muonic molecules are suppressed compared to measurements in liquid hydrogen but yet they are not entirely negligible. After a muon stops in the TPC and forms a $\mu^- p$ atom, collisions with other hydrogen can lead to the formation of molecular hydrogen $pp\mu^-$ at the rate $\lambda_{pp\mu}$. Muon capture from the molecular state is slower than from the singlet state and $\lambda_{pp\mu}$ must be known to correctly extract Λ_S from the data. The current knowledge of $\lambda_{pp\mu}$ introduces a systematic error contribution that is almost of the same magnitude as the final MuCap statistical precision. Therefore, it is necessary to improve the measurement of $\lambda_{pp\mu}$.

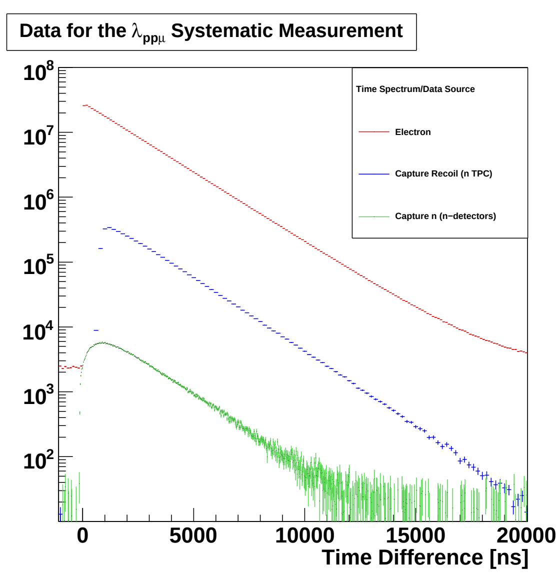

Figure 4.2.2-1. Time spectra of the argon-doped hydrogen data. The electron decay spectra with $\sim 5 \times 10^8$ statistics is shown in red. The histograms in blue and green are the time spectra for the recoiling nuclei (4×10^6) and neutrons (5×10^5) from muon capture onto the Ar nucleus.

*University of Illinois at Urbana-Champaign, Urbana, IL.

A new determination of $\lambda_{pp\mu}$ is in progress based on data obtained using argon-doped hydrogen gas (18.5 ppm atomic concentration) in the TPC which is otherwise operated identically to the undoped data. Argon introduces additional atomic processes involving the muon. These are a transfer rate $\Lambda_{p\mathrm{Ar}}$ from the singlet $\mu^- p$ state that leaves the μ^- in a bound state with the Ar nucleus in an energetically favorable transition, and a capture rate on the Ar nucleus Λ_{Ar}, which is $\sim Z^4$ larger than the Λ_S capture rate. These kinetics are observed in the muon decay electron and the direct capture time spectra, which are then fit to extract the rate $\lambda_{pp\mu}$. Fig. 4.2.2-1 shows the three relevant time spectra of this analysis. The first and highest statistics spectrum is the muon decay electron time distribution, which is the most precise constraint in the fits. The other two spectra are obtained from capture events onto Ar, stemming from the observation of either the capture neutrons or the recoiling nuclei. Currently the analysis for the electron time distribution is at an advanced state. Overall, we expect to measure the effective molecular formation rate to 4%, which is a five fold improvement over the current world average.

MuSun

4.3 Muon capture on deuterium, the MuSun experiment

D. W. Hertzog, P. Kammel, S. Kizigul*, M. H. Murray, and P. Winter

The goal of the MuSun experiment[1] is a measurement of the rate Λ_D for the semileptonic weak process $\mu^- + d \rightarrow \nu_\mu + n + n$ to a precision of better than 1.5%. Λ_D denotes the capture rate from the doublet hyperfine state of the muonic deuterium atom in its $1s$ ground state.

Muon capture on deuteron is the simplest weak interaction process on a nucleus that can both be calculated and measured to a high degree of precision (see the discussion in a recent review of this field[2]). The basic pseudoscalar coupling g_P required for such calculations has been measured by the MuCap experiment and will be more precisely determined by its ongoing final analysis. At the same time, effective field theories (EFTs) have been developed to calculate electro-weak observables in few-body systems, following Weinberg's pioneering work. The standard nuclear physics approach, based on impulse approximation with explicit modeling of two-body current contributions, is being replaced by less model-dependent hybrid EFT[3] and pionless EFT[4] calculations. Several theory groups are preparing fully self-consistent calculations in a rigorous QCD-based EFT scheme.

While μd capture could serve as the benchmark for the axial current interaction in the two-nucleon system, the present experimental situation is inadequate to provide much guidance.

---

*University of Illinois at Urbana-Champaign, Urbana, IL.

[1] http://muon.npl.washington.edu/exp/MuSun.

[2] P. Kammel, K. Kubodera, Annu. Rev. Nucl. Part. Sci. **60**, 327 (2010).

[3] S. Ando, T. S. Park, K. Kubodera, and F. Myhrer, Phys. Lett. **B533**, 25 (2002); P. Ricci, and E. Truhlik, arXiv:1012.2216 (2010); L. E. Marcucci *et al.*, submitted to Phys. Rev. C (2010).

[4] J.-W. Chen, X.-d. Ji, and Y.-c. Li, Phys. Lett. **B620**, 33 (2005).

The best existing experiments[1] are not precise enough and the most precise result differs from modern theory by three standard deviations. If true, such a discrepancy would have major ramifications for important astrophysics processes, which are discussed below. The MuSun measurement, based on novel techniques, should exceed the precision of previous efforts by nearly an order of magnitude.

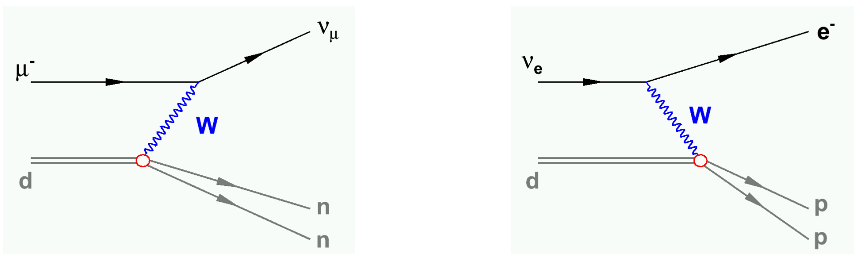

Figure 4.3-1. Muon capture on deuterium (left) and the νd scattering reactions observed at SNO (right), depend on the same weak hadronic matrix element (red circle). The MuSun experiment will determine the low-energy constant that characterizes the short-distance physics in the two-nucleon axial current.

Muon capture on deuterium is closely related to fundamental reactions of astrophysical interest (see Fig. 4.3-1). These include one of the most important nuclear reactions of the universe, *pp* fusion, which is the primary energy source in the sun and the main sequence stars, and the νd reaction, which provided convincing evidence for solar neutrino oscillations at the Sudbury Neutrino Observatory[2]. Direct experiments on the axial-vector interaction within the two-nucleon system are scarce and have not reached the required precision[3]. Here again, the development of EFTs during the last years has led to an important model-independent connection. It was proved that, up to the required precision in the systematic chiral expansion, these weak reactions are related by a two-nucleon current term, whose strength is parametrized by a single, but poorly-known low-energy constant. The constant integrates all the short-distance physics, which is considered the main theoretical uncertainty in these processes. For the foreseeable future, the MuSun experiment is the cleanest and only way to determine this constant to a precision 5 times greater than presently available.

The MuSun experiment must be performed under conditions such that the result leads to an unambiguous extraction of Λ_D, independent of muonic atomic physics complications occurring after the muon stops in deuterium. The transition between the upper μd quartet to the lower μd hyperfine state is slow and, once a $dd\mu$ molecule is formed, nuclear dd fusion occurs at a time scale of nanoseconds (because of the process of muon-catalyzed fusion). Our studies demonstrated that atomic physics uncertainties are reduced to a negligible level at optimized target conditions of T = 30 K and 6% liquid hydrogen density. To achieve such conditions, a new high-density cryogenic ionization chamber filled with ultra-pure deuterium is being developed. This TPC will define the muon stop, identify impurities, and observe muon-catalyzed reactions. The new TPC must have very good energy resolution and full

[1] G. Bardin *et al.*, Nucl. Phys. **A453**, 591 (1986); M. Cargnelli *et al.*, in Proceedings of the XXIII Yamada Conf. on Nuclear Weak Processes and Nuclear Structure, Osaka, Japan, (1989).

[2] B. Aharmim *et al.*, Phys. Rev. Lett. **101**, 111301 (2008).

[3] M. Butler, J.-W. Chen and P. Vogel, Phys. Lett. **B549**, 26 (2002); J.-W. Chen, K. M. Heeger, and R. G. H. Robertson, Phys. Rev. **C67**, 025801 (2003).

analog readout using flash ADCs. This information is critical to avoid systematic uncertainties in the muon stop definition and to detect the charged particles induced by the fusion and impurity capture processes. The 5-times higher target density of MuSun, compared to MuCap, implies that the chamber does not have internal gas gain and that drift voltages up to 100 kV are needed.

In 2010 the MuSun TPC became operational. A short engineering run in spring 2010 demonstrated successful operation of the MuSun detector with the TPC stably working under nominal cryo-conditions. After rectifying several shortcomings of this initial test - in particular noise, spark and grounding issues - the whole system was fully commissioned during 8 weeks of beam time in $\pi E3$ in fall 2010, including several weeks of quality data taking. The progress was recognized by the PSI advisory committee in Feb. 2011. A requested 12-week long beam time in summer 2011 was approved, which should result in the first physics result of MuSun. Moreover, the construction of a new high intensity beam line at PSI was recommended, which should provide optimal conditions for the completion of the experiment during 2012-2013.

4.3.1 TPC performance

D. W. Hertzog, P. Kammel, S. Kizigul*, M. H. Murray and P. Winter

The CryoTPC plays a central role in cleanly measuring the 3-dimensional stopping position of the incoming muons, observing the reaction products of the muon catalyzed fusion branches $dd\mu \rightarrow ^3\text{He}+\mu$ and $dd\mu \rightarrow p+t+\mu$, and monitoring nuclear recoils of typically some 100 keV resulting from muon capture on trace impurities. The TPC vessel is a cylindrical shell capped by a beryllium window on one end, serving as an entrance for the muon beam, and a stainless steel flange on the other end, containing electronic and gas line feed-throughs. With no gas amplification at our operational conditions of 6% LD_2 density and 30K, signals are small and electronic noise minimization and optimal signal processing are essential.

Because the measurement of Λ_D to 1.5% requires measurement of the muon lifetime to 10-ppm precision, even small systematic effects must be well understood and accounted for. Current analysis challenges include defining pulse-fitting and muon track-finding algorithms that are robust against small time-dependent effects on the muon lifetime. As an example, a fusion pulse (see Fig. 4.3.1-1, right) could overlap with the muon signal. If the resulting additional ionization charge enhances the efficiency of selecting a good muon, it would introduce a time-dependent distortion of the lifetime fit. During the commisioning run in 2010, 10% of the full expected data was collected. It is currently being analyzed and used to develop and optimize the analysis algorithms and selection criteria so that systematic distortions of the lifetime fits can be identified and minimized.

*University of Illinois at Urbana-Champaign, Urbana, IL.

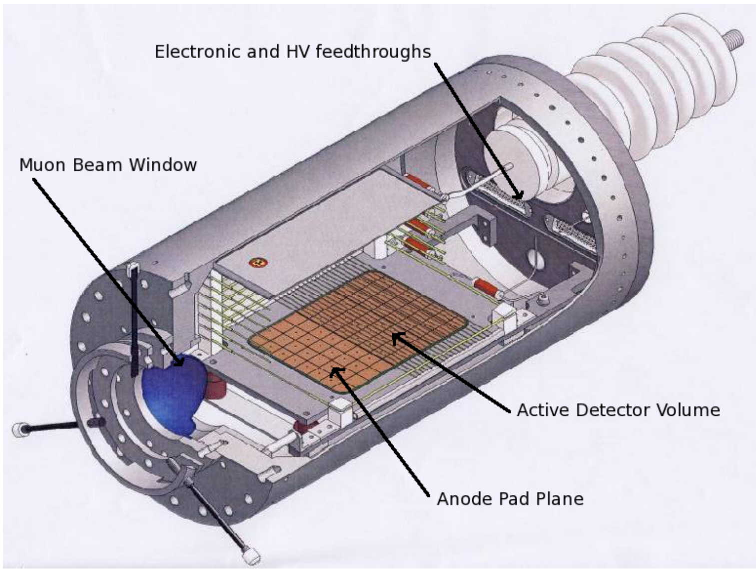

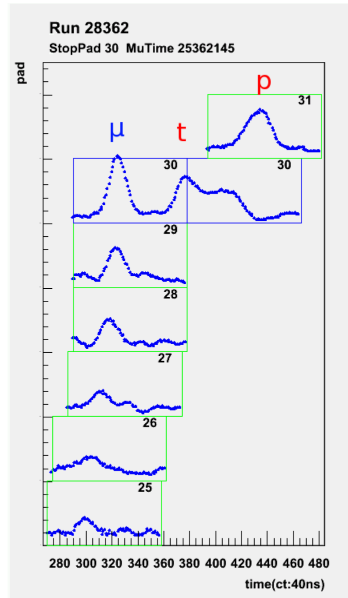

Figure 4.3.1-1. *Left:* TPC drawing. *Right:* Example of TPC signals for a muon stopping. This trace shows muon charge deposition in 6 pads followed by a proton-triton fusion. Such a fusion is catalyzed with 2.5% probability per stopped muon.

g-2

4.4 Overview of the g-2 experiment: physics, technique and project status

J. D. Crnkovic, A. García, D. W. Hertzog, P. Kammel, M. H. Murray, A. Trautner, P. Winter, and T. Zhao

The anomalous magnetic moment of the muon, a_μ, can be calculated and measured precisely. The "$g-2$ test" is a comparison between theory and experiment and it represents one of the most sensitive tests of the completeness of the standard model (SM). The SM theory and the Brookhaven E821 measurement[1] have uncertainties of 0.42 ppm and 0.54 ppm, respectively. The difference, Δa_μ(Expt-SM), is $(287 \pm 80) \times 10^{-11}$, a 3.6 σ significance and a very tantalizing hint of new physics. To establish discovery, a 5 σ or greater level of significance is the generally accepted threshold and to pin down what type of new physics is causing the deviation, a combination of high-energy LHC data and low-energy observables—measured to the highest precision possible—will be required.

The SM error is dominated by quantum loops involving hadrons—hadronic vacuum polarization (HVP) and hadronic light-by-light (HLbL) scattering, with relative uncertainties of 0.35 ppm and 0.22 ppm, respectively. The HVP contribution is obtained from data, principally $e^+e^- \to$ *hadrons* cross sections, which can be folded with a dispersion relation to

[1] Muon G-2 Collaboration: G.W. Bennett*et al.*, Phys. Rev. D73 072003, (2006).

accurately determine a_μ(HVP). The uncertainty is "data driven" and future efforts suggest a reduction to ~ 0.25 ppm in the next 5 years. The HLbL scattering contribution must be determined from low-energy QCD models or from Lattice QCD. A recent workshop[1] held here at the Institute for Nuclear Theory was devoted to improving the accuracy and precision of the HLbL contribution. An outcome of the workshop was the belief that a goal of 0.05 ppm could be achieved on the lattice for HLbL in ~ 5 years, with a byproduct of an independent determination of HVP at a level comparable to the cross section measurements. On the measurement side of the "$g-2$ test," the uncertainty in the BNL experiment was limited by statistics (0.46 ppm). Thus, a new experiment following the proven method will lead to better precision if appropriate conditions are obtained to collect more muon decays, while reducing systematic uncertainties.

We are co-leading the next-generation $g-2$ experiment E989 at Fermilab. The goal is an overall precision of 0.14 ppm. It will be achieved by a data sample more than 20 times larger than BNL, which can be collected in just over 1 year of running. The basic idea of E989 is to relocate the BNL storage ring (Fig. 4.4-1) to Fermilab and to use the accelerator complex to fill the ring 4 times more frequently compared to BNL with a five- to ten-fold stored muon flux improvement per proton and a considerable reduction in beam-related background. An upgraded suite of detectors and associated electronics will be required as well as improvements in the magnetic field mapping system. In 2010, the experiment was reviewed favorably in the DOE's Intensity Frontier Review competition, being rated as the #1 project. Official stage-1 approval by Fermilab came in January, 2011. We have been working with laboratory and DOE management to establish a funding profile and construction timeline ever since. At the time of this update, $g-2$ is scheduled for running beginning in mid 2015.

Figure 4.4-1. Photo of the $g-2$ Storage Ring that will be relocated to Fermilab.

The University of Washington (UW) group has taken on a number of responsibilities in this experiment. We developed many aspects of the beam delivery plan, including design of lattices to transport muons from in-flight pion decay, establishing the baseline pion production

[1] http://www.int.washington.edu/PROGRAMS/11-47w/.

optics, and developing an initial end-to-end flux accounting that determined the rates used in the proposal. Kammel is co-leading the beam team. We have developed a new high-density, ultra-fast electromagnetic calorimeter based on thin sheets of tungsten alternated with ribbons of scintillating fiber. In 2010, we completed a near full-size prototype having 25 independent readouts. The detector was evaluated in the MTest beam at Fermilab, confirming many of the expected properties that were predicted in our prior simulation work. This work has been led by Hertzog and he co-leads the detector team. One of the exciting new ideas is the possibility to read out such calorimeters using the new silicon photomultiplier (SiPM) devices (also known as Geiger mode avalanche photodiodes). SiPMs are immune to magnetic fields, so they can be placed directly on the calorimeter modules inside the storage ring. As they are new, many R&D questions remain before we can commit to their deployment. Tianchi Zhao, a leading detector physicist at UW, has recently joined our effort and is spearheading this development. A modest success is the fact that several SiPMs were used in the MTest experiment on one of the sub-modules, obtaining equally good performance compared to PMTs. With approval of E989, additional members are joining from UW, including faculty member Garcia. Finally, we note that Hertzog was elected co-spokesman of the experiment.

4.4.1 Current Status of Cross Section Measurements via ISR at Belle

J. D. Crnkovic, D. W. Hertzog, and A. Trautner

Comparing the current standard model (SM) prediction of the muon anomalous magnetic moment (a_μ) to measurement has hinted at the possibility of new physics. The SM contribution to a_μ with the largest current error is the leading-order hadronic vacuum polarization (HVP). The HVP has low-energy (up to 2 GeV), non-perturbative components that are currently calculated from data using exclusive cross sections of electron-positron to hadrons, $\sigma(e^+e^- \to hadrons)$. Components of the HVP contribution can also in principle be calculated from τ-spectral functions. For the case of an isovector (I=1) $\sigma(e^+e^- \to hadrons)$, it is possible to calculate $\sigma(e^+e^- \to hadrons)$ from the corresponding $\tau \to hadrons\ + \nu_\tau$ by the assumptions of isospin invariance and the conserved vector current relations[1]. The final state hadron system in both cases is the same except for one less charged hadron in the τ case to account for the τ having a charge. For instance, $\tau^- \to \pi^+\eta\ \nu_\tau$ corresponds to $e^+e^- \to \pi^+\pi^-\eta$. Historically there have been significant differences between the predicted $(g-2)_\mu$ from the e^+e^- data vs. the τ data[2]. Better precision measurements of (I=1) $\sigma(e^+e^- \to hadrons)$ and the corresponding τ-spectral functions may be needed to help resolve this discrepancy. Theoretical work on this discrepancy has continued, and a recent breakthrough has been reported that effectively moves the τ data into excellent agreement with the e^+e^- data[3].

The direct method of obtaining these cross sections is to vary the center-of-mass energy of the initial electron-positron system. Fixed-energy colliders, such as B-factories, can alternatively use events having a high energy initial state radiation (ISR) photon. The ISR photon

[1] R. Alemany, M. Davier and A. Hocker, Eur. Phys. J. C **2**, 123 (1998) [arXiv:hep-ph/9703220].
[2] F. Jegerlehner, Acta Phys. Polon. B **38**, 3021 (2007) [arXiv:hep-ph/0703125].
[3] F. Jegerlehner and R. Szafron, arXiv:1101.2872 [hep-ph].

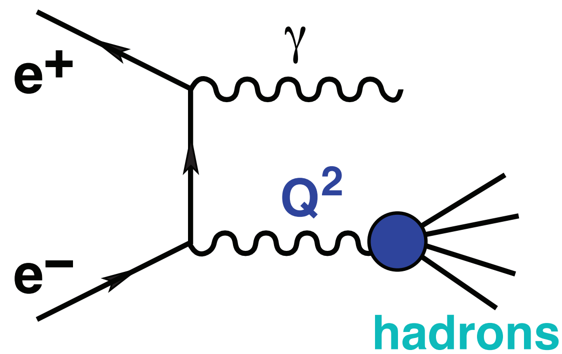

Figure 4.4.1-1. Leading-order Feynman diagram for ISR.

lowers the effective invariant mass of the hadron system. Fig. 4.4.1-1 shows the leading-order ISR Feynman diagram.

The $\sigma(e^+e^- \rightarrow \pi^+\pi^-\pi^0)$ and $\sigma(e^+e^- \rightarrow \pi^+\pi^-\eta)$ are two such HVP contributions to a_μ. The $\pi^+\pi^-\pi^0$ channel provides the second largest contribution to a_μ[1], and the $\pi^+\pi^-\eta$ channel has a corresponding τ-spectral function for comparison. The relative contribution of $\pi^+\pi^-\eta$ channel to a_μ is small, but relevant to the precision goals of the new Fermilab E989 experiment[2]. The aim of our current research is to precisely measure both of these cross sections using the ISR method on Belle data obtained at the KEK-B factory in Tsukuba, Japan. Preliminary cross sections for these two processes have been calculated. The major focus of the analysis is now to carry out systematic studies. There are also recent efforts to locally calculate components of the HVP contribution from the cross section measurements. This work has been extended into a detailed examination of the output from the PHOKHARA next-to-leading-order ISR event generator. The hope is to gain a better local understanding of ISR physics and its effect on cross section measurements by ISR. This work forms the basis of the thesis for Illinois Ph.D. student Crnkovic.

[1] M. Davier, A. Hoecker, B. Malaescu, Z. Zhang, Eur. Phys. J. C (2011) 71: 1515.

[2] `http://gm2.fnal.gov/public_docs/proposals/Proposal-APR5-Final.pdf`.

5 Axion searches

ADMX[1]

5.1 ADMX axion search

M. Hotz, D. Lyapustin, L. J Rosenberg, G. Rybka, A. Wagner, and D. I. Will

The Axion Dark Matter eXperiment (ADMX) is a large-scale RF-cavity search for galactic dark-matter axions. This experiment has been in operation since the mid-1990s, and has recently completed the "Phase I" upgrade and data-taking run. This goal of this upgrade was to significantly improve the experiment sensitivity by replacing the key technology in the experiment, cryogenic microwave amplifiers, with Superconducting Quantum Interference Device (SQUID) amplifiers. This upgrade was successful and the first-year data set has been published. The experiment has been moved to CENPA from Lawrence Livermore Lab, and is being upgraded again to increase further the sensitivity. This "Phase II" upgrade, sited at CENPA, will be a "definitive" experiment: it will have sufficient sensitivity to either detect or rule out the QCD-axion hypothesis at high confidence.

The axion was postulated three decades ago to explain why QCD conserves the discrete symmetries P (parity) and CP (charge conjugation times parity). QCD's predictions depend upon a parameter θ. When θ differs from zero, QCD violates P and CP. Since the strong interactions appear P- and CP-symmetric in the laboratory, θ must be very small. The upper limit on the neutron electric dipole moment requires $|\theta| < 10^{-10}$. However, in the Standard Model, P- and CP-violation by the weak interactions feeds into the strong interactions so that the expected value of θ is of order unity. The inability of the Standard Model to account for P- and CP-conservation by the strong interactions is called the "strong CP problem". Peccei and Quinn proposed a solution to this problem in which the Standard Model is modified whereby θ becomes a dynamical field and relaxes to zero. The theory's underlying broken continuous symmetry results in the existence of a new particle, called the axion. The axion is the quantum of oscillation of the θ field and has zero spin, zero electric charge, and negative intrinsic parity. So, like the neutral pion, the axion can decay into two photons.

However, despite of the prodigious local density of dark-matter axions (in the neighborhood of 10^{14}/cc), the expected electromagnetic signal would be extraordinarily weak, around 10^{-23} Watts in the ADMX apparatus. Our present ADMX Collaboration (with original core institutions Washington, LLNL, Florida, NRAO and Berkeley) constructed and operated a large-scale dark matter axion experiment that, for the first time, reached sensitivity to plausible dark-matter axions. This experiment consists of a large microwave cavity immersed in a static magnetic field. Nearby galactic halo axions scatter off the static field and convert into microwave photons within the cavity. The present ADMX experiment, fitted with SQUID amplifiers in the Phase I upgrade, has just completed a scan of the $1.9 - 3.5$-μeV axion mass range. The ADMX detection apparatus is essentially an extraordinarily low-noise

[1]ADMX is supported by the DOE Office of High-Energy Physics and makes use of CENPA resources by recharge to the cost center.

radio receiver with a RF cavity forming a tuned tank circuit. A short electric-field probe couples power from the cavity into a cryogenic amplifier, which is cooled to near the cavity temperature, (around 2 K for the original ADMX and Phase I upgrade).

The motivation for lowering the system noise temperature is clear: (i) for a given axion-photon coupling, the scan rate grows as the square of the system temperature, and (ii) for a given scan rate, the power sensitivity which can be reached increases linearly at the system temperature. In ADMX the system noise temperature is essentially the noise temperature of the amplifier plus the cavity physical temperature. We developed SQUID amplifiers in the 100-1000-MHz range specifically for ADMX and this development allowed more than an order-of-magnitude reduction in system noise temperature. We have retrofitted these SQUIDs (but not yet a dilution refrigerator) to ADMX for the Phase I upgrade and published the results.

Commissioning of the Phase I experiment began in 2007, and the first LHe cool-down was on September 20, 2007. In January 2008, in-situ SQUID amplification was demonstrated, where a weak test-signal injected into a weakly-coupled cavity port was tracked through the full receiver chain. Shortly thereafter, field cancellation using the bucking coil was confirmed to over 7 Tesla in the main coil. By the summer of 2008, operation of each component of the new Phase I system had been demonstrated and science data-taking began.

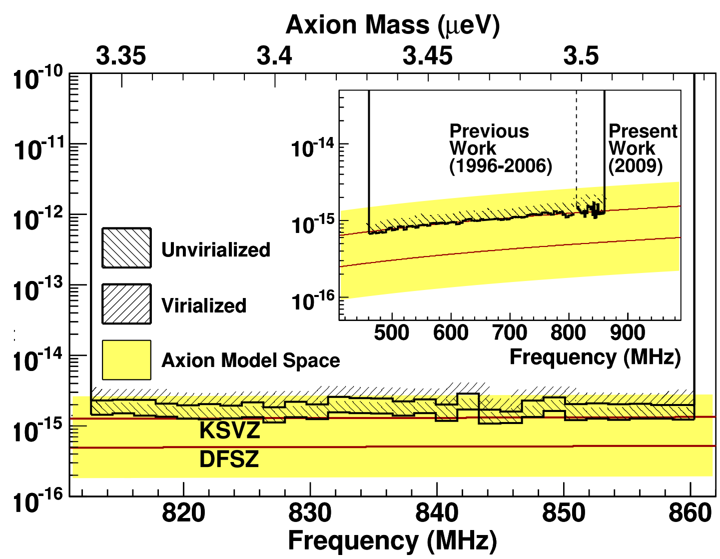

Figure 5.1-1. Axion mass and coupling limits from Phase I upgrade.

As of Feb 2011, the Phase I upgrade has scanned the previously unexplored axion mass region of 812-890 MHz at the "KSVZ" level of sensitivity (one of two benchmark axion models). All technical goals were met and had characterized the RF and cryogenic systems. The first results from this experiment were published in a Physical Review Letter, where we have reported results from the medium-resolution data channel at KSVZ sensitivity. This publication[1] marked the last major milestone of the Phase I program (Fig. 5.1-1).

[1]S. J. Asztalos *et al.*, Phys. Rev. Lett. **104**, 041301 (2010).

Since ADMX is the most sensitive microwave receiver in the world, it is ideal to search for weakly-coupled beyond-standard-model particles besides axions. One such study is a search for scalar chameleons. Chameleons are nonlinearly self-coupled particles whose mass depends on the local density of matter. They are conjectured to play a role in the dark energy of our universe, but their unusual properties evade detection by the short-range gravity experiments traditionally used to search for new light scalars. A different approach is to search for photon-chameleon-photon mixing using the "afterglow" effect, so-called because the slow decay of chameleons after their production by photons may cause a residual "glow" of photons after a source is removed. The GammeV experiment at FNAL used the absence of "afterglow" in their apparatus to exclude a limited region of chameleon-photon coupling parameter space for a range of masses.

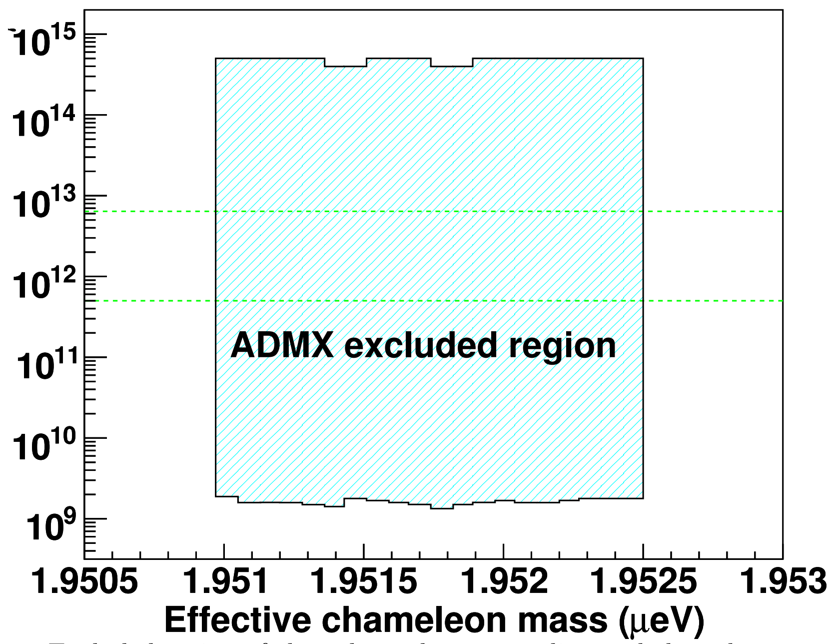

Figure 5.1-2. Excluded region of chameleon-photon coupling and chameleon masses from the chameleon-search operation of ADMX. Results from a FermiLab experiment are also shown as dotted green lines for comparison.

The ADMX experiment was run for one day in a configuration to search for chameleon scalars. In this experiment, an RF source was used to excite the TE_{010} mode of the ADMX RF cavity for a period of 10 minutes. During this period, photons in the electromagnetic cavity mode would have mixed with chameleons in an approximately similarly shaped chameleon mode. The RF source was then shut off, and the usual high-sensitivity ADMX receiver chain recorded the power spectrum of the ADMX cavity over another 10 minutes. The cavity resonance was shifted and the process repeated. With these data, we were able to exclude a large region of chameleon-photon coupling over a range of chameleon masses. That such a short run produced this result demonstrates the power for these searches of having high sensitivity to electromagnetic radiation. The results of this search were published this year[1] (Fig. 5.1-2).

[1]Rybka *et al.*, Phys. Rev. Lett. **105**, 051801 (2010).

Another search for beyond-standard-model particles using ADMX is a search for hidden sector photons. These particles arise in theories with extra hidden symmetries. Such new photons behave like extremely weakly-coupled photons having mass. These low-mass hidden sector photons may mix with normal photons, and this mixing can be exploited in a search by the use of two microwave cavities tuned to the same frequency. If one cavity is excited by a signal source, the photons in the cavity may mix with hidden sector photons, which due to their feeble coupling to normal matter and radiation, are then free to escape the cavity. They may then reconvert to photons in the other cavity, thereby providing a means to weakly-couple the two cavities. Additionally, this search is able to take place during normal axion-search operations with only the addition of a source cavity tuned to the frequency of the detector cavity. A demonstration run of this type of search has been completed and published this year[1] (Fig. 5.1-3). Note how competitive is the short ADMX test-run result, another consequence of the high sensitivity of ADMX to electromagnetic radiation.

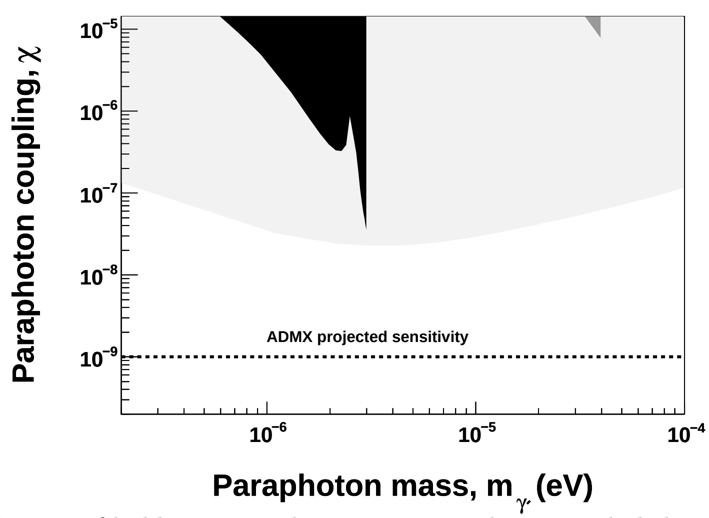

Figure 5.1-3. Region of hidden-sector photon mixing and mass excluded at 95% confidence by the ADMX demonstation is shown in black. Results from a similar cavity experiment reported this year are shown in light grey, and the exclusion from indirect measurements of Coulomb's law are shown lightly shaded.

In summer of 2010, the ADMX main magnet was moved to CENPA (Fig. 5.1-4) and successfully ramped to operating field as a demonstration of functionality. The east end of the accelerator tunnel is being prepared to install the magnet and support equipment, and the next generation insert is being designed. Fabrication of the insert will begin by the end of the year. In the meantime, more sophisticated analyses of Phase I data are being performed by graduate students.

[1]Wagner *et al.*, Phys. Rev. Lett. **105**, 171801 (2010).

Figure 5.1-4. Doug Will observes as the ADMX magnet cryostat is unloaded at CENPA.

Axion torsion balance experiment

5.2 Improved constraints on an axion-mediated force

E. G. Adelberger, F. Fleischer, B. R. Heckel, and S. A. Hoedl

After extensive analysis and investigation of systematic effects, we have published a result[1] from our torsion-balance axion-search. As shown in Fig. 5.2-1, we were able to improve existing limits on a parity and time-reversal violating force mediated by axion-like particles with masses lying in the astrophysical window by up to 10 orders of magnitude. This challenging experiment was limited by systematic effects, especially by a large degauss scatter between data-taking cycles. The figure also shows the sensitivity achievable with a pendulum operating at the room temperature thermal noise limit, which motivates us to develop an upgraded version of the apparatus (see Sec. 5.3).

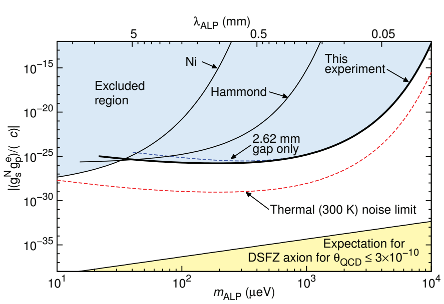

Figure 5.2-1. Experimental 95% confidence upper limits on a parity and time-reversal violating force. The force mediated by the DFSZ axion would appear below the bottom-most line. The thermal noise limit represents an ideal torsion pendulum with a magnet-on Q of 3000.

[1] S.A. Hoedl, F. Fleischer, E.G. Adelberger, B.R. Heckel, Phys. Rev. Lett. **106**, 041801 (2011).

5.3 A magnet upgrade for the "axion" torsion-balance experiment

E. G. Adelberger, F. Fleischer, B. R. Heckel, C. D. Hoyle* and H. E. Swanson

The search for axion like particles (ALPs) using a torsion balance is discussed in this and previous CENPA annual reports[1,2,3] and a recent publication[4].

The dominant contribution to statistical errors in Ref 4 came from nonreproducible effects in the demagnetizing procedure. We are upgrading the instrument, beginning with the magnet. The new magnet will be made from perfection annealed CO-NETIC AA which has a high permeability and a low saturation field and should achieve more reproducible demagnetized states.

Semicircular laminations are cut from sheets of 1/16th-inch material using electric discharge machining to preserve its annealed status. The magnet core is assembled by alternating the laminations with strips of 1.5-mil Integral adhesive film cut to the same shape. The assembled half cores are clamped and heated above 120°C to bond the laminations together. The completed core has an outer diameter of 12 cm, an inner diameter of 6 cm with pole faces that are 3 cm × 3 cm. The adhesive film is non-conducting so any eddy currents produced while demagnetizing the core are constrained to the thickness of the individual laminations and are therefore negligible. The completed core sections are shown in Fig. 5.3-1.

Figure 5.3-1. The completed core sections with the laminations clearly visible

The coils will be wound on 4 individual coil forms, each forming about one quarter of a hollow torus that slides over the core. We are currently in the process of winding these coils.

*Department of Physics, Humbolt State University, Arcata, CA.

[1]CENPA Annual Report, University of Washington (2011) p. 45.
[2]CENPA Annual Report, University of Washington (2010) p. 59.
[3]CENPA Annual Report, University of Washington (2009) p. 42.
[4]S.A. Hoedl, F. Fleischer, E.G. Adelberger, B.R. Heckel, Phys. Rev. Lett. **106**, 041801 (2011).

6 Relativistic Heavy Ions

6.1 UW URHI program overview

D. T. Kettler, D. J. Prindle, and T. A. Trainor

This activity emphasizes the study of two-particle angular and transverse momentum (p_t) correlations from nuclear collisions at the relativistic heavy ion collider (RHIC). Unique features of the program include construction of *minimum-bias* angular correlations (no special p_t cuts), implementation of a *per-particle* correlation measure, application of angular *autocorrelations* adopted from linear time-invariant (LTI) systems analysis, accurate A-A centrality determination extended to very peripheral A-A (∼N-N) collisions directly comparable to p-p collisions, utilization of a *Glauber linear superposition* (GLS) reference system based on p-p data and representation of A-A centrality by *mean participant path length* $\nu = 2N_{part}/N_{bin}$.

Our model-independent analysis of the structure of angular autocorrelations and p_t correlations has revealed two major components, interpreted subsequently as minimum-bias jets (minijets) and an azimuth quadrupole conventionally interpreted as elliptic flow. Minijet angular correlations dominate the quadrupole structure. Interpretation of correlations has required extension of our research program to differential studies of single-particle p_t spectrum structure and construction of parton fragment distributions from pQCD parton scattering cross sections and parton *fragmentation functions*. We have established a self-consistent description including three elements: correlations, single-particle spectra and pQCD theory.

Significant jet-related discoveries include an unexpected large minijet abundance in more-central Au-Au collisions which contradicts claims of jet quenching and parton thermalization to a dense partonic medium, strong elongation on pseudorapidity η of the same-side jet peak in Au-Au angular correlations, strong elongation of the same-side peak on azimuth ϕ in p-p collisions and a *sharp transition* in jet correlation properties at a Au-Au centrality corresponding to a per-event jet multiplicity per unit η comparable to unity.

Significant azimuth-quadrupole-related discoveries include factorization of the per-particle p_t-integral quadrupole amplitude on centrality and collision energy. The centrality variation is determined only by fractional impact parameter b/b_0 approximately independent of system size A. The collision-energy dependence above 13 GeV is a simple linear function of $\log\{\sqrt{s_{NN}}\}$. Study of the p_t dependence of the azimuth quadrupole reveals a further factorization. Our p_t-differential v_2 data obtained from fits to 2D angular correlations can be expressed in terms of a *quadrupole m_t spectrum* from a boosted source. The source boost distribution is approximately independent of Au-Au centrality and strongly contradicts a Hubble flow collective expansion description. The quadrupole m_t spectrum common to several hadron species is nearly Maxwell-Boltzmann, with a low temperature $T \approx 0.1$ GeV.

This combination of several novel results strongly suggests that the conventional description of RHIC data in terms of formation of a strongly-coupled dense, thermalized partonic medium is incorrect. Instead, RHIC collisions appear to be nearly transparent to low-energy partons, but the color field geometry is strongly affected leading to substantial changes in jet systematics. The azimuth quadrupole is surprisingly insensitive to the A-A environment, depending only on the geometry of two intersecting spheres independent of absolute size. A significant quadrupole component in p-p collisions is consistent with our data.

6.1.1 Minijets (minimum-bias jets) in correlations and spectra

Quantitative understanding of parton fragment distributions in RHIC collisions was significantly advanced with our discovery of the spectrum hard component in p-p collisions[1], leading to the realization that characteristic features representing minimum-bias parton scattering and fragmentation (minijets) are directly accessible in spectra and correlations. To better understand minijet phenomenology we conducted a detailed study of parton fragentation in e^+-e^- collisions[2]. The apparent abundance of minijets in more-central Au-Au collisions conflicts with the picture of a dense flowing medium nearly opaque to low-energy partons. We therefore searched for evidence of radial flow in a differential study of single-particle p_t spectra but instead found that structure previously identified as evidence for radial flow matches the properties of parton fragment distributions—spectrum hard components[3]. Combining two-component spectrum analysis with a pQCD description of parton fragmenation lead to a quantitative description of A-A spectrum hard components as fragment distributions[4].

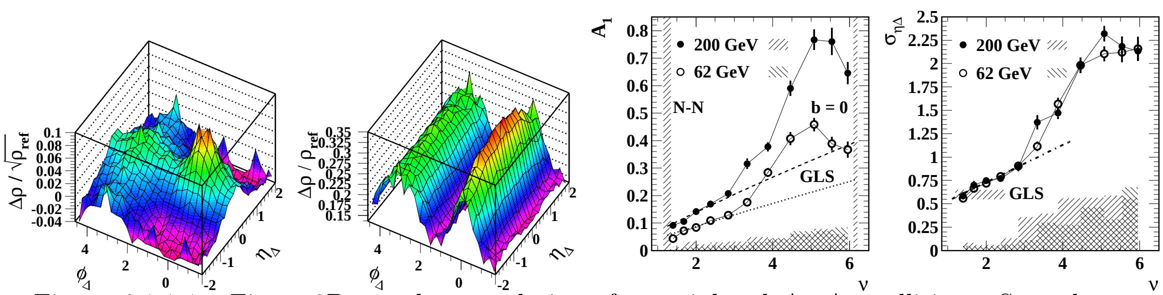

Figure 6.1.1-1. First: 2D angular correlations for peripheral Au-Au collisions, Second: Angular correlations for central Au-Au collisions, Third: Amplitude of the same-side 2D jet peak, Fourth: η width of the same-side 2D peak.

Fig. 6.1.1-1 shows examples of *minimum-bias* (no "trigger-associated" p_t cuts) angular correlations dominated by minijets which directly correspond to single-particle p_t spectra. The centrality evolution of the minijet structure exhibits several remarkable features. 1) Minijet correlations follow the Glauber linear superposition (GLS) trend up to a particular centrality. 2) At that centrality the same-side jet peak (intrajet correlations) undergoes a sharp transition: 3) the jet peak amplitude A_1 increases much faster than N-N binary collisions and 4) the η width of the same-side peak σ_{η_Δ} greatly increases. 5) The ϕ width of the same-side peak (not shown) actually decreases.

We have recently provided a quantitative description of the relationship among jet an-

[1] J. Adams *et al.* (STAR Collaboration), Phys. Rev. D **74**, 032006 (2006).
[2] T. A. Trainor and D. T. Kettler, Phys. Rev. D **74**, 034012 (2006).
[3] T. A. Trainor, Int. J. Mod. Phys. E **17**, 1499 (2008).
[4] T. A. Trainor, Phys. Rev. C **80**, 044901 (2009).

gular correlations, spectrum hard components and pQCD[1]. The importance of the minijet scenario for the interpretation of RHIC collisions is indicated by the intensity of some recent responses. We have provided rebuttals to some of the more significant initiatives[2]. We have also demonstrated the effects of using flawed v_2 data to estimate backgrounds in dihadron correlation analysis: severe underestimation of jet yields and strong distortion of jet correlations leading to inference of "Mach cones[3]." We have reviewed evidence presented in support of hydro interpretations of RHIC collisions in constrast with our increasingly detailed quantitative understanding of minimum-bias jets. We conclude that some claimed hydro phenomena should be reinterpreted in terms of parton fragmentation, and other phenomena are inconsistent with hydro expectations and may represent a new QCD phenomenon[4].

6.1.2 The azimuth quadrupole in correlations and spectra

The other major component of minimum-bias angular correlations is the azimuth quadrupole conventionally intepreted as elliptic flow. We first completed p_t-integral measurements of quadrupole measure $v_2\{2D\}$, where $2D$ denotes inference of v_2 from model fits to 2D angular correlations[5]. The 2D method provides the first accurate separation of jet-related structure (nonflow) from the non-jet quadrupole associated with intial-state geometry. Fig. 6.1.2-1 (left panels) shows p_t-integral $v_2\{2D\}$ data exhibiting very simple centrality and energy systematics including *factorization* of the two trends. The $v_2\{2D\}$ systematics share no common features with minijet centrality systematics, providing one of several strong arguments against the reality of a dense, flowing partonic medium opaque to low-energy partons.

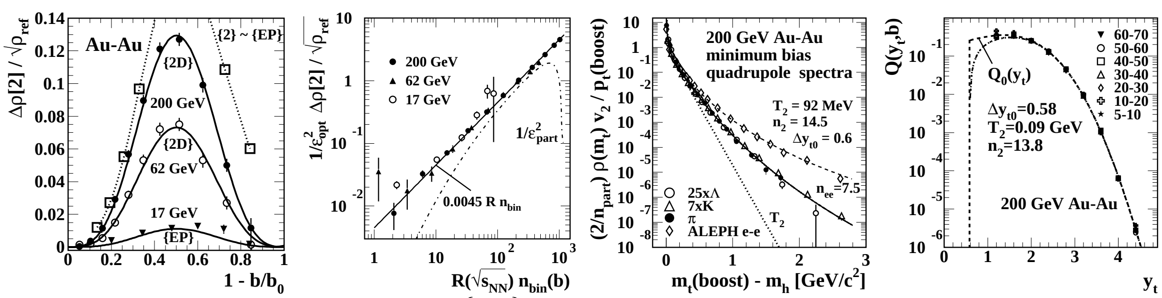

Figure 6.1.2-1. First: p_t-integral $v_2\{2D\}$ centrality dependence, Second: Systematics of $v_2\{2D\}$ data on Au-Au centrality and collision energy, Third: Quadrupole spectra for minimum-bias Au-Au collisions, Fourth: Quadrupole spectra for Au-Au centralities.

In order to better understand the v_2 historical context we conducted a broad survey of analysis methods and interpretations[6]. Our p_t-intregral systematics already suggested

[1] T. A. Trainor and D. T. Kettler, arXiv:1008.4759, to be published in Phys. Rev. C.

[2] T. A. Trainor, arXiv:1012.2373.

[3] T. A. Trainor, Phys. Rev. C **81**, 014905 (2010).

[4] T. A. Trainor, J. Phys. G **37**, 085004 (2010).

[5] D. T. Kettler (STAR Collaboration), Proceedings of Hot Quarks 2008: Workshop For Young Scientists On The Physics Of Ultrarelativistic Nucleus-Nucleus Collisions, Aspen Lodge at Estes Park, Colorado, 18-23 August 2008, Eur. Phys. J. C **62**, 175 (2009).

[6] T. A. Trainor and D. T. Kettler, Int. J. Mod. Phys. E **17**, 1219 (2008).

alternative interpretations for the azimuth quadrupole mechanism[1]. We then extended our studies to p_t-differential $v_2(p_t)$ and developed novel methods to define and extract *quadrupole spectra*[2]. Fig. 6.1.2-1 (third panel) shows published $v_2(p_t)$ data from minimum-bias Au-Au collisions for three identified hadron species transformed to quadrupole spectra in the particle-source boost frame. Remarkably, the quadrupole spectra for three hadron species agree in form within the limits of data and are cold ($T \approx 100$ MeV). The inferred source boost distribution is inconsistent with Hubble expansion, the basis for hydro theory descriptions of RHIC collisions. The quadrupole spectra are also compared directly to a p_t spectrum from LEP dijets (open diamonds). Our results further demonstrate that invocation of identified-hadron $v_2(p_t)$ data to support claims of so-called *constituent-quark scaling* is unjustified.

We have extended our $v_2\{2D\}$ methods to accurate measurements of both the p_t and centrality dependence of v_2[3]. From those data we have determined the A-A centrality dependence of the quadrupole source boost distribution and quadrupole spectrum properies. Fig. 6.1.2-1 (fourth panel) shows the surprising result[4]. Quadrupole spectra for all centralities lie on a common spectrum shape (Lévy distribution). The source boost and quadrupole spectrum properties are, to good approximation, *independent of A-A centrality*, providing another strong argument against hydro interpretations. The overall result is complete factorization of v_2 data above 13 GeV on collision energy, hadron transverse momentum and A-A centrality. We have thus obtained a very simple and accurate parametrization of all $v_2\{2D\}$ data from Au-Au collisions, with negligible contamination from jet correlations (nonflow).

6.1.3 Current status and plans

In recent years our program has lead to a new RHIC paradigm based on abundant minijet survival to the final state and an azimuth quadrupole with newly-revealed properties, both emerging from nearly-transparent A-A collisions and possibly indicating new QCD phenomena[5]. As an example of the general utility of these results in other areas we have combined minijet and quadrupole systematics to provide a simple explanation for the *CMS ridge* recently observed in 7-TeV p-p collisions at the LHC[6]. Our results have elicited strong reactions from a number of hydro proponents, typically consisting of attempts to reinterpret minijet structure as a form of flow manifestation, so far unsuccessful. At the same time the minijet/quadrupole picture continues to improve in substance and internal consistency. In the near future our efforts shift to publishing a similar Cu-Cu analysis, processing new STAR time-of-flight (ToF) data which should provide for the first time access to identified-hadron

[1] T. A. Trainor, Mod. Phys. Lett. A **23**, 569 (2008).

[2] T. A. Trainor, Phys. Rev. C **78**, 064908 (2008).

[3] D. T. Kettler (STAR Collaboration), Proceedings of the XXXIX International Symposium on Multiparticle Dynamics, Gold Sands, Gomel, Belarus, 4-9 September 2009, Nonlin. Phenom. Compl. Syst. **12**, 195 (2010).

[4] D. T. Kettler (STAR Collaboration), Proceedings of Hot Quarks 2010: Workshop for young scientists on the physics of ultrarelativistic nucleus-nucleus collisions, 21-26 June, 2010, La Londe-les-Maures, Côte d'Azur, France, J. Phys. Conf. Ser. **270**, 012058 (2011).

[5] D. T. Kettler (STAR Collaboration), to be published in Proceedings of the Workshop on Critical Examination of RHIC Paradigms, University of Texas at Austin, Austin, Texas, 14-17 April 2010, arXiv:1011.5254.

[6] T. A. Trainor and D. T. Kettler, arXiv:1010.3048.

correlations over broad p_t intervals, and data from lower collision energies (BES program) since we expect minijet production to cease below 13 GeV according to current systematics. That combination will greatly expand our understanding of parton scattering and fragmentation in A-A collisions, and perhaps reveal the true mechanism for the azimuth quadrupole.

6.2 Global parametrization of the azimuth quadrupole in Au-Au collisions

D. T. Kettler and T. A. Trainor

We have developed a detailed description of the centrality-dependent quadrupole spectrum described in the previous section. We rearrange the definition of Q to derive:

$$v_2\{2D\}(p_t, b) = \left\langle \frac{1}{p_t} \right\rangle p_t v_2\{2D\}(b) \left[\frac{\rho_0(b) Q_0(p_t)}{\rho_0(p_t, b)} \right]. \tag{1}$$

The quantity in square brackets has a p_t dependence described by the ratio of a Lévy distribution to the single-particle spectrum. This ratio is observed to be approximated by an exponential for larger values of p_t. We can then construct a revised parametrization of the form

$$v_2\{2D\}(p_t, b) \approx \left\langle \frac{1}{p_t} \right\rangle p_t v_2\{2D\}(b) \exp(-p_t/4) \times f(p_t, b), \tag{2}$$

where $f(p_t, b)$ is an $O(1)$ dimensionless factor needed to describe deviations from the exponential form at low p_t. $f(p_t, b)$ can be fit to the data with the form $f(p_t, b) = 1 + C(b)[\mathrm{erf}(y_t - 1.2) - \mathrm{erf}(1.8 - 1.2)]$, where $C(b) = 0.12 - (\nu - 3.4)/5 - [(\nu - 3.4)/2]^5$. The factor $f(p_t, b)$ is approximately 1 above about 0.75 GeV/c. Above that point the p_t dependence of the quadrupole is entirely described by the factor $p_t \exp(-p_t/4)$. This leads to a factorization of the p_t and centrality dependence of $v_2(p_t, b)$ for higher p_t.

Fig. 6.2-1 shows this parametrization for 20-30%, 10-20%, 5-10%, and 0-5% central collisions. It compares favorably with the data (points) even in these more-central collisions where the conventional parametrization (light dotted curves) fails. Viscous hydro theory (dashed curves) also fails to describe the data. In our parametrization we have obtained a simple, accurate, and complete description of the azimuth quadrupole centrality and p_t dependence for 200-GeV Au-Au collisions.

6.3 p_t and charge dependence of the same-side jet peak in Au-Au collisions

D. T. Kettler and T. A. Trainor

We have observed that charge-independent (CI) two-particle correlations in heavy ion collisions are dominated by a quadrupole term, an away-side dipole—producing the away-side ridge—and a 2D Gaussian jet peak centered at $(0, 0)$ in $(\eta_\Delta, \phi_\Delta)$. This jet peak is a major

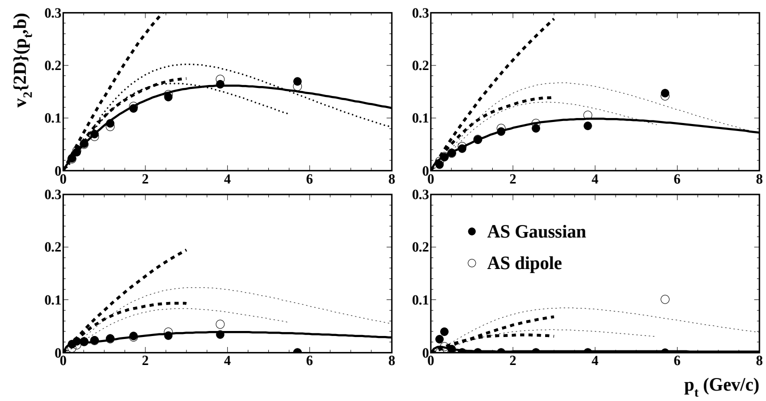

Figure 6.2-1. Examples of this parametrization of $v_2\{2D\}(p_t, b)$ (solid curves) for 20-30% (upper left), 10-20% (upper right), 5-10% (lower left) and 0-5% (lower right) most central collisions. The points are measured $v_2\{2D\}(p_t, b)$ with two different fit models, the dashed curves are hydro theory, and the thin dotted curves are an existing parametrization used at STAR.

contribution to the correlation structure for all centralities and p_t, and we can measure its properties using model fits.

Charge dependence is an important distinguishing property of the jet peak. Instead of constructing a two-particle correlation histogram from all pairs of particles in an event it is possible to construct histograms for only like-sign (LS) or unlike-sign (US) pairs. Some elements of our description of heavy-ion collisions—such as the quadrupole—appear to be completely charge-independent. However, the jet peak exhibits a strong dependence on charge-pair combination. This is expected in a fragmentation process, but it holds true even in the more-central collisions in which the jet peak is significantly modified from what we observe in proton-proton collisions and peripheral Au-Au collisions. The physics behind the modification of the peak is not well understood, but charge dependence is an important property that must be included in any complete description.

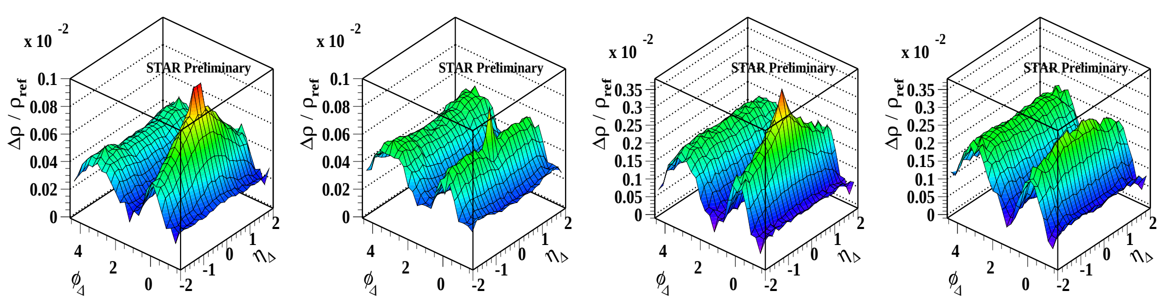

Figure 6.3-1. Example correlation histograms for unlike-sign (US) and like-sign (LS) pairs in 10-20% central 200-GeV Au-Au collisions with the quadrupole term subtracted. The left two panels show US and LS pairs for marginal p_t between 0.41 and 0.62 GeV/c. The right two panels show US and LS pairs for marginal p_t between 2.10 and 3.13 GeV/c.

The left two panels in Fig. 6.3-1 show histograms for 200-GeV 10-20% central Au-Au collisions with a marginal p_t cut between 0.41 and 0.62 GeV/c for unlike-sign and like-sign pairs, respectively. The quadrupole term—based on fits to the corresponding CI correlations—has been subtracted to isolate the jet structure. For this p_t bin the US pairs (first panel) also contain a strong contribution from e^+e^- pair production that produces an exponential peak centered at $(0, 0)$, but it has been cut off in the scale shown. There is a dramatic difference between LS and US in the peak structure. There is actually a dip near $(0, 0)$ in the LS pairs (second panel), though it is obscured by another smaller peak from HBT correlations. The right two panels show the same Au-Au centrality but now with a marginal p_t cut between 2.10 and 3.13 GeV/c. There is still a clear charge-dependence, but the effect is smaller than in the lower-p_t case. In both cases there are still significant LS correlations at large η_Δ. The suppression of the LS peak compared to the US peak for smaller values of η_Δ is consistent with local charge conservation in the fragmentation process.

6.4 Quadrupole Spectrum

D. T. Kettler and T. A. Trainor

Previously we showed a transformation from the convention $v_2(p_t, b)$ measure of the quadrupole component to a *quadrupole* spectrum for unidentified particles. Now we discuss $v_2(p_t)$ for minimum-bias identified pions, kaons, and Lambdas. The first panel of Fig. 6.4-1 shows published data in the conventional $v_2(p_t)$ vs. p_t format.

We have found that if we instead plot these data as $v_2(p_t)/p_t$ vs. transverse rapidity $y_t = \ln((m_t + p_t)/m)$ (second panel) there appears to be a common boost of $y_t \approx 0.6$ for all particle species. This is more evident for heavier particles. This type of narrow boost seems to be incompatible with hydro models of heavy ion collisions, which require some sort of Hubble expansion with a broad boost distribution. We also found a similar boost for unidentified particle $v_2(p_t, b)$ that appears to be independent of Au-Au centrality.

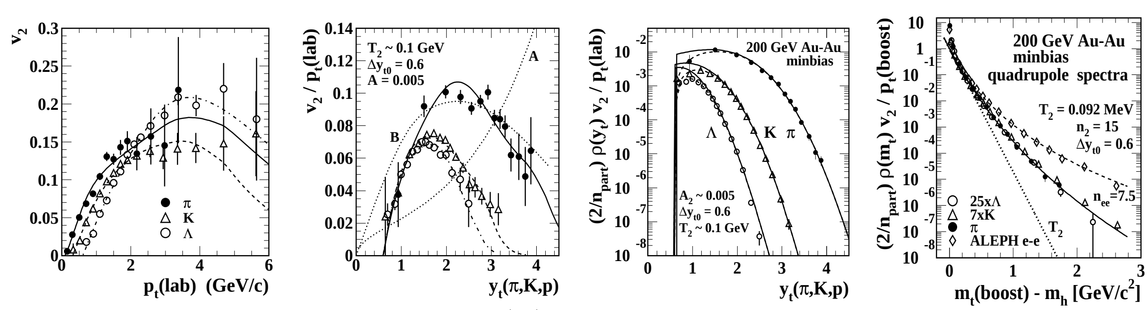

Figure 6.4-1. First Panel: Published $v_2(p_t)$ values for identified pions, kaons, and lambdas. Second Panel: Transformation of these data to $v_2(p_t)/p_t$ as a function of transverse rapidity. Third Panel: Transformation of these data to the quadrupole spectrum variable $\rho_0(p_t)v_2(p_t)/p_t$ normalized by $2/n_{part}$ as a function of transverse rapidity. Last Panel: The same quadrupole spectrum variable but plotted on $m_t - m_0$.

We access the quadrupole spectrum with the quantity $\rho_0(p_t)v_2(p_t)/p_t$, where $\rho_0(p_t)$ is the single-particle spectrum. In our previous study this quantity was normalized by its own p_t-integral to define the unit-normal quantity $Q(p_t, b)$, but in this case we have scaled it by $2/n_{part}$. The result is shown as a function of y_t in the third panel. In this format we can describe the data with boosted Lévy distributions (solid curves). Previously we found that when plotted in this format unidentified particles could be described by a single Lévy distribution over a wide range of centralities, which we denote $Q_0(p_t)$.

In the last panel of Fig. 6.4-1 we have transformed the data to $m_t - m_0$ and scaled the spectra as in the legend. Data plotted in the conventional format (first panel) have been used to claim that there is evidence for constituent-quark scaling. When plotted on $m_t - m_0$ we see that it is possible to describe these three hadron species with a single cold m_t spectrum from a moving source with a boost independent of centrality. This result conflicts with the idea of constituent quark scaling.

6.5 Single-particle jet fragment yields from two-particle jet correlations - comparisons with pQCD

D. T. Kettler and <u>T. A. Trainor</u>

During the past year a major effort has emerged to reinterpret jet-like angular correlations from RHIC Au-Au collisions in terms of initial-state geometry fluctuations coupled with collective expansion, thus reassigning all nominal minimum-bias jet (minijet) structure to hydrodynamics. Initial-state structure has been described variously in terms of "triangularity," Glasma flux tubes and A-A geometry fluctuations. As part of a program to counter such initiatives we have established quantitative connections among pQCD theory, single-particle hadron spectra and jet-related hadron-hadron correlations (minijets). Fig. 6.5-1 (first panel) shows the volume of the same-side 2D peak (solid curve) attributed to minijets vs centrality measure ν. Fig. 6.5-1 (second panel) shows a pQCD calculation of the expected number of jets in the detector angular acceptance as a function of Au-Au centrality. The upper hatched region at $\nu \approx 2.5$ indicates the centrality where multiple jets per event are first expected. That is also the point where a "sharp transition" in jet-like angular correlations is observed.

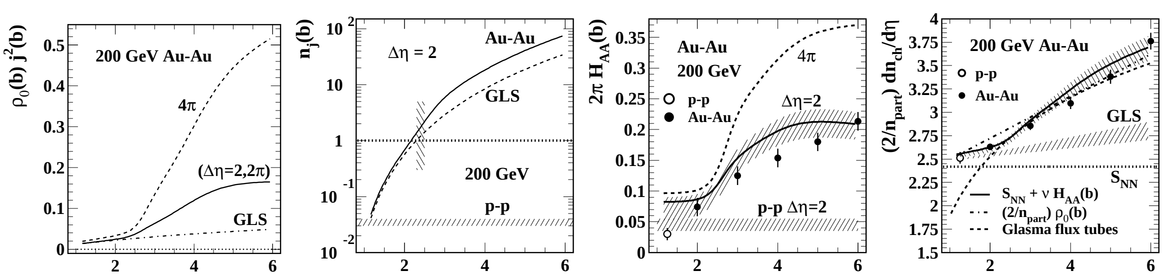

Figure 6.5-1. First: Same-side 2D jet peak volume vs centrality, Second: Predicted jet number within angular acceptance vs centrality, Third: Jet fragment density per N-N binary collision inferred from Au-Au angular correlations and pQCD compared to spectrum yields, Fourth: Jet correlations compared with single-particle yields and a novel theory conjecture.

Fig. 6.5-1 (third panel) shows the angular density of parton fragments per N-N binary collision (solid curve) inferred by combining the first two plots. The open symbol is the result from a two-component analysis of p-p p_t spectra. Solid symbols were obtained from a two-component analysis of Au-Au spectra. The transition from the p-p trend to a 4.5×

increase in fragment production occurs at $\nu \approx 2.5$. Fig. 6.5-1 (fourth panel) combines the previous results in a two-component spectrum model to predict the total hadron yield in Au-Au collisions vs centrality (bold solid curve). The correspondence with single-particle spectrum yields (points) is excellent. The bold dashed curve in the fourth panel represents a prediction based on conjectured Glasma flux tubes as the initial-state source of final-state jet-like particle production. An overall constant has been adjusted to match theory to data. The shape of the prediction (curvature sign) is falsified by both spectrum and correlation data. We conclude that the combination of pQCD, angular correlation data and spectrum data relevant to minimum-bias parton scattering and fragmentation are quantitatively consistent over the full range of Au-Au centralities, including an interesting sharp transition in jet properties. At least one novel proposal for hydrodynamic production of jet-like angular correlation structure via collective expansion (Glasma flux tubes) is qualitatively inconsistent with the same data.

6.6 Interpretation of the same-side "ridge" observed in LHC p-p angular correlations

D. T. Kettler and T. A. Trainor

The CMS collaboration at the LHC has reported the first results for two-particle angular correlations from p-p collisions at 7 TeV. When a certain combination of multiplicity and p_t cuts is applied a same-side "ridge" appears at zero azimuth difference ϕ_Δ, extending uniformly over a large pseudorapidity difference η_Δ interval. The CMS ridge has been compared to a similar feature in angular correlations with p_t cuts from more-central Au-Au collisions interpreted by some to indicate formation of a dense flowing partonic medium.

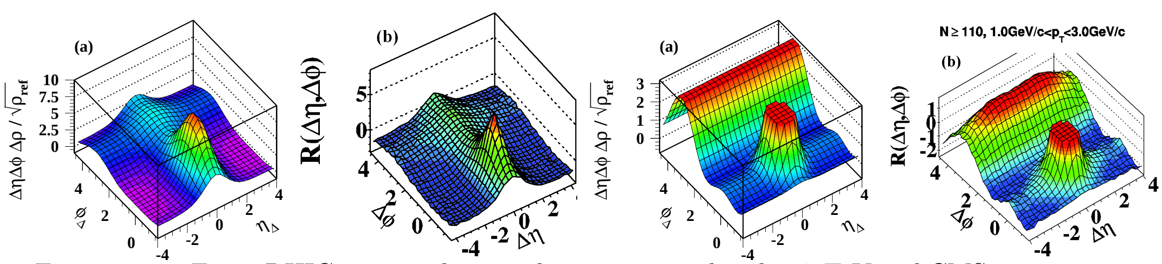

Figure 6.6-1. First: RHIC p-p angular correlations extrapolated to 7 TeV and CMS measure R, Second: CMS angular correlations for 7-TeV p-p collisions, Third: Extrapolated RHIC correlations with quadrupole amplitude increased by 6×, Fourth: CMS angular correlations showing the same-side ridge extending from the cut-off 2D peak at the azimuth origin.

We have applied our correlation measurements from Au-Au collisions at the RHIC to test the hypothesis that the novel ridge structure in CMS data is simply a manifestation of the azimuth quadrupole measured by v_2. We extrapolate our results from RHIC to LHC energies and invoke the CMS cut system. Fig. 6.6-1 (first panel) shows minimum-bias p-p angular correlations at 200 GeV extrapolated to 7 TeV by the logarithmic energy dependence we established for such correlations within 17 - 200 GeV. Fig. 6.6-1 (second panel) shows CMS minimum-bias correlations at 7 TeV. There is good quantitative agreement in all features.

Given the baseline minimum-bias agreement we determine what modifications to our extrapolation are required to describe correlations with CMS applied multiplicity and p_t cuts. The result is shown in Fig. 6.6-1 (third panel). The seven-fold increase in event multiplicity resulting from the CMS n_{ch} cut apparently leads to a three-fold increase in jet correlation yields, interpreted as increased dijet production resulting from bias toward more-central p-p collisions. The other required change in the correlation model is a six-fold increase in the azimuth quadrupole amplitude. Application of CMS p_t cuts reduces jet correlations by the amount expected from RHIC measurements, leaving the quadrupole component unchanged.

Fig. 6.6-1 (fourth panel) shows the CMS data with the same-side ridge at $\phi_\Delta = 0$ approximately uniform on η_Δ. The agreement between our model and the CMS data (third and fourth panels) is excellent. This study reveals that the CMS same-side ridge is the result of two opposite-signed curvatures competing at the azimuth origin: the azimuth quadrupole has a negative curvature and the away-side ridge (back-to-back jets) has a positive curvature. CMS applied cuts change the relative contributions and the net curvature at the origin changes sign, producing the ridge feature. The action is similar to an electronic comparator.

6.7 First correlation analysis of low-energy RHIC data at 39 and 7.7 GeV

D. J. Prindle

In the year-10 operation at RHIC we have commenced a beam energy scan with the goal of identifying the QGP critical point. In our two-particle autocorrelations we have seen an interesting transition in the amplitude and shape of the same-side 2D Gaussian that appears to happen at the same centrality in $\sqrt{s_{NN}}$ = 200-GeV and 62-GeV Au-Au collisions. It will be interesting to see how far down in beam energy the transition structure persists and if the transition centrality changes.

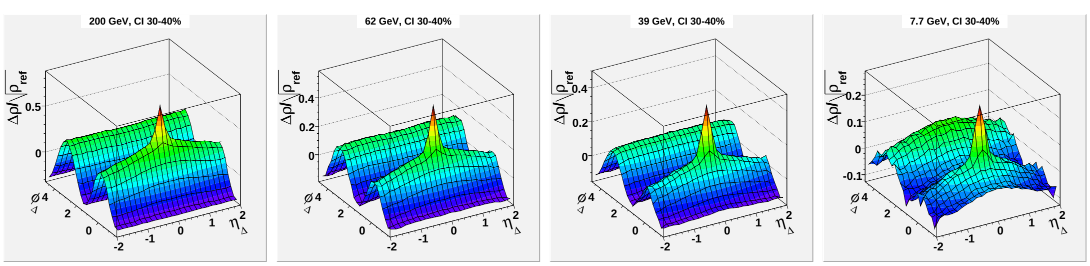

(a) 200 GeV (b) 62 GeV (c) 39 GeV (d) 7.7 GeV

Figure 6.7-1. 2D angular correlations for the 30 to 40% centrality bin and four energies.

During the most recent experimental running period we have taken a significant amount of $\sqrt{s_{NN}}$ = 39-GeV and 7.7-GeV data. In Fig. 6.7-1 we show charge-independent angular correlations for the 30 to 40% centrality bin and for four different beam energies. The correlation amplituded generally decreases as the beam energy is reduced. But the shapes of the 200-GeV, 62-GeV and 39-GeV beam energies are generally similar. In contrast, the 7.7-GeV correlation structure is substantially different. There is an overall strong curvature on η_Δ for both same-side and away-side structure. And the same-side peak is well described by a single sharp 2D exponential with no requirement for a 2D Gaussian. Based on our correlation measeurements at 62 and 200 GeV we predicted that jet production should cease at and below 13.5 GeV. The lack of an observable same-side 2D Gaussian at 7.7 GeV is therefore not surprising.

The 7.7-GeV data exhibit two other interesting features. The amplitude of the away-side dipole term $\cos(\phi_\Delta - \pi)$ for peripheral collisions increases rapidly with centrality but quickly saturates at a constant value instead of continuing to increase raplidly with centrality as at the higher energies. In contrast, the nonjet quadrupole term $\cos(2\phi_\Delta)$ has the same centrality dependence as for the higher energies. The uniform $\cos(\phi_\Delta)$ value indicates that at the lowest collision energy the away-side dipole is due to global transverse momentum conservation across the entire system, not momentum conservation between back-to-back pairs of scattered partons.

6.8 Consequences of event-pileup corrections to inferred minijet systematics

D. J. Prindle and T. A. Trainor

We have noted previously that pileup has a significant affect on the shape of our two-particle angular correlations[1]. In Fig. 6.8-1(a) and Fig. 6.8-1(b) we show 2-particle correlations without and with pileup cuts and corrections for mid-central $\sqrt{s_{NN}} = 62$-GeV Au-Au collisions. For this data sample we estimate that about 0.5% of collisions are affected by pileup. Although the pileup rate is small in absolute terms we see that the pileup effect is still a substantial modification to the correlation shape: a W-shaped distortion on η_Δ clearly visible along the away-side ridge ($|\phi_\Delta| > \pi/2$) in the first panel. Fig. 1(b) shows corrected data with uniform ridge.

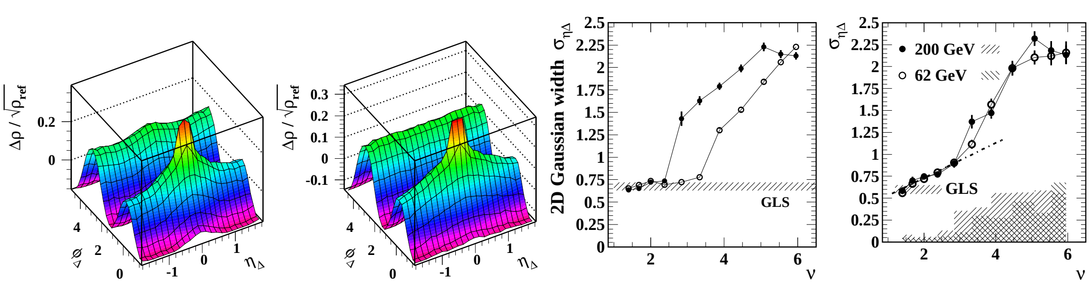

(a) no pileup cuts (b) pileup corrected (c) fit with no pileup cuts (d) fit with pileup corrected

Figure 6.8-1. Pileup, its effect on 2D angular correlations and inferred fit parameters

Our standard fit model includes five components, $\cos(\phi_\Delta)$, $\cos(2\phi_\Delta)$, a 1D Gaussian on η_Δ, a 2D Gaussian centered at $(\eta_\Delta, \phi_\Delta) = (0, 0)$ and a sharp 2D exponential. Of these components the 1D Gaussian on η_Δ is the most strongly affected by pileup, but that structure

[1] CENPA Annual Report, University of Washington (2009) p. 58.

falls to zero amplitude in more-central Au-Au collisions. Properties of the same-side 2D peak are also strongly affected by the pileup contribution. For example, the η_Δ width of the 2D peak varies strongly with centrality, increasing to large values in more-central Au-Au collisions above a specific "transition point" on centrality measure ν.

In Fig. 6.8-1(c) we show σ_{η_Δ} values for the 2D Gaussian model determined by fits to correlation histograms before the pileup correction was developed. From those data it appears that same-side 2D peaks for $\sqrt{s_{NN}} = 62$ GeV and 200 GeV transition to extended Gaussians at substantially different centralities. The difference was interpreted in terms of a dependence on transverse particle density. Fig. 6.8-1(d) shows σ_{η_Δ} values from data histograms after the pileup correction was developed and applied. The most striking feature of the centrality trend, the large broadening along η_Δ "switching on" at a specific centrality, is still present. But the centrality trends for two beam energies are no longer significantly different. The transverse density model was abandoned. These anomalous centrality trends place severe constraints on theory. It is essential that systematic biases such as pileup distortions be eliminated.

6.9 Testing the HIJING Monte Carlo as a linear-superposition reference for Au-Au collisions

D. J. Prindle and T. A. Trainor

The Glauber linear superposition (GLS) reference represents A-A collisions as simply linear superpositions of N-N binary collisions determined by a Glauber model of the A-A interaction. For example, in the case of linear superposition we would expect the amplitude of the same-side 2D jet peak in *per particle* angular correlations to scale as $X_{pp}\,\nu/(1 + x(\nu - 1))$, where X_{pp} is the correlation amplitude measured in p-p collisions, and x represents the fractional hadron yield per N-N binary collision from semihard parton collisions (hard component). The HIJING Monte Carlo (jet quenching off) nominally represents just such a linear superposition, and might therefore serve as a GLS reference for RHIC A-A collisions. New phenomena would then be revealed by significant deviations from the HIJING reference.

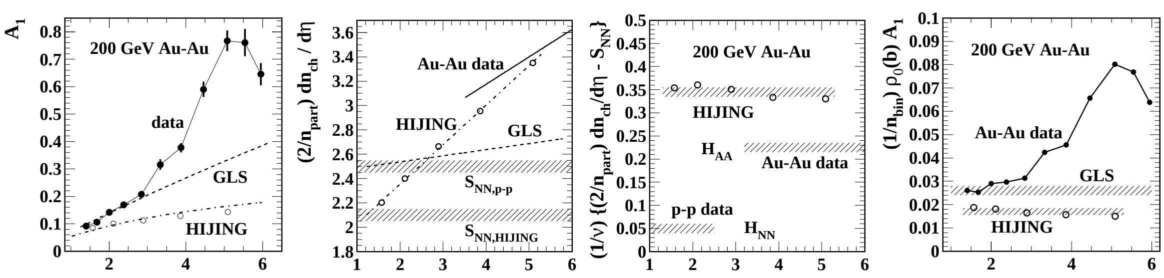

Figure 6.9-1. First: Same-side jet peak amplitude for Au-Au angular correlation data (solid dots) and the HIJING Monte Carlo (open points) vs centrality measure $\nu = 2N_{bin}/N_{part}$, Second: Per-participant-pair charged hadron yields, Third: Hard-component (jet fragment) yields per binary N-N collision, Fourth: Jet-correlated pairs per binary N-N collision.

In Fig. 6.9-1 (first panel) the correlation results from HIJING (open points) are very different from the GLS expectation based on p-p measurements (dashed curve). The explanation is found in the last three panels. Fig. 6.9-1 (second panel) shows single-particle yields per participant-nucleon pair. The HIJING trend (open points) has a binary-collision component (slope) *seven times* that observed in p-p collisions and even larger than observed in central Au-Au collisions. The third panel shows the hard-component hadron production per N-N binary collision, making the HIJING disagreement with p-p collisions more evident.

In contrast, Fig. 6.9-1 (fourth panel) shows the number of jet-correlated *pairs* measured by the same-side 2D peak amplitude per binary N-N collision for HIJING (open points) and Au-Au data (solid points) compared to p-p data (GLS). The jet-correlated pair yield from HIJING is significantly *less* than the p-p observation. The combination of excess single-particle spectrum hard-component yields and deficient jet-correlated pair yields from the HIJING Monte Carlo leads to the trend in the first panel: the per-particle measure of jet correlations from HIJING falls far below the GLS trend extrapolated from p-p data in more-central Au-Au collisions. HIJING is based on linear superposition of PYTHIA as a model of p-p collisions. While PYTHIA is tuned to certain aspects of p-p data, other aspects apparently are not correctly described, and the consequences become apparent only in more-central A-A collisions. Thus, HIJING is not a reliable GLS reference for A-A collisions.

6.10 Glasma flux tubes and collective expansion vs minimum-bias jets

T. A. Trainor

The same-side 2D peak in minimum-bias angular correlations can be interpreted as jet-correlated fragment pairs (minijets) resulting from the minimum-bias parton spectrum. The abundant survival of minijets in more-central Au-Au collisions strongly contradicts the current interpretation of RHIC data in terms of a dense partonic medium opaque to lower-energy partons. To counter the minijet interpretation several theoretical mechanisms have been proposed that couple initial-state structure to collective expansion (radial flow). One proposal invokes "Glasma flux tubes" (related to the color glass condensate or CGC) as the initial structure. A theoretical prediction for the centrality dependence of the same-side peak amplitude based on that mechanism can be falsified in several ways.

Fig. 6.10-1 (first panel) shows the centrality variation of the same-side 2D jet peak volume (solid curve) which can be converted via pQCD dijet cross sections to hard-component (jet fragment) spectrum yields (second panel, solid curve) which agree quantitatively with measured spectrum yields (solid points). The CGC prediction for the total particle yield is $\propto \ln(8\nu)$ (dashed curve), with an unpredicted coefficient adjusted to agree with the data. Even the sign of the curvature (the theory prediction) disagrees with yields and correlations.

The Glasma flux tube prediction of the correlation amplitude is based on an argument by analogy with fluctuations. The last term in this final-state fluctuation measure

$$\frac{\sigma_N^2 - \bar{N}}{\bar{N}} = \frac{\sigma_n^2 - \bar{n}}{\bar{n}} + \lambda \frac{\sigma_{n_1 n_2}^2}{\bar{n}} + \bar{n} \left[\frac{\sigma_K^2 - \bar{K}}{\bar{K}} \right] + \bar{n}, \tag{1}$$

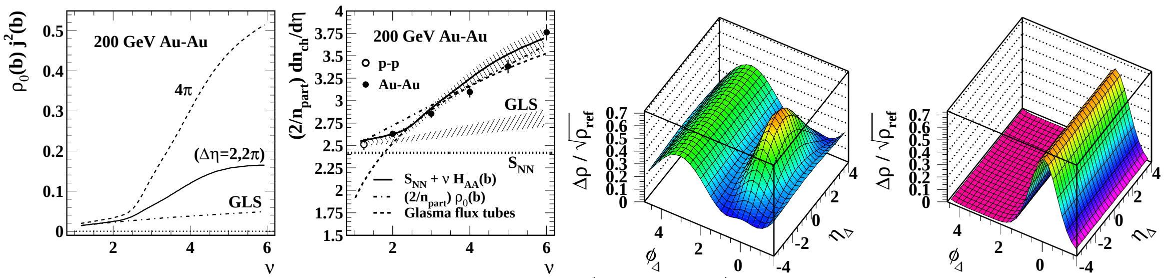

Figure 6.10-1. First: Same-side peak volume (solid curve), Second: Particle production centrality trends from correlations (solid curve) and CGC theory (dashed curve), Third: Jet angular correlations for more-central 200 GeV Au-Au collisions, Fourth: Flux-tube model of the same-side correlation peak.

is attributed to the number of initial-state flux tubes, and the same-side peak amplitude is derived therefrom. However, it is the *first* term in Eq. (1) that actually represents the same-side peak, and the peak *volume* not the amplitude. The theoretical model includes no η_Δ dependence. The model peak thus has infinite volume, and there is no actual quantitative relation between same-side peak properties and the flux-tube theory. Fig. 6.10-1 (third and fourth panels) compare the measured same-side peak in more-central Au-Au collisions with the flux-tube model. Whereas the peak volume from the third panel corresponds quantitatively to measured spectrum yields, the Glasma flux tube prediction in the fourth panel has no such relation and is actually falsified by both angular correlation and spectrum yield data.

6.11 "Triangular flow" vs minimum-bias jets in long-range (on η) correlations

T. A. Trainor

It has been proposed recently that two intriguing features of 2D angular correlations from RHIC Au-Au collisions, the same-side "ridge" and strong distortions of the away-side azimuth peak (interpreted in terms of "Mach cones"), represent "triangular flow" arising from coupling of a "triangularity" component of the A-A initial-state transverse geometry to collective expansion (radial flow). By that means nominal jet phenomena are reinterpreted as flow phenomena. Close inspection of analysis results and methods reveals that claimed triangular flow in the final state is actually a manifestation of the same-side jet peak, and the away-side ridge distortion is the result of v_2 oversubtraction arising from a "nonflow" or jet contribution to v_2 data: effectively, jets are subtracted from jets.

Triangular flow analysis relies on restricting the pair pseudorapidity difference to $|\eta_\Delta| > 2$, nominally intended to eliminate "short-range" jet contributions. The remaining "long-range" correlations are the intended focus. Fig. 6.11-1 (first panel) shows the measured Gaussian η_Δ width of the minimum-bias same-side 2D jet peak as a function of centrality, including a sharp transition to strong η elongation above $\nu = 2.5$. Fig. 6.11-1 (second panel) shows v_2^2 from the AMPT Monte Carlo (thin solid curve) and from our measurements of nonjet quadrupole $v_2\{2D\}$ (dashed curve). The dash-dotted curve is the quadrupole component of that part of the same-side 2D jet peak appearing within the selected η_Δ acceptance interval.

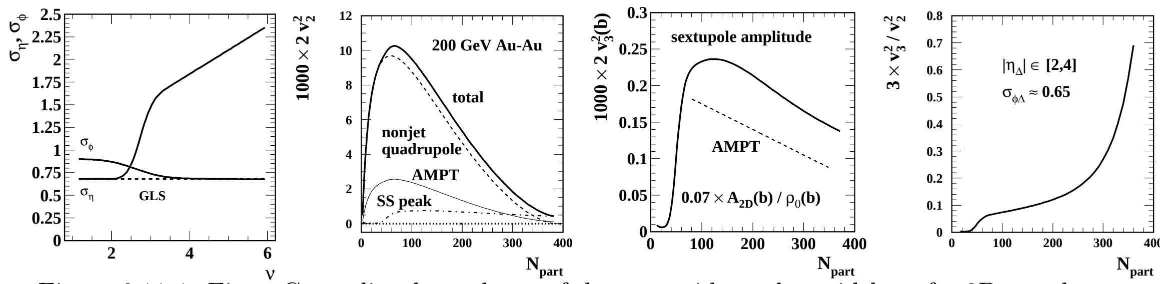

Figure 6.11-1. First: Centrality dependence of the same-side peak η width σ_η for 2D angular correlations from 200-GeV Au-Au, Second: Centrality dependence of quadrupole v_2^2 from the AMPT Monte Carlo (thin solid curve), from nonjet quadrupole data (dashed curve) and from combined nonjet and jet-related quadrupoles (bold solid curve), Third: "Triangular flow" v_3^2 derived from the measured same-side 2D jet peak, Fourth: Ratio v_3^2/v_2^2.

Fig. 6.11-1 (third panel) shows the "triangular flow" v_3^2 Fourier component arising from the same-side jet peak observed within the same η_Δ interval. The fourth panel shows the corresponding v_3^2/v_2^2 ratio. The last three panels correspond quantitatively to results from an analysis of RHIC data which claims to demonstrate the presence of "triangular flow." The present results reveal that the triangular-flow manifestation is explained entirely by η elongation of the same-side jet peak. Above the sharp transition at $\nu \approx 2.5$ or $N_{part} \approx 40$ the elongated same-side jet peak first appears within the restricted η cut acceptance, producing the nonzero v_3^2 as one Fourier component of the projected 1D Gaussian on azimuth (jet peak). There is no evidence to support a triangularity component of the initial-state geometry, or any coupling to a conjectured collective expansion.

7 Radiation and detectors and other research

7.1 Interaction of charged particles with matter

H. Bichsel, Z. Chaoui*, P. Christiansen†, P. Renschler‡, F. Salvat§, and D. Y. Smith¶

Methods for the calculation of the interaction of charged particles for special applications have been developed here for over 20 years. Some have been described in earlier annual reports. Studies are made for the detection of primary and secondary interactions of high speed particles such as electrons, mesons and fully ionized light ions with $z < 10$. Emphasis is on the processes for very thin absorbers. A quantity frequently used is the stopping power (usual symbol dE/dx, here the symbol M_1 is used). For most of the systems described here it is a most unsuitable quantity. Instead the number of collisions per unit length, M_0, is needed. For a more detailed description the collision cross sections that are differential in energy loss $\sigma(E, \beta)$ are needed. The ion speed is β and E is the energy loss of the ion in one collision (within a narrow band dE). For present purposes two methods are used to calculate $\sigma(E, \beta)$, M_0 and M_1: the Bethe-Fano (B-F) method and the Fermi Virtual Photon(FVP) method[1,2,3]. Differences between the two methods are given below (see Sec. 7.1.1) The moments of the collision cross section are defined by

$$M_\nu(v) = N \int E^\nu \ \sigma(E, v) \ \mathrm{d}E \tag{1}$$

where N is the number of electrons per unit volume, and $\nu = 0, 1, 2, 3...$ For large energy losses the Coulomb cross section can be used.

$$\sigma_R(E, \beta) = \frac{k}{\beta^2} \frac{(1 - \beta^2 E/E_M)}{E^2}, \ k = \frac{2\pi e^4}{mc^2} \cdot z^2 = 2.54955 \cdot 10^{-19} \ z^2 \ \mathrm{eVcm}^2 \tag{2}$$

It is a 5-10% approximation for $E > 10 \ I_K$ where I_K is the ionization energy of K-shell electrons in the absorber. More complex expressions are needed for smaller energy losses[4]. The Bethe-Fano method (B-F) is quite accurate for this purpose. The Fermi-Virtual-Photon method (FVP) requires less input data and thus is used frequently.

Both methods[1,2] give results for the stopping power M_1 (usually expressed as dE/dx) which agree to better than 1%.

*University of Setif, Setif, Algeria.
†Lund University, Lund, Sweden.
‡Karlsruhe Institute of Technology, Karlsruhe, Germany.
§Universitat de Barcelona, Barcelona, Spain.
¶University of Vermont, Burlington, VT and Argonne National Laboratory, Argonne, IL.

[1] H. Bichsel, *Interaction of radiation with matter*, in Landolt-Boernstein, New Series, Group I, Vol.21, Elementary Particles, Subvolume B, Detectors for Particles and Radiation, H. Schopper and C. Fabjan Eds., Springer (2011).
[2] H. Bichsel, Nucl. Instrum. Methods A **562** 154 (2006).
[3] R. P. Saxon, Phys. Rev. A **8** 839 (1973).
[4] Fano's description of interactions with solids is especially useful: Ann. Rev. Nucl. Sci. **13** 1 (1963).

M_0 gives the mean number of collisions of the particles and is important for calculating the straggling functions. The results from B-F and FVP may differ by as much as 20% and are described below (see Sec. 7.1.1).

7.1.1 Differences in M_0 and M_1 for B-F and FVP.

Tables of M_0 and M_1 for Si are given in[1,2]. For M_0 the differences are 8% at $\beta\gamma = 0.316$ and 6% for $\beta\gamma > 3$. For M_1, the differences are 0.9% at $\beta\gamma = 0.316$ and less than 0.5% for $\beta\gamma > 3$.

For gases a B-F study of $M_0 = \sigma_{tot}$ was made by Saxon[3]. Comparisons with FVP M_0 are given in the Table. In order to show the equivalence with Lindhard's L for dE/dx the values of M_0 are multiplied by $2\beta^2$.

T(MeV)	L_0 (Ne)	$_sL_0$ (Ne)	diff%	L_0 (Ar)	$_sL_0$ (Ar)	diff%
10	13.59	11.89	14.3	34.56	31.02	11.4
30	15.65	13.93	12.3	39.37	35.82	9.9
100	17.81	16.06	11.1	44.40	40.85	8.7
300	19.69	17.87	10.2	48.68	45.13	7.9
500	20.58	18.73	9.9	50.70	47.15	7.5
1000	21.95	20.05	9.5	53.81	50.26	7.1
3000	24.76	22.81	8.5	60.31	56.77	6.2
10000	28.66	26.70	7.3	69.40	65.96	5.2
30000	32.57	30.67	6.2	78.01	75.30	3.6

Table 7.1.1-1. Comparison of $L_0 = 2\beta^2 M_0$ for Ne (left columns) and Ar (right columns) calculated with FVP and $_sL_0 = 2\beta^2\sigma_{tot}$ (using $\mathcal{J}_1 - \mathcal{J}_2 = 2.852$[3]) for protons with energy T (for $\beta\gamma = 0.316$ $T = 46$ MeV).

Differences between M_0 and σ_{tot} for Ar are similar to those for Si[2], and somewhat larger for Ne. The stopping power M_1 for both gases calculated with FVP differs by less than 1% from ICRU 49.

At present we are not aware of any study of the consequences of these differences (see Sec. 7.1.2). For very thin absorbers, i.e. with less than say 10 collisions on the average (i.e. 3 mm in Ar or 7 mm in Ne) the errors of FVP will become evident[5].

7.1.2 Applications for STAR, ALICE, ILD, etc.

The PID (Particle Identification) program[2] has been used extensively for the STAR and ALICE time projection chambers (TPC). The problem of the conversion of the ionization in

[5]H. Bichsel, Advances in Quantum Chemistry **46** 329 (2004).

the gas into ADC signals is still under study[6,7]. Other problems have been described[8,9].

The exchange of results, opinions and advice about the practical applications of the studies of the interaction of radiation with matter outlined here continues. In particular the effects in very thin layers of absorbers (mm in gases, μm in solids) in detectors such as gas electron multipliers (GEMs) must be explored in great detail[5]. Estimates have been calculated for energy deposition in plastic detectors related to calorimetry.

7.1.3 Applications in KATRIN

A short report about the progress with the simulations for the interactions of the 18.6-keV electrons from the tritium decay has been made[10]. A detailed report will be given[11]. Good agreement between calculations and experiment has been found[12].

Studies about the production of delta rays by cosmic ray muons in the steel wall of the large electrostatic spectrometer have been initiated[13].

7.1.4 Dosimetry of C-ion beams for radiation therapy

An invited presentation of the study of the stochastics of the dosimetry of C-ions described last year[14] was given at the Annual Meeting of the Radiation Research Society in Sept. 2010. Further refinements of the correlation between physical and biological radiation effects are progressing.

7.1.5 Comparisons with functions calculated with GEANT4

The programs mentioned above are complementary to the more universal programs such as GEANT4 and many others. Calculations with the methods described here are compared with two other systems[7]. Differences between calculations with specialized methods and with GEANT4 are found frequently[15].

---

[6] Y. Fisyak, Private communication, February 2011.

[7] P. Christiansen *et al.*, Nucl. Instrum. Methods A **609** 149 (2009) and Private communication, February 2011.

[8] M. Shao, *et al.*, Nucl. Instrum. Methods A **558** 419 (2006).

[9] Y. Xu, H.Bichsel *et al.*, Nucl. Instrum. Methods A **614** 28 (2011).

[10] P. Renschler, M. Babutzka, H. Bichsel, Z. Chaoui, M. Steidl, Nucl. Phys. B (Proc. Suppl.) (2010) [pending].

[11] P. Renschler, thesis, to be finished in May 2011.

[12] Z. Chaoui, Z.J. Ding and K. Goto, Phys. Lett. A **373** 1679 (2009).

[13] M. Prall, Prog. Part. Nucl. Phys. (2011), doi:10.1016/ j.ppnp.2011.01.044.

[14] CENPA Annual Report, University of Washington (2010) p. 98.

[15] E. Poon, J. Seuntjens and F. Verhaegen, Phys. Med. Biol. **50** 681 (2005).

7.2 Status of nonlocal quantum communication test

J. G. Cramer, K. Hall, B. Parris, and D. B. Pengra

The question we have been investigating in this experiment is whether the intrinsic nonlocality of standard quantum mechanics is the private domain of Nature, as is generally assumed by the physics community, or whether in special circumstances the nonlocal connection between subsystems can be used to send signals from one observer to another. With the aid of generous private contributions and some use of CENPA resources, we have continued the work on this test of nonlocal quantum communication, which has been reported in the past four years[1,2,3,4]. The initial configuration of the experiment, as described in the first two references, employed a high power argon-ion laser operating at about 1 W in the ultraviolet at 351 nm that pumped nonlinear crystals (BBO or $LiIO_3$) to produce pairs of momentum-entangled 702-nm photons, on which measurements were subsequently performed. It was concluded that signal-to-noise limitations from fluoresence photons competing with the downconverted photons prevented that planned measurements using that initial configuration.

In January, 2010, the experiment was moved from the basement of the Physics-Astronomy Building to the Optics Laboratory on the 2nd floor, which offered the advantage that the experimental area can be darkened without interference with other experiments. A new experimental configuration was mounted in this location. The new configuration uses periodically-poled potassium titanyl phosphate (ppKTP) crystal with a 10-μm poling length and dimensions 1 mm$\times$2 mm$\times$30 mm from Raicol, Inc. The ppKTP crystal is maintained at 50° C in a precision crystal oven. The ppKTP crystal is pumped with a Littow-type grating-stabilized diode laser capable of delivering up to 100 mW at 405 nm of vertically polarized light. The laser light is rotated from vertical to horizontal with a half-wave plate, inducing the ppKTP crystal to produce pairs of colinear 810-nm momentum-entangled photons.

For the interference measurements required by the experiment, two "half-slit" momentum-sensitive interferometers described in last year's report[5] were employed. To more effectively prevent the pump laser light from entering the interferometers, a quartz 60° prism has been added after the nonlinear crystal. The prism's dispersion provides separate angular paths for the 405-nm pump radiation and the 810-nm entangled photons of interest. The new Mark IV experimental configuration is shown in Fig. 7.2-1. The basic idea of the experiment is that if the beam splitter in the "Alice" interferometer is out, the detection of an Alice photon determines which path through the interferometer the photon took and, because of the transverse momentum entanglement of the photon pair, gives path information about *both* photons, leading to suppression of any two-path interference pattern in the "Bob" interferometer. If the Alice beam-splitter is in place, no path information is available and Bob detects a two-path interference pattern. The presence or absence of the interference pattern thus provides a medium for nonlocal signaling.

[1] CENPA Annual Report, University of Washington (2007) p. 52.
[2] CENPA Annual Report, University of Washington (2008) p. 42.
[3] CENPA Annual Report, University of Washington (2009) p. 41.
[4] CENPA Annual Report, University of Washington (2010) p. 93.
[5] CENPA Annual Report, University of Washington (2010) p. 95.

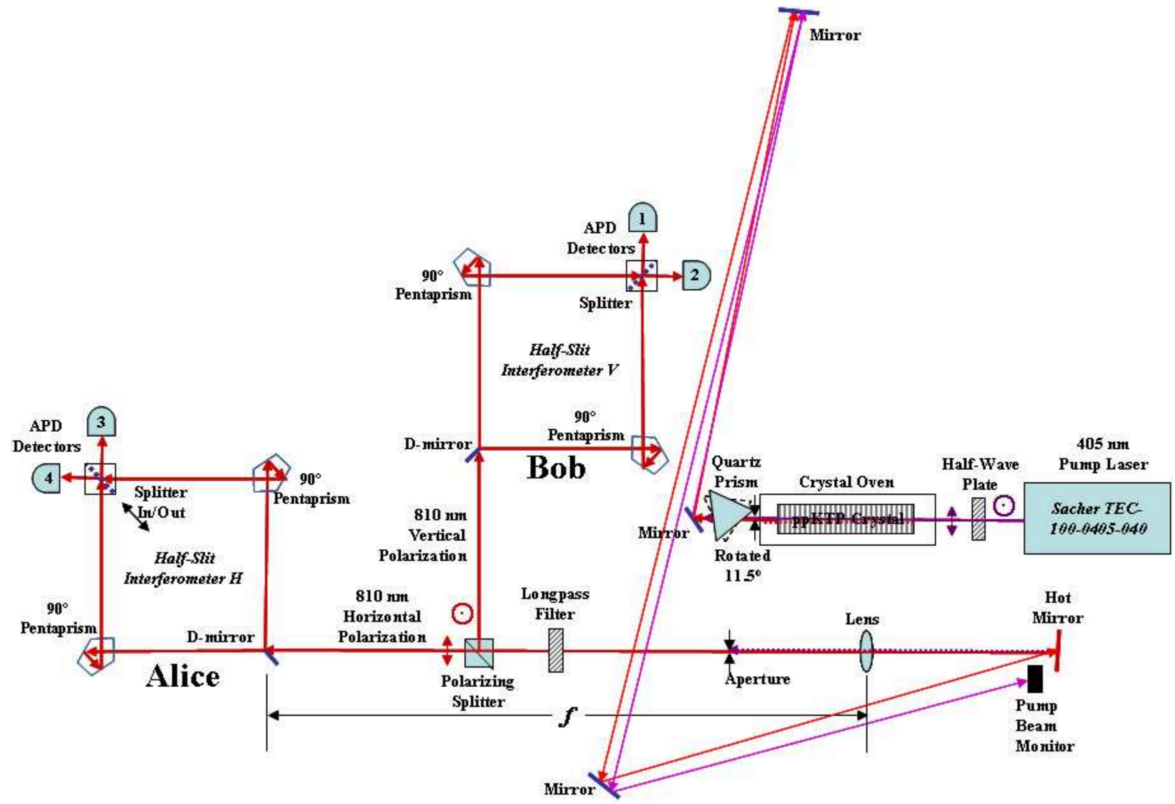

Figure 7.2-1. Schematic diagram of the Mark III quantum nonlocal communication test setup

We have identified the source of the insensitivity of our avalanche photodiode (APD) detector system mentioned in last year's report. It arises from operation of the avalanche diodes in the linear mode driving charge sensitive preamplifiers. At the high gains needed for single-photon detection, the large avalanche signal was saturating the preamplifiers, locking up the electronics, and preventing coincidence measurements. In the present setup we have eliminated the preamplifier, and we operate the APDs in the single-photon-sensing "Geiger" mode of operation. We have obtained new APDs from Pacific Semiconductor with sensitivity curves centered on 810 nm, and we operate them with an upstream 2 megohm current-limit resistor in series with the APD in series with a 50-ohm load resistor to ground, the latter directly driving a 50-ohm coaxial cable to the electronics. The two APD signals are sent to Ortec 474 Timing-Filter Amplifiers and two sections of a 934 Quad Constant Fraction Discriminator with about 35 ns of delay between the inverted and normal signals. The system works well in tests using light-pulser photons from pairs of red LEDs. We have also constructed a large light-tight box to house the experiment, and we are presently seeking to detect 810-nm entangled photon pairs with the new setup. We are also investigating techniques for cooling the APDs to reduce spontaneous-avalanche "dark current" that is present in the Geiger mode.

7.3 Detection of airborne fission products from the Fukushima reactor incident

J. Diaz Leon, J. Kaspar, A. Knecht, M. L. Miller, R. G. H. Robertson, and
A. G. Schubert

The recent earthquake and tsunami in Japan on 11 March, 2011 resulted in severe damage to the nuclear reactor complex in Fukushima. Due to the uncertainty of the situation, limited quantitative information, and its potential impact on both local public health as well as our low-background fundamental physics program, we began monitoring local air samples for the potential arrival of airborne radioactive fission products.

Our samples consist of air filters taken from the intake to the ventilation system of the Physics and Astronomy building at the University of Washington. This allows us to sample 114000 ± 8000 m^3 of air per day, $\sim$10 times more air than what had been done here previously[1]. This proved to be one of the key points for the successful detection of the radioactive fission products. In order to search for characteristic γ rays stemming from radioactive fission products we place the samples inside a lead shield of 5 to 20 cm thickness next to a 0.5-kg P-type point contact germanium detector for low-level counting.

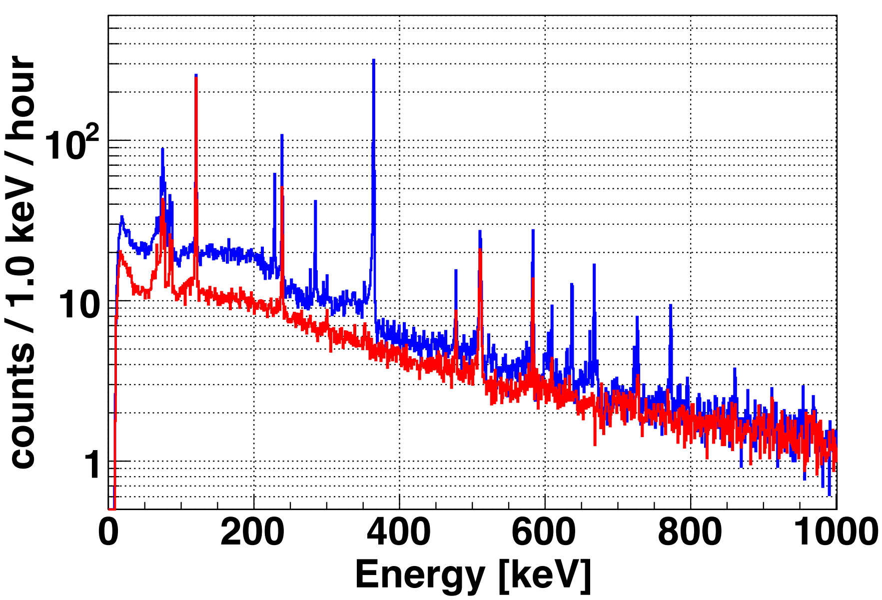

Figure 7.3-1. Comparison of the gamma spectra from the measurements of air filters exposed during 16-17 March (red, bottom) and 17-18 March (blue, top) showing clearly the additional peaks due to the arrival of radioactive fission products at the US west coast. The dominant peak at 364 keV is from ^{131}I.

We started the air monitoring campaign on 16 March. No fission products were detected in the first air filter and we were able to attribute all the visible γ lines to known background radioactivity from cosmic-ray induced processes, various radioactive isotopes of the uranium and thorium decay chains, cosmogenic ^{7}Be, and ^{40}K. The subsequent sample immediately

[1] CENPA Annual Report, University of Washington (1986) p. 59.

revealed the onset of several characteristic gamma lines from fission products. The identified isotopes are ^{131}I, ^{132}I, ^{132}Te, ^{134}Cs, and ^{137}Cs. Fig. 7.3-1 shows the comparison between the γ-ray spectra from the first two air filters where the additional γ peaks are clearly identifiable. The extracted activity for ^{131}I amounts to $\lesssim$32 mBq/m^3 and is at least a factor of $\sim$100 below the limit given by the Environmental Protection Agency. A full report on the first five days of our measurements is available at J. Diaz Leon et al., arXiv:1103.4853. Updates on the current measurements are posted at http://www.npl.washington.edu/monitoring.

8 Facilities

8.1 Facilities overview

G. C. Harper

As new experiments emerge and as the demands of research change with time, CENPA constantly adjusts and improves its facilities in order to provide the best possible resources and research environment for its users. Faculty and staff work together to shape the future of the facility and to ensure that these goals are met. Efforts are always being made to provide improvements over a wide spectrum of modern technical support. Modifications within the existing building are frequently made to ensure that researchers have adequate upgraded office space and experimental space.

The computational facilities at CENPA remain at the front edge of technology. We have improved management of server resources by utilizing virtual technology (e.g. Xen). The benefits of virtualization include reduced power consumption and server footprint, improved server management, and increased server resource allocation efficiency. Network security was scrutinised and enhanced by replacing the antiquated firewall appliance, updating server operating systems, hardening public facing servers, and tightening user access rules. Previously providing only Microsoft Windows support, we now provide a secure backup solution and client software to support backups on our heterogeneous operating system environment. Other notable improvements this year include improved wireless security and coverage, license server consolidation, CENPA managed printer server, and a new IMAP/SMTP email server with up-to-date spam engine and filters. As always, personal desktop and portable computers are maintained and the technology kept current.

The NPL Data Center (NPLDC) previously contained a single high performance cluster, ATHENA, and now provides the infrastructure to multiple clusters and department appliances. The ATHENA high performance computing (HPC) cluster has evolved into multiple smaller computational clusters. One of these clusters, CENPA, currently runs a Rocks 5.3 cluster which provides computing power to CENPA faculty and students. We are investigating the possibility of scaling the cluster to a hybrid cloud by leveraging publicly available clouds resources. In addition, NPLDC supports a wide range of server appliances: virtual web/wiki/gateway servers, SQL servers, file servers, backup servers, shared storage arrays and security appliances.

The CENPA electronics shop provides modern surface-mount technology and miniature cable manufacturing equipment on site and in appropriately clean areas. The shop continues to do custom design work for specialty pre-amps as well as dedicated multichannel DAQ systems and contracts with outside vendors to efficiently produce custom printed circuit boards for these projects in a cost-effective manner. The shop also interacts with the on-campus Washington Technology Center taking advantage of much of the capital-intensive, high-tech equipment there that is more effectively used as a cost-shared facility. The electronics shop staff also provides training for students and other staff members so that they may quickly and easily design, build, and repair their own small projects.

The CENPA instrument shop and student shop provide a unique climate for a research facility. Our instrument shop is manned by two highly skilled instrument makers with decades of experience working in the university and research environments. The shop equipment is kept up to date as evidenced by the recent addition of a CNC mill and CNC lathe. The instrument makers interact with students, staff, and faculty on a daily basis providing instruction on how to design physically realizable devices and how to correctly document design changes. In this sense it is an instructional facility as well as a shop facility. The student shop is headed by an instrument maker who himself does small machining jobs but more importantly provides safety training and instruction to students, staff, and faculty on the operation of a wide variety of machine tools.

The FN tandem Van de Graaff accelerator and its associated ion sources and experimental caves undergo changes regularly to accommodate new experiments and provide support for accelerator related projects. The accelerator lab is also a true, hands-on training facility for students. The entering graduate students and the undergraduate hourly employees are trained to operate the accelerator and ion sources and there have even been some provisions made for undergraduate course credit using the accelerator to perform simple nuclear physics experiments. The accelerator can be quickly switched between two different operational modes to provide a wide accessible energy range with high beam intensity over the entire range. The ion sources are modified as needed to accommodate a wide variety of experimental requirements. Dedicated beam lines and target areas in the experimental caves are regularly disassembled, redesigned, and rebuilt for new experiments.

This year the ion sources and accelerator provided proton beams for the ^{21}Ne$(p,\gamma)^{22}$Na, ^{22}Na$(p,\gamma)^{23}$Mg, and ^{33}S$(p,\gamma)^{34}$Cl experiments, production of a ^{83}Rb source for Project 8, and tests of a liquid scintillator for SNO+ PMT development. A 17.75-MeV deuteron beam was provided for the ^{6}He experiment. The ion sources and injector deck provided beams of ^{21}Ne, ^{23}Na, and ^{27}Al with energies of a few tens of keV for implantation. A beam line previously devoted to heavy ion research was disassembled and a newly designed beam line, vacuum control, and target for the ^{21}Ne$(p,\gamma)^{22}$Na experiment was installed in its place. This work was done primarily by undergraduate students who were also trained to operate the accelerator and all of the ion sources.

Laboratory space is reallocated as needed as new large experiments are initiated at or move to CENPA. The entire east end of the accelerator tunnel is presently being modified to house the ADMX experiment. New lab space is being opened up to provide testing facilities for the development of experiments and detectors for the muon and neutrino programs. Old, poorly used shop space is being converted to modern office space to house the increase in personnel associated with growing experiments.

Computing

8.1.1 Laboratory computer systems

R. Coffey, J. Gardner, G. T. Holman, D. B. Kaplan, M. L. Miller, T. Quinn, and D. I. Will

CENPA is a mixed shop of Windows 7, XP, Vista, Mac OS X and various flavors of Linux. Windows 7 is installed on new systems, however we are still running Windows XP and Vista. This year the IT focus was directed toward server consolidation, network security, process documentation and removal of redundant processes. Utilizing Xen virtualization, hardware was reduced from twelve servers to three. Most web, Elogs, wiki, calendar, tracking and document servers are all now running in the virtualized environment. The Cenpa website and research group web pages are now on a virtual Debian server and utilize the Drupal web framework. The NPL mail server and spam filters were upgraded however all NPL email is now relayed to user's UW email hardware.

Linux and Windows backups are saved to Crunch4's 6TB RAID farm, from whence they are written to LTO tape by the Physics Computer Center on a three month backup retention plan. Two Dell 510 20TB servers were purchased to replace Crunch4 and offer increased user storage, print server and improved backup policy. The new backup server now supports Linux, MAC, Windows and Solaris operating systems and provides differential and encrypted backups. Crunch4 will be transitioned into a virtual appliance for CENPA user and research group domains.

The NPL Data Center (NPLDC) provides the critical infrastructure supporting high performance scientific computing applications that cannot be efficiently executed on typical commodity server infrastructures (e.g., the Amazon EC2 Cloud). NPLDC space is shared by Physics, the Institute for Nuclear Theory (INT), CENPA, and the Astronomy departments. Prior to this year the space housed a single cluster that was treated as one computational resource.

Today, to meet the wide and highly specialized array of research requirements, the cluster has been separated into specific instances. The computational hardware infrastructure supports six different instances of cluster: three cluster instances that leverage Infiniband interconnects (classified as HPC clusters) and three clusters that primarily run single-threaded applications (non-HPC clusters.) The HPC clusters primarily use Torque/Maui via the three cluster's dedicated frontends. The three other clusters use Condor or user driven scheduling and resource management.

The data requirements in the NPLDC have also rapidly grown. Approximately one-third rack space is dedicated to non-cluster hardware: NFS scratch storage, SQL, MySQL, and backup servers. These servers constitute over 200TB of raw disk space. The computational clusters instances continue to use 23.7 TB of SAN storage on a HP/Polyserve NFS Cluster. This is an order of magnitude increase in specialized, low-cost storage for both cluster and desktop scientific computing.

Our computing and analysis facility consists of:

- The NPL data center as a shared resource with Physics, the Institute for Nuclear Theory (INT), and the Astronomy department.
- A mix of Linux systems: Debian, Redhat, and Ubuntu distributions.
- One VMS/VAXstation and two VMS Alphas for legacy computing.
- The SNO, KATRIN, MAJORANA and emiT groups rely upon Macintosh systems.
- One SunBlade 100 workstation serves CADENCE circuit design, analysis and layout duties.
- A VAXstation is the linac and vacuum systems control and display system.
- Various Windows XP desktop JAM systems (Java based software for acquisition and analysis), plus two laptops for taking to other installations.
- The bulk of CENPA's PCs and servers are now behind a Shorewall Linux-based logical firewall.
- Although not directly used by lab personnel, we provide additional legacy co-location services for the INT and the Physics Nuclear Theory group in the form of one VMS Alphastation 500.

Planning is underway to Migrate serial/VAX based controllers to TCP/Labview this year. In addition we plan to implement true video conferencing thereby reducing associated travel costs.

CENPA electronics shop

8.1.2 Electronic equipment

D. A. Peterson and T. D. Van Wechel

The electronics shop is responsible for the design and construction of new laboratory electronic equipment, as well as the maintenance and repair of existing CENPA electronics. Projects undertaken by the electronics shop included the following:

1. Significant progress has been made in the reorganization and clean up of the electronics shop and stock room.

2. The development of a forward biased reset pre-amplifier (see Sec. 1.3.2) for the Majorana experiment has been one of the most significant design projects this year.

3. A test circuit for the evaluation of the noise characteristics of JFETs over the frequency range of 10 Hz to 10 MHz has been developed and constructed. We will be evaluating both triode and tetrode JFETs for the use in pre-amplifiers for Majorana and other projects.

4. We are acquiring training at the Washington Technology Center to learn the processes and the use of the tools needed for the construction of hybrid electronics on a fused silica based substrate.
5. An optical pulser for the electronic calibration of the KATRIN focal plane detector was developed and constructed.
6. A VMEbus veto summing board for the KATRIN project was constructed.
7. Constructed a beam line gate controller for the ^{6}He experiment.
8. Ongoing modification and testing of approximately 70 NCD preamps for the HALO project in Sudbury.

Accelerator

8.1.3 Van de Graaff accelerator and ion source operations and development

N. M. Boyd, T. M. Cope, G. C. Harper, D. A. Peterson, S. P. R. Steininger, T. D. Van Wechel, and D. I. Will

The tandem was entered seven times this year. During two openings the accelerator was switched between single-ended and tandem operation. Gas bottles of H_2 were installed or refilled and the gradient was changed for single-ended running during two openings. Repairs took place during five of the openings as follows. A resistor was replaced. Faulty fiber optics were removed and replaced. The bottom high energy charge pickup wheel in the terminal was replaced. One of the low energy idler wheels was replaced. The left steering feed through as well as the Southeast port vacuum seal were replaced. In addition, new stripper foils were installed during two openings and the alignment of the foil box, foils, as well as the high energy aperture were measured during one opening.

ACTIVITY SCHEDULED	**DAYS SCHEDULED**	**PERCENT of TIME**
Ion implantation, deck ion sources	102	28
Nuclear physics research, terminal ion source	21	6
Subtotal, ion implant or nuclear physics research	123	34
Development, maintenance, or crew training	64	18
Grand total	187	51

Table 8.1.3-1. Tandem Accelerator Operations 1 April, 2010 to 31 March, 2011

During the 12 months from 1 April, 2010 to 31 March, 2011 the tandem pellet chains operated 1214 hours, the SpIS operated 157 hours, and the DEIS operated 1428 hours. Additional statistics of accelerator operations are given in Table 8.1.3-1.

Development of the DEIS for the production of the positive ion beams of the noble gases was completed this year. An implantation of the rare isotope ^{21}Ne from natural abundance neon using this ion source was successful.

CENPA instrument shop

8.1.4 CENPA instrument shop and student shop

J. H. Elms, D. R. Hyde, and H. Simons

The CENPA instrument shop has used its CNC machine tools in very productive and innovative ways this year, especially the more recently acquired CNC lathe. Both the 4-axis CNC mill and the newly acquired CNC lathe are currently being used to produce high precision parts for the NCD detectors. The CNC lathe is being used in mass-production mode for some of these parts. The NCD detectors are scheduled to be reused in the HALO experiment after modification.

The CNC mill is regularly used to make one-off, specialty components for the KATRIN collaboration and Majorana project. High quality vacuum welds and seals are routinely made to provide equipment for first class research. Most recently, an elegant thermal break has been formed and welded together in sections for KATRIN.

The main instrument shop and the student shop continue to provide technical support for CENPA. The student shop especially provides safety training and training in the operation of machine tools for all of the faculty, staff, and students.

Building modifications

8.1.5 Buildings, accommodating the ADMX cryostat

N. M. Boyd, J. A. Heilman*, A. P. Wagner, and D. I. Will

The move of the Axion Dark Matter Experiment (ADMX) from Lawrence Livermore National Laboratory to the Center for Experimental Nuclear Physics and Astrophysics (CENPA) at the University of Washington occurred this past summer. Relocating necessitated changes to the east end of the CENPA accelerator tunnel. The following equipment has been removed and surplused or scavenged: three well-used RS Helium Compressors, one plate-fin heat exchanger, four water pumps, and one motor control center for the preceding. Then about ten meters each of supply and return piping for the following systems were removed and recycled: tower cooling water, process cooling water, and helium compressor (plus one line to the helium gas buffer tank).

*Now in graduate school, University of California, Riverside, CA.

The 12-ton annular magnet cryostat is 12 feet tall with outer diameter 51 inches and inner bore 22 inches. The magnet cryostat must remain upright. The 11-foot tall experimental insert is being improved for the next phase of the experiment. Because the insert is raised and lowered by crane for placement in the magnet bore, the total height below the top position of the crane hook must be about 24 feet to avoid damage to magnet or insert. Achieving this height required cutting through the tunnel floor into the service alleyway underneath and further cutting down through the service alley floor. In the pit excavated below the service alley floor a concrete well with a new floor three foot below the existing floor is under construction now. Finally, power is being run to the new experimental location.

9 CENPA Personnel

9.1 Faculty

Eric G. Adelberger[1]	Professor Emeritus
Hans Bichsel[1]	Affiliate Professor
John G. Cramer[1]	Professor Emeritus
Peter J. Doe	Research Professor
Sanshiro Enomoto	Research Assistant Professor; CENPA Fellow
Alejandro García	Professor
Jens H. Gundlach[1]	Professor
Blayne R. Heckel[1]	Professor; Chair
David W. Hertzog[2]	Professor
C. D. Hoyle[1,3,4]	Affiliate Assistant Professor
Michael L. Miller	Research Assistant Professor; CENPA Fellow
R. G. Hamish Robertson	Professor; Director
Peter Kammel[2]	Research Professor
Leslie J Rosenberg[1]	Professor
Stephan Schlamminger[1,5]	Research Assistant Professor
Kurt A. Snover[1]	Research Professor Emeritus
Derek W. Storm[1]	Research Professor Emeritus
Nikolai R. Tolich	Assistant Professor
Thomas A. Trainor	Research Professor
Robert Vandenbosch[1]	Professor Emeritus
William G. Weitkamp[1]	Research Professor Emeritus
John F. Wilkerson[1,6]	Affiliate Professor
Tianchi Zhao[7]	Research Associate Professor

9.2 CENPA External Advisory Committee

Baha Balantekin	University of Wisconsin
Stuart Freedman	UC Berkeley and Lawrence Berkeley National Laboratory
Wick Haxton	UC Berkeley and Lawrence Berkeley National Laboratory
William Zajc	Columbia University

[1] Not supported by DOE CENPA grant.
[2] Arrived August, 2010.
[3] Affiliated faculty, Humboldt State University, Arcata, CA.
[4] Arrived June, 2010.
[5] On leave to N.I.S.T., November, 2010.
[6] Affiliated faculty, University of North Carolina, Chapel Hill, NC.
[7] Arrived April, 2011.

9.3 Postdoctoral Research Associates

Frank Fleischer[1,2]
Seth Hoedl[1,3]
Jarek Kaspar
Andreas Knecht
Diana Parno[4]
Gray Rybka[1]
Brent VanDevender[5]
Hok Wan Chan Tseung
Krishna Venkateswara[6]
Andrew Wagner[1]
Peter Winter[7]
Chris Wrede

9.4 Predoctoral Research Associates

Laura Bodine
Ted Cook[1]
Ian Derrington[1]
Jonathan Diaz Leon
Brent Graner
Charles Hagedorn[1]
Ran Hong
Michael Hotz[1]
Robert Johnson[8]
David Kettler
Sara Knaack[1,7]
Jared Kofron
Dmitry Lyapustin[1,9]
Michael Marino[10]
Eric Martin
Michael Murray[7]
Anne Sallaska[11]
Alexis Schubert
Daniel Scislowski
William Terrano[1]
Matthew Turner[1]
Todd Wagner[1]
Brandon Wall
Brett Wolfe
David Zumwalt

9.5 NSF Research Experience for Undergraduates participants

Morgan Askins	Florida State University
Gregory Dooley	Princeton University
Jessica Gifford	Oregon State University

[1]Not supported by DOE CENPA grant.
[2]Feodor Lynen Fellow.
[3]Departed October, 2010, Civatech Oncology, Inc., Research Triangle Park, N.C.
[4]Arrived April, 2011.
[5]Departed September, 2010, Pacific Northwest National Laboratory, Richland, WA.
[6]Arrived December, 2010.
[7]Arrived August, 2010.
[8]Ph.D., August, 2010. Postdoctoral Fellow, University of Colorado, Boulder, CO.
[9]Arrived April, 2010.
[10]Ph.D., August, 2010. Postdoctoral Fellow, Excellence Cluster Universe, Munich, Germany.
[11]Ph.D., December, 2010. Postdoctoral Fellow, University of North Carolina, Chapel Hill, NC.

9.6 University of Washington graduates taking research credit

Rachel Rosten	Hamish Robertson, Advisor

9.7 University of Washington undergraduates taking research credit

Jennie Chen	Blayne Heckel, Advisor
Brent Delbridge	Andreas Knecht, Chris Wrede, Advisors
Blake Freeman	Chris Wrede, Advisor
Matthew Haefele	Ted Cook, Advisor
William Norton Haycox[1]	Michael Miller, Advisor
Holly Hess	Eric Adelberger, Seth Hoedl, Advisors
Eric Lee-Wong	Blayne Heckel, Advisor
Daniel McInally	Nikolai Tolich, Advisor
James Mulligan	Nikolai Tolich, Advisor
Evan Nelson[1]	Michael Miller, Brent VanDevender, Advisors
Andrew Palmer[2]	A. García, Advisor
Satoshi Utsuno[3]	Chris Wrede, Advisor
David Williams	A. García, Advisor
Thomas Wolowiec	Leslie Rosenberg, Advisor

9.8 Professional staff

John F. Amsbaugh	Research Engineer	KATRIN vacuum systems
Nora M. Boyd[4]	Research Engineer	ADMX install, accelerator
Tom H. Burritt	Research Engineer	Design of KATRIN detector system
Gregory C. Harper	Associate Director	Accelerator, ion sources
Gary T. Holman	Computer Systems	Systems Manager
Duncan J. Prindle, Ph.D.	Research Scientist	Heavy ion research
Hendrik Simons	Instrument Maker	Shop Supervisor
H. Erik Swanson, Ph.D.	Research Physicist	Precision experimental equipment
Timothy D. Van Wechel	Electronics Engineer	Analog and digital electronics design
Douglas I. Will	Research Engineer	Cryogenics, ion sources

[1] Graduated June, 2010.
[2] Departed September, 2010.
[3] Visiting from Keio University, Japan.
[4] Arrived October, 2010.

9.9 Technical staff

James H. Elms	Instrument Maker
David R. Hyde	Instrument Maker
David A. Peterson	Electronics Technician

9.10 Administrative staff

Victoria A. Clarkson	Administrator
Kate J. Higgins	Fiscal Specialist
Robert S. Shupe[1]	Fiscal Specialist

9.11 Part time staff and student helpers

Tyler Cope
Robert Fiszer[1]
Jesse Heilman[2]
Draza Miloshevich
Andrew Palmer
Jonathan Rollins[2]
Devin Short
Arielle Steger[2]
Steven Steininger
Kyle Tracy[2]
Kevin Wald[3]
Kevin Wierman

[1] Arrived October 2010.
[2] Departed August 2010.
[3] Departed May 2010.

10 Publications

Publications and presentations with a date of 2010 or 2011 are included below. Some entries from early 2010 may therefore also appear in the 2010 Annual Report.

10.1 Published papers

"A SQUID-based microwave cavity search for dark-matter axions," S. J. Asztalos, G. Carosi, C. Hagmann, D. Kinion, K. van Bibber, M. Hotz, L. Rosenberg, G. Rybka, J. Hoskins, J. Hwang, P. Sikivie, D. B. Tanner, R. Bradley, J. Clarke, Phys. Rev. Lett. **104**, 041301 (2010).

"Search for Chameleon Scalar Fields with the Axion Dark Matter Experiment," G. Rybka, M. Hotz, L. J. Rosenberg, S. J. Asztalos, G. Carosi, C. Hagmann, D. Kinion, K. van Bibber, J. Hoskins, C. Martin, P. Sikivie, D. B. Tanner, R. Bradley, J. Clarke, Phys. Rev. Lett. **105**, 051801 (2010).

"Search for Hidden Sector Photons with the ADMX Detector," A. Wagner, G. Rybka, M. Hotz, L. J. Rosenberg, S. J. Asztalos, G. Carosi, C. Hagmann, D. Kinion, K. van Bibber, J. Hoskins, C. Martin, P. Sikivie, D. B. Tanner, R. Bradley, J. Clarke, Phys. Rev. Lett. **105**, 171801 (2010).

"Upper bound on parity-violating neutron spin rotation in ^{4}He," W. M. Snow, C. D. Bass, T. D. Bass, B. E. Crawford, K. Gan, B. R. Heckel, D. Luo, D. M. Markoff, A. M. Micherdzinska, H. P. Mumm, J. S. Nico, A. K. Opper, M. Sarsour, E. I. Sharapov, H. E. Swanson, S. B. Walbridge, V. Zhumabekova, Phys. Rev. C **83**, 022501(R) (2011).

"Polarized neutron beam properties for measuring parity-violating spin rotation in liquid ^{4}He," A. M. Micherdzinska, C. D. Bass, T. D. Bass, K. Gan, D. Luo, D. M. Markoff, H. P. Mumm, J. S. Nico, A. K. Opper, E. I. Sharapov, W. M. Snow, H. E. Swanson, V. Zhumabekova, Nucl. Instrum. Methods A **631**, 80 (2011).

"Removal of zero-point drift from AB data and the statistical cost," H. E. Swanson and S. Schlamminger, Meas. Sci. Technol. **21**, 115104 (2010).

"Measurement of the Positive Muon Lifetime and Determination of the Fermi Constant to Part-per-Million Precision," D. M. Webber *et al.*, Phys. Rev. Lett. **106**, 041803 (2011).

"Preparation of ^{20}Ne, ^{24}Mg, ^{28}Si, ^{32}S, and ^{36}Ar targets by ion implantation into thin carbon foils," C. Wrede, K. Deryckx, B. M. Freeman, A. García, G. C. Harper, A. S. C. Palmer, D. A. Short, D. I. Will, Nucl. Instrum. Methods B **268**, 3482 (2010).

"Absolute Determination of the ^{22}Na(p,γ) Reaction Rate in Novae," A. L. Sallaska, C. Wrede, A. García, D. W. Storm, T. A. D. Brown, C. Ruiz, K. Snover, D. F. Ottewell, L Buchmann, C. Vockenhuber, D. A. Hutcheon, J. A. Caggiano, J. José, Phys. Rev. C **83**, 034611 (2011).

"Determination of the axial coupling constant from polarized ultracold neutrons," J. Liu, M. P. Mendenhall, A. T. Holley, H. O. Back, T. J. Bowles, L. J. Broussard, S. Clayton, S. Currie, B. W. Filippone, A. P. Galvan, A. García, P. Geltenbort, K. P. Hickerson, J. Hoagland, G. E. Hogan, B. Hona, T. M. Ito,C. -Y. Liu, M. Makela, R. R. Mammei, J. W. Martin, D. Melconian, N. Meier, C. L. Morris, R. W. Pattie Jr., B. Plaster, J. C. Ramsey, R. Rios, R. Russell, A. Saunders, S. Seestrom, W. E. Sondheim, E. Tatar, R. B. Vogelaar, B. VornDick, C. Wrede, H. Yan, A. R. Young, J. Yuan, Phys. Rev. Lett. **105**, 181803 (2010).

"Direct measurements of ^{22}Na(p,γ)^{23}Mg resonances and consequences for ^{22}Na production in classical novae," A. L. Sallaska, C. Wrede, A. García, D. W. Storm, T. A. D. Brown, C. Ruiz, K. A. Snover, D. F. Ottewell, L. Buchmann, C. Vockenhuber, D. A. Hutcheon, J. A. Caggiano, Phys. Rev. Lett. **105**, 152501 (2010); *ibid.* **105**, 209901 (2010).

"Properties of ^{20}Na, ^{24}Al, ^{28}P, ^{32}Cl, and ^{36}K for studies of explosive hydrogen burning," C. Wrede, J. A. Clark, C. M. Deibel, T. Faestermann, R. Hertenberger, A. Parikh, H. Wirth, S. Bishop, A. A. Chen, K. Eppinger, B. M. Freeman, R. Krücken, O. Lepyoshkina, G. Rugel, K. Setoodehnia, Phys. Rev. C **82**, 035805 (2010).

"Structure of ^{30}S with ^{32}S(p,t)^{30}S and the thermonuclear ^{29}P(p,γ)^{30}S reaction rate," K. Setoodehnia, A. A. Chen, J. Chen, J. A. Clark, C. M. Deibel, S. D. Geraedts, D. Kahl, P. D. Parker, D. Seiler, C. Wrede, Phys. Rev. C **82**, 022801(R) (2010).

"Toward precise Q_{EC} values for the superallowed $0^+ \to 0^+$ β decays of $T = 2$ nuclides: The masses of ^{20}Na, ^{24}Al, ^{28}P, and ^{32}Cl," C. Wrede, J. A. Clark, C. M. Deibel, T. Faestermann, R. Hertenberger, A. Parikh, H.-F. Wirth, S. Bishop, A. A. Chen, K. Eppinger, A. García, R. Krücken, O. Lepyoshkina, G. Rugel, K. Setoodehnia, Phys. Rev. C **81**, 055503 (2010).

"First direct measurement of the ^{23}Mg(p,γ)^{24}Al reaction," L. Erikson, C. Ruiz, F. Ames, P. Bricault, L. Buchmann, A. A. Chen, J. Chen, H. Dare, B. Davids, C. Davis, C. Deibel, M. Dombsky, S. Foubister, N. Galinski, U. Greife, U. Hager, A. Hussein, D. A. Hutcheon, J. Lassen, L. Martin, D. F. Ottewell, C. V. Ouellet, G. Ruprecht, K. Setoodehnia, A. C. Shotter, A. Teigelhöfer, C. Vockenhuber, C. Wrede, A. Wallner, Phys. Rev. C. **81**, 045808 (2010).

"New constraints on Lorentz invariance violation from the neutron electric dipole moment," I. Altarev *et al.*, Eur. Phys. Lett. **92**, 51001 (2010).

"An efficient gravitational spectrometer for ultracold neutrons," P. Geltenbort *et al.*, Nucl. Instrum. Methods A **624**, 168 (2010).

"Diffuse reflection of ultracold neutrons from low-roughness surfaces," F. Atchison *et al.*, Eur. Phys. J. A **44**, 23 (2010).

"Cubic boron nitride: A new prospective material for ultracold neutron application," Y. Sobolev *et al.*, Nucl. Instrum. Methods A **614**, 461 (2010).

"Study of Astrophysically Important Resonant States in ^{30}S Using the ^{32}S(p,t)^{30}S Reaction," K. Setoodehnia, A. A. Chen, J. Chen, J. A. Clark, C. M. Deibel, D. Kahl, W. N. Lennard, P. D. Parker, C. Wrede, J. Phys.: Conf. Ser. **202**, 012042 (2010).

"Study of Astrophysically Important Resonant States in ^{30}S Using the ^{32}S(p,t)^{30}S Reaction," K. Setoodehnia, A. A. Chen, J. Chen, J. A. Clark, C. M. Deibel, D. Kahl, W. N. Lennard, P. D. Parker, C. Wrede, Nucl. Phys. **A834**, 205c (2010).

"Destruction of ^{22}Na in novae: surprising results from an absolute measurement of ^{22}Na(p,γ) resonance strengths," A. L. Sallaska, C. Wrede, A. García, D. W. Storm, T. A. D. Brown, C. Ruiz, K. A. Snover, D. F. Ottewell, L. Buchmann, C. Vockenhuber, D. A. Hutcheon, J. A. Caggiano, accepted for publication in PoS **NIC XI** 051.

"Precision measurements of ^{20}Na, ^{24}Al, ^{28}P, ^{32}Cl, and ^{36}K for the *rp* process," C. Wrede, J. A. Clark, C. M. Deibel, T. Faestermann, R. Hertenberger, A. Parikh, H.-F. Wirth, S. Bishop, A. A. Chen, K. Eppinger, B. M. Freeman, R. Krücken, O. Lepyoshkina, G. Rugel, K. Setoodehnia, PoS **NIC XI** 198.

"Destruction of ^{22}Na in novae: surprising results from an absolute measurement of ^{22}Na(p,γ)^{23}Mg resonance strengths," A. L. Sallaska, C. Wrede, A. García, D. W. Storm, T. A. D. Brown, C. Ruiz, K. A. Snover, D. F. Ottewell, L. Buchmann, C. Vockenhuber, D. A. Hutcheon, J. A. Caggiano, PoS **NIC XI** 122.

"The ^{33}S(p,γ)^{34}Cl reaction in classical nova explosions," A. Parikh, T. Faestermann, R. Krücken, V. Bildsten, S. Bishop, K. Eppinger, C. Herlitzius, O. Lepyoshkina, P. Maierbeck, D. Seiler, K. Wimmer, R. Hertenberger, H.-F. Wirth, J. Fallis, U. Hager, D. A. Hutcheon, C. Ruiz, L. Buchmann, D. Ottewell, B. Freeman, C. Wrede, A. García, B. Delbridge, A. Knecht, A. L. Sallaska, A. A. Chen, J. A. Clark, C. M. Deibel, B. Fulton, A. Laird, U. Greife, B. Guo, E. Li, Z. Li, G. Lian, Y. Wang, P. D. Parker, K. Setoodehnia, PoS **NIC XI** 052.

"Solar fusion cross sections II: the pp chain and CNO cycles," E. G. Adelberger, A. B. Balantekin, D. Bemmerer, C. A. Bertulani, J.-W. Chen, H. Costantini, M. Couder, R. Cyburt, B. Davids, S. J. Freedman, M. Gai, A. García, D. Gazit, L. Gialanella, U. Greife, M. Hass, K. Heeger, W. C. Haxton, G. Imbriani, T. Itahashi, A. Junghans, K. Kubodera, K. Langanke, D. Leitner, M. Leitner, L. E. Marcucci, T. Motobayashi, A. Mukhamedzhanov, K. M. Nollett, F. M. Nunes, T.-S. Park, P. D. Parker, P. Prati, M. J. Ramsey-Musolf, R. G. H. Robertson, R. Schiavilla, E. C. Simpson, K. A. Snover, C. Spitaleri, F. Strieder, K. Suemmerer, H.-P. Trautvetter, R. E. Tribble, S. Typel, E. Uberseder, P. Vetter, M. Wiescher, L. Winslow, Rev. Mod. Phys. (2010, in press).

"Understanding RHIC Collisions: Modified QCD fragmentation vs quark coalescence from a thermalized flowing medium," T. A. Trainor, to be published in the Proceedings of the XL International Symposium on Multiparticle Dynamics (ISMD2010), University of Antwerp, Antwerp, Belgium, 21-25 September 2010, arXiv:1011.6351.

"Parton fragmentation in nuclear collisions," T. A. Trainor, Proceedings of the Workshop on Critical Examination of RHIC Paradigms (CERP2010), University of Texas at Austin, Austin, Texas, 14-17 April 2010, PoS **CERP2010** 003, arXiv:1008.4757.

"Systematics of parton fragmentation in e^+-e^- and nuclear collisions," T. A. Trainor, Proceedings of the XXXIX International Symposium on Multiparticle Dynamics (ISMD2009), Gold Sands, Gomel, Belarus, 4-9 September 2009, Nonlin. Phen. in Comp. Syst. **12**, 323 (2010), arXiv:0910.1125.

"Heavy Flavor and Jets," D. J. Prindle (STAR Collaboration), to be published in the Proceedings of the 6th International Conference on Physics and Astrophysics of Quark Gluon Plasma (ICPAQGP 2010), Goa, India, 5-10 December 2010, arXiv:1103.6053.

"Review of minimum-bias jet systematics at RHIC," D. J. Prindle (STAR Collaboration) Proceedings of the Workshop on Critical Examination of RHIC Paradigms (CERP2010), University of Texas at Austin, Austin, Texas, 14-17 April 2010, PoS **CERP2010** 013, arXiv:1104.0046.

"$v_2(p_t)$ from 2D angular correlations and centrality evolution of the azimuth quadrupole p_t spectrum," D. T. Kettler (STAR Collaboration), Proceedings of the XXXIX International Symposium on Multiparticle Dynamics (ISMD2009), Gold Sands, Gomel, Belarus, 4-9 September 2009, Nonlin. Phen. in Comp. Syst. **12**, 195 (2010), arXiv:1011.6351.

"The azimuth quadrupole in nuclear collisions," D. T. Kettler (STAR Collaboration), Proceedings of the Workshop on Critical Examination of RHIC Paradigms (CERP2010), University of Texas at Austin, Austin, Texas, 14-17 April 2010, PoS **CERP2010** 011, arXiv:1011.5254.

"Azimuth quadrupole systematics in Au-Au collisions," D. T. Kettler (STAR Collaboration), Proceedings of Hot Quarks 2010: Workshop for young scientists on the physics of ultrarelativistic nucleus-nucleus collisions, La Londe-les-Maures, Côte d'Azur, France, 21-26 June, 2010, J. Phys.: Conf. Ser. **270**, 012058 (2011), arXiv:1008.4793.

"Monte Carlo simulations of the detector response to low energy electrons for KATRIN," P. Renschler, M. Babutzka, H. Bichsel, Z. Chaoui, M. Steidl, Nucl. Phys. B (Proc. Suppl.) **00**, 1 (2010).

"Interaction of radiation with matter," H. Bichsel in Landolt-Boernstein, New Series, Group I, Vol.21, Elementary Particles, Subvolume B, Detectors and Data Handling, H. Schopper ed., Springer (2011).

"A proposed STAR microvertex detector using Active Pixel Sensors with some relevant studies on APS performance," S. Kleinfelder, S. Li, F. Bieser, R. Gareus, L. Greiner, J. King, J. Levesque, H. S. Matis, M. Oldenburg, H. G. Ritter, F. Retiere, A. Rose, K. Schweda, A. Shabetai, E. Sichtermann, J. H. Thomas, H. H. Wieman, H. Bichsel, Nucl. Instrum. Methods A **565**, 132 (2006).

"Improving the dE/dx calibration of the STAR TPC for the high-pT hadron identification," Y. Xu, H. Bichsel *et al.*, Nucl. Instrum. Methods A **614**, 28 (2010).

"Muon capture in hydrogen," P. Kammel, Nucl. Phys. **A844**, 181c (2010).

"Precision Muon Capture," P. Kammel and K. Kubodera, Annu. Rev. Nucl. Part. Sci. **60**, 327 (2010).

"High Precision Study of Muon Catalyzed Fusion in D_2 and HD Gas," D. V. Balin *et al.*, Phys. Elem. Part. At. Nuclei **42**, 185 (2011).

"Measurement of the Positive Muon Lifetime and Determination of the Fermi Constant to Part-per-Million Precision," D. M. Webber *et al.*, Phys. Rev. Lett. **106**, 041803 (2011).

"The 10 bar hydrogen time projection chamber of the MuCap experiment," J. Egger *et al.*, Nucl. Instrum. Methods A **628**, 199 (2011).

"Picoradian deflection measurement with an interferometric quasi-autocollimator using weak value amplification," M. D. Turner, C. A. Hagedorn, S. Schlamminger, J. H. Gundlach, Opt. Lett., doc. ID 142777 (posted 23 March 2011, in press).

"Preparation of ^{114m}In low energy conversion electron sources," C. Wrede, B. W. Filippone, A. García, G. C. Harper, S. Lassell, J. Liu, M. P. Mendenhall, A. S. C. Palmer, R. W. Pattie, Jr., D. I. Will, A. R. Young, Nucl. Instrum. Methods B **269**, 1113 (2011).

"Improving the ^{30}P(p,γ)^{31}S rate in ONe novae: constraints on J^π values for proton-threshold states in ^{31}S," A. Parikh, K. Wimmer, T. Faestermann, R. Hertenberger, J. José, R. Longland, H.-F. Wirth, V. Bildstein, S. Bishop, A. A. Chen, J. A. Clark, C. M. Deibel, C. Herlitzius, R. Krücken, D. Seiler, K. Straub, C. Wrede, accepted for publication in Phys. Rev. C.

"Branches of ^{33}S(p,γ)^{34}Cl at oxygen-neon nova temperatures," B. M. Freeman, C. Wrede, B. Delbridge, A. García, A. Knecht, A. Parikh, A. L. Sallaska, Phys. Rev. C **83**, 048801 (2011).

"Low Energy Threshold Analysis of the Phase I and Phase II Data Sets of the Sudbury Neutrino Observatory," B. Aharmim *et al.* [SNO Collaboration], Phys. Rev. C **81**, 055504 2010; arXiv:0910.2984

"The calibration of the Sudbury Neutrino Observatory using uniformly distributed radioactive sources," K. Boudjemline, B. Cai, B. T. Cleveland, H. C. Evans, J. Farine, R. J. Ford, E. Guillian, A. L. Hallin, E. D. Hallman, C. Howard, P. Jagam, N. A. Jelley, K. J. Keeter, J. R. Klein, C. Kraus, C. B. Krauss, R. Lange, I. T. Lawson, J. R. Leslie, J. C. Loach, A. B. McDonald, G. McGregor, A. J. Noble, H. M. O'Keeffe, S. J. M. Peeters, A. W. P. Poon, S. D. Reizner, K. Rielage, R. G. H. Robertson, V. L. Rusu, S. R. Seibert, P. Skensved, M. J. Thomson, Nucl. Instrum. Methods A **620**, 171 (2010).

"Energy spectra of electron yields from silicon: Theory and experiment," Z. Chaoui, Z. J. Ding, K. Goto, Phys. Lett. A **373**, 1679 (2009).

"Explain it in 60 Seconds: Shielding," R. G. H. Robertson, symmetry **07**, vol. 01, Feb. 2010.

"Searches for High Frequency Variations in the ^{8}B Neutrino Flux at the Sudbury Neutrino Observatory," B. Aharmim *et al.* [SNO Collaboration], Ap. J. **710**, 540 (2010).

"Solubility, Light Output and Energy Resolution Studies of Molybdenum-Loaded Liquid Scintillators," V. M. Gehman, P. J. Doe, R. G. H. Robertson, D. I. Will, H. Ejiri, R. Hazama, Nucl. Instrum. Methods A **622**, 602 (2010).

"Theory of Neutrino Oscillations with Entanglement," B. Kayser, J. Kopp, R. G. H. Robertson, P. Vogel, Phys. Rev. D **82**, 093003 (2010).

"Low Multiplicity Burst Search at the Sudbury Neutrino Observatory," B. Aharmim *et al.* [SNO Collaboration], Ap. J. **728**, 83 (2011); arXiv:1011.5436 [hep-ex].

"New Constraints on Axion-mediated Forces," S. Hoedl, F. Fleischer, E. G. Adelberger, B. R. Heckel, Phys. Rev. Lett. **106**, 041801 (2011).

10.2 Papers submitted or to be published 2011

"Decay studies for neutrino physics: Electron capture decays of ^{100}Tc and ^{116}In," A. García, S. Sjue, H. E. Swanson, C. Wrede, D. Melconian, A. Algora, I. Ahmad, submitted to Hyperfine Interactions.

"Four methods for determining the composition of trace radioactive surface contamination of low-radioactivity metal," H. M. O'Keeffe, T. H. Burritt, B. T. Cleveland, G. Doucas, N. Gagnon, N. A. Jelley, C. Kraus, I. T. Lawson, S. Majerus, S. R. McGee, A. W. Myers, A. W. P. Poon, K. Rielage, R. G. H. Robertson, R. C. Rosten, L. C. Stonehill, B. A. VanDevender, T. D. Van Wechel, Nucl. Instrum. Methods A (submitted March 2011), arXiv:1103.5788 (2011).

"Arrival time and magnitude of airborne fission products from the Fukushima, Japan, reactor incident as measured in Seattle, WA, USA," J. Diaz-Leon, J. Kaspar, A. Knecht, M. L. Miller, R. G. H. Robertson, A. G. Schubert, (preprint) arXiv:1103.4853v1 (2011).

"Constraints on θ_{13} from a three-flavor oscillation analysis of reactor antineutrinos at KamLAND," A. Gando *et al.* [KamLAND Collaboration], Phys. Rev. D **83**, 052002 (2011).

10.3 Invited talks, abstracts, and other conference presentations

"Destruction of ^{22}Na in Novae: Surprising Results from an Absolute Measurement of ^{22}Na(p,γ) Resonance Strengths," A. L. Sallaska, 11th Symposium on Nuclei in the Cosmos, Heidelberg, Germany, 2010.

“Nucleosynthesis in classical novae,” C. Wrede, Seminar, Department of Physics and Astronomy, Michigan State University, East Lansing, MI, USA, March 2011.

“Destruction of ^{22}Na in Novae: Surprising Results from an Absolute Measurement of ^{22}Na(p,γ) Resonance Strengths,” A. L. Sallaska, Triangle Universities Nuclear Laboratory Seminar, Durham, NC, USA, 2010.

“Destruction of ^{22}Na in Novae: Surprising Results from an Absolute Measurement of ^{22}Na(p,γ) Resonance Strengths,” A. L. Sallaska, MIT-Laboratory for Nuclear Science Seminar, Cambridge, MA, USA, 2010.

“Destruction of ^{22}Na in Novae: Surprising Results from an Absolute Measurement of ^{22}Na(p,γ) Resonance Strengths,” A. L. Sallaska, RadiaBeam Technologies Seminar, Santa Monica, CA, USA, 2010.

“Destruction of ^{22}Na in Novae: Surprising Results from an Absolute Measurement of ^{22}Na(p,γ) Resonance Strengths,” A. L. Sallaska, Poster at the National Nuclear Physics Summer School, Vancouver, BC, Canada, 2010.

“Muon capture at PSI, P. Winter, arXiv:1012.3859, 2nd International Workshop on the Physics of fundamental Symmetries and Interactions, Villigen, Switzerland (PSI2010).

“In a muon’s lifetime: From Fermi’s constant to “calibrating” the sun,” P. Winter, 12th Annual Meeting of the Northwest Section of the APS, Walla Walla, WA, USA.

“Simulating GeV particles in a very large scintillator detector,” J. Kaspar, S. Enomoto, N. R. Tolich, H. S. Wan Chan Tseung, Neutrino 2010, Athens, Greece, June 2010.

“Simulating GeV particles in a very large scintillator detector,” J. Kaspar, Advances in Neutrino Technology, Santa Fe, NM, USA, September 2010.

“Nucleosynthesis in classical novae,” C. Wrede, Colloquium, Department of Physics, The George Washington University, Washington, D.C., USA, March 2011.

“Astrophysics and particle physics with rare isotope beams,” C. Wrede, Lunch Research Discussion, National Superconducting Cyclotron Laboratory, Michigan State University, East Lansing, MI, USA, March 2011.

“Nucleosynthesis in classical novae,” C. Wrede, Seminar, Department of Physics and Astronomy, Michigan State University, East Lansing, MI, USA, March 2011.

“Thermonuclear reaction rates and nova nucleosynthesis,” C. Wrede, Nuclear Physics Seminar, Department of Physics and Astronomy, Rutgers University, Piscataway, NJ, February 2011.

“Nucleosynthesis in classical novae,” C. Wrede, Colloquium, Department of Physics, Louisiana State University, Baton Rouge, LA, USA, January 2011.

“Absolute resonance strength measurements of the ^{22}Na(p,γ)^{23}Mg reaction,” C. Wrede, Presentation, Canadian Workshop on the Nuclear Astrophysics of Stars, TRIUMF, Vancouver, BC, Canada, December 2010.

“Thermonuclear reaction rates and nova observables,” C. Wrede, Lunch Research Discussion, Joint Institute for Nuclear Astrophysics, Michigan State University, East Lansing, MI, USA, November 2010.

“Properties of ^{20}Na, ^{24}Al, ^{28}P, ^{32}Cl, and ^{36}K for the *rp* process,” C. Wrede, Presentation, 11th International Symposium on Nuclei in the Cosmos, Heidelberg, Germany, July 2010.

“Mass measurements of $T = 2$ nuclides,” C. Wrede, Presentation, TITAN collaboration meeting, TRIUMF, Vancouver, BC, Canada, May 2010.

“Stochastics in specific energy imparted to cells in radiation therapy,” H. Bichsel, 56th Annual Meeting, Radiation Research Society, Maui, Hawaii, USA, September 25-29, 2010.

“Searches for new physics using the nucleus,” A. García, Invited talk at Meeting of SACNAS (Society for the Advancement of Chicanos and Native Americans in Science), Anaheim, CA, USA, October 1, 2010.

“Weak Interactions with Rare Isotopes,” A. García, Lectures at the Ninth Exotic Beam Summer School, Oak Ridge National Lab, August 2-6, 2010.

“Kinematic Measurements,” R. G. H. Robertson, Invited talk, INT Workshop: The Future of Neutrino Mass Measurements, Seattle, WA, Feb. 8-11, 2010.

“Neutrino Experiments: A Summary,” R. G. H. Robertson, Invited Conference Summary, XXIV International Conference on Neutrino Physics and Astrophysics (Neutrinos 2010), Athens, Greece, June 14-19, 2010.

“The Neutrino @ 80,” R. G. H. Robertson, Invited talk, The INT @ 20: The Future of Nuclear Physics and its Intersections, Institute for Nuclear Theory, Seattle, WA, July 1-2, 2010.

“Measuring a Moment in a Lifetime with Muons,” D. W. Hertzog, Nucleon Structure and Electroweak Precision Tests: Past and Future, Symposium, Urbana, IL, May 20, 2010.

“Measurement of the Positive Muon Lifetime and Determination of the Fermi Constant to Part-per-Million Precision,” D. W. Hertzog, Physics of Fundamental Symmetries and Interactions, Paul Scherrer Institute, Switzerland, Oct. 11-14, 2010.

“The New Muon g-2 (and μEDM) Experiment at Fermilab,” D. W. Hertzog, Physics of Fundamental Symmetries and Interactions, Paul Scherrer Institute, Switzerland, Oct. 11-14, 2010.

“Muons and Fundamental Symmetries,” D. W. Hertzog, Invited Talk, 2010 Fall Meeting of the APS Division of Nuclear Physics, Santa Fe, NM, Nov. 3, 2010.

"Muons and Fundamental Symmetries," D. W. Hertzog, Seminar, Department of Energy, Germantown, MD, March 16, 2011.

"Towards a new study of the electron-neutrino angular correlation in the decay of magneto-optically trapped ^{6}He," A. Knecht, INPC 2010, Vancouver B.C., Canada, July 2010.

"Towards a new study of the electron-neutrino angular correlation in the decay of magneto-optically trapped ^{6}He," A. Knecht, CINP Workshop on Fundamental Symmetries, Vancouver B.C., Canada, July 2010.

"Towards a new study of the electron-neutrino angular correlation in the decay of magneto-optically trapped ^{6}He," A. Knecht, PSI2010, Villigen PSI, Switzerland, October 2010.

"Geo-neutrino review," N. Tolich, Neutrinos, Athens, Greece, June 2010.

"SNO latest results and future prospects," N. Tolich, Neutrino Oscillations Workshop, Brindisi, Italy, September 2010.

"Pulse-Shape Analysis of the Proportional Counter Data from the Third Phase of the Sudbury Neutrino Observatory," R. Martin, N. Oblath, N. Tolich, Neutrinos, Athens, Greece, June 2010.

"SNO+ Liquid Scintillator Characterization: Timing, Quenching, and Energy Scale," E. O'Sullivan, H. S. Wan Chan Tseung, N. Tolich, H. M. O'Keeffe, M. Chen, Neutrinos, Athens, Greece, June 2010.

10.4 Patents

"In-114*m* low energy electron source," U.S. Patent Application No. 61/441,913, unpublished (filing date Feb. 1, 2011) (Christopher Wrede *et al.*, applicants).

10.5 Ph.D. degrees granted

Alpha Backgrounds and Their Implications for Neutrinoless Double-Beta Decay Experiments Using HPGe Detectors, Robert A. Johnson (August, 2010).

Dark matter physics with p-type point contact germanium detectors: extending the physics reach of the MAJORANA experiment, Michael G. Marino (August, 2010).

Absolute Determination of the ^{22}Na(p,γ)^{23}Mg *Reaction Rate: Consequences for Nucleosynthesis of* ^{22}Na *in Novae*, Anne L. Sallaska (December, 2010).